

University of Leicester

ADVANCED CONTROL OF PHOTOVOLTAIC CONVERTERS

Thesis submitted to the Department of Engineering,
University of Leicester for the degree of Doctor of Philosophy

by Ying LIU
April 2009



ADVANCED CONTROL OF PHOTOVOLTAIC CONVERTERS

by

Ying LIU

Thesis submitted to the Department of Engineering, University of Leicester for
the degree of Doctor of Philosophy

April 2009

ABSTRACT

It is essential to always track maximum power from photovoltaic (PV) sources. Failure to track the global maximum power point under partial shading conditions is one of the major reasons that lead to significant power losses. Several maximum power point tracking methods have been proposed to deal with this problem. However, none of them were able to effectively identify the occurrence of partial shading. With the facility of Matlab modelling and simulation as well as the aid of a constructed solar emulator, the power-voltage characteristics of a PV panel under uniform and non-uniform irradiance conditions have been studied and some useful conclusions have been identified from observation. Based on these conclusions, a novel maximum power point tracking algorithm has been proposed, which is capable of identifying the occurrence of partial shading hence determining the need for a global scan over the operation range of PV panels for the true maximum power point.

In the meantime, the effect of PV dynamics, due to the capacitance of PV cells, on maximum power point trackers has been investigated and some initial results and suggestions have been presented in this work.

Key words: maximum power point, maximum power point tracking, partial shading, photovoltaic, capacitance

ACKNOWLEDGEMENTS

Firstly, I would like to thank my supervisor, Dr Hans Bleijs, for his extensive guidance, support and help throughout this research. Also his comments and suggestions during the writing of this thesis are invaluable and are highly appreciated.

I would also like to thank my colleague Mr Luigi Alessandro, who is warm-hearted and very helpful and shared a lot of ideas for this work.

Special thanks to Mr Stuart Tranter (Alanod Limited) who kindly offered two large MIRO-SUN reflective aluminum sheets for free, which are used as the mirrors in the constructed solar emulator.

Also I would like to thank all other colleagues in the Department of Engineering for their support, advice and help during my PhD study.

Finally, words alone cannot express the thanks I owe to my husband and my parents for their understanding, patience, support and encouragement.

LIST OF CONTENTS

Chapter 1. Introduction.....	1
1.1 Renewable Energy and Solar Energy	1
1.1.1 Renewable Energy and Energy Policies	1
1.1.2 Solar Energy.....	4
1.1.3 Solar energy at the University of Leicester.....	7
1.2 Photovoltaic Cells and Photovoltaic Systems.....	8
1.2.1 Photovoltaic Effect.....	8
1.2.2 PV technologies	10
1.2.3 Terminal Characteristics of PV cells	12
1.2.4 PV Systems	16
1.3 Maximum Power Point Tracking Algorithms.....	21
1.3.1 Conventional MPPT methods under uniform irradiance.....	22
1.3.2 MPPT methods under partial shading conditions	24
1.4 Existing Experimental Set Up.....	27
1.5 Objective of Research and Structure of Thesis.....	30
Chapter 2. Basic Comparative Study of MPPT Algorithms.....	33
2.1 Introduction.....	33
2.2.1 Modelling of steady-state PV sources.....	34
2.2.2 Modelling of Multiple PV Sources under Non-Uniform Conditions	44
2.3 Simulation of MPPT Algorithms	46
2.3.1 Perturbation & Observation Methods	48
2.3.2 Incremental Conductance Methods.....	49
2.3.3 An MPPT Algorithm Based on Intrinsic Ripple.....	52
2.4 Comparison of MPPT Algorithms and Conclusions	53
Chapter 3. Effect of PV Dynamics on MPPT Algorithms	57
3.1 Introduction.....	57
3.2 Modelling of PV Dynamics due to Capacitance of PV Cells	58
3.2.1 Experimental Test	58
3.2.2 MATLAB Modelling.....	60
3.3 Effects of PV Dynamics on Operation of MPPT Algorithms.....	62
3.4 Conclusions.....	65
Chapter 4. Novel MPPT Method to Identify Partial Shading.....	67
4.1 Introduction.....	67
4.2 PV Characteristics without Partial Shading.....	71
4.3 PV Characteristics under Partial Shading Conditions and Identification of Partial Shading	74
4.4 A Novel MPPT Algorithm Adopting Partial Shading Identification	78
4.5 Conclusions.....	80
Chapter 5. Design and Construction of a Solar Emulator	81
5.1 Introduction.....	81
5.1.1 Why a Solar Emulator Is Needed.....	81
5.1.2 Spectral Sensitivity of PV cells.....	85
5.1.3 Standards for Solar Simulators	89
5.1.4 Existing Commercial Solar Simulators.....	90
5.1.5 Design Requirements for the Solar Emulator	92

5.2 Facilities to Test Lamp Characteristics.....	94
5.2.1 Radiometric and Photometric Quantities.....	94
5.2.2 Irradiance Measuring Device.....	97
5.3 Design of a Solar Emulator Using Power LEDs.....	99
5.4 Design of a Solar Emulator Using Halogen Lamps.....	103
5.4.1 Selecting the Lamp Type.....	103
5.4.2 Testing the Lamp Characteristics.....	108
5.5 Construction and Testing.....	109
5.5.1 Mechanical and Electrical Design of the Solar Emulator.....	109
5.5.2 Testing the Solar Emulator.....	115
5.6 Conclusions.....	118
Chapter 6. Implementation of Intelligent MPP Tracking Using a DSP controller.....	119
6.1 Introduction.....	119
6.2 TMS320F2812 Digital Signal Processor.....	121
6.3 Intelligent MPPT Controller with Partial Shading Identifier.....	122
6.4 Testing and Performance.....	129
6.4.1 Measurement of Power-Voltage Curves under Partial Shading Conditions.....	129
6.4.2 Test of the Proposed MPPT Algorithm with Partial Shading Identifier.....	130
6.5 Conclusions.....	136
Chapter 7. Original Contributions, Conclusions and Future Work.....	138
7.1 Original Contributions.....	138
7.2 Overview of Conclusions.....	140
7.3 Future Work.....	141

Appendices

Appendix 1 Matlab model of a PV source with only 1st quadrant characteristics
Appendix 2 Matlab model of a PV source with 2nd quadrant characteristics
Appendix 3 Matlab model of a PV source with bypass diodes
Appendix 4 Matlab function program of the Perturbation & Observation MPPT algorithm
Appendix 5 Matlab function program of the Incremental Conductance MPPT algorithm
Appendix 6 Matlab function program of the MPPT algorithm based on Intrinsic Ripple
Appendix 7 Matlab program for irradiance distribution calculation
Appendix 8 Diagrams of existing and modified circuits
Appendix 9 Interface board circuit
Appendix 10 DSP code

References

Publications

Chapter 1. Introduction

1.1 Renewable Energy and Solar Energy

1.1.1 Renewable Energy and Energy Policies

Energy is essential for our life and economy. Since the Industrial Revolution, energy demand has greatly increased, not only in the western world, but also in other parts of the world. This has resulted in two problems: energy crisis and more recently climate change (global warming). The sustainability of our civilization is seriously threatened. The worldwide energy demand and energy related greenhouse gas emissions are still increasing. It is a global challenge to tackle climate change by reducing carbon dioxide emissions and ensuring secure, clean and affordable energy [1], and to achieve more sustainable energy systems.

Saving energy is one cost effective solution but not enough to meet the increasing worldwide energy demand. On the other hand, moving towards renewable energy supplies is a solution that can solve these problems simultaneously. They are green and clean with little or no carbon dioxide emission, and they are ‘renewable’ hence sustainable.

Renewable energy is energy generated from renewable natural resources, such as solar radiation, wind, rainfall, tides, geothermal heat, etc. [2]. The main renewable energy technologies include biomass, hydropower, solar heating, solar electricity, wind power, ocean energy, etc. They have been applied in four sectors: power generation, hot water

and space heating, transport fuels, and rural (off-grid) energy. In 2006, renewable energy supplied 18% of the world's final energy consumption, taking into account the traditional use of biomass [3].

Compared to conventional fossil fuel energy sources (coal, oil and natural gas), renewable energy sources have the following major advantages: firstly, they are replenished from natural resources, therefore they are sustainable and will never run out; secondly, they produce little or no carbon dioxide. Therefore, using renewable energy will be the key to tackle climate change as well as to achieve sustainable energy [1].

To encourage the use of renewable energy, more than 65 countries in the world now have set goals for their own renewable energy future [3]. In 2007, all 27 European Union countries reached an agreement to commit the EU to achieve a 20% reduction in the greenhouse gas emissions and to meet the target of deriving 20% of the EU's final energy consumption from renewable sources, both by 2020 [4]. In order to achieve this, for UK it was suggested that 15% of its energy be derived from renewable energy by 2020 [4][5].

In UK, it is estimated that in 2020, 10% transport fuel and 5% to 10% heat energy will be renewable, so it will be necessary to have 35% to 40% of renewable electricity by 2020 to reach the 15% target [5]. In 2007, total electricity generation from renewable energies was 19,664 GWh, which is 4.98% of the electricity generated in the UK in 2007 [6].

To achieve the renewable energy target, more and more funds have been and will be invested in the research and development of the renewable energy. Fig. 1-1 shows the growth of the annual investment in new renewable energy capacity since 1995 [3]. It can be seen that wind power and solar (photovoltaic) energy are two major areas. In 2007,

\$71 billion was invested in new renewable energy capacity. Approximately 47% of the investment goes into wind power and 30% into solar energy.

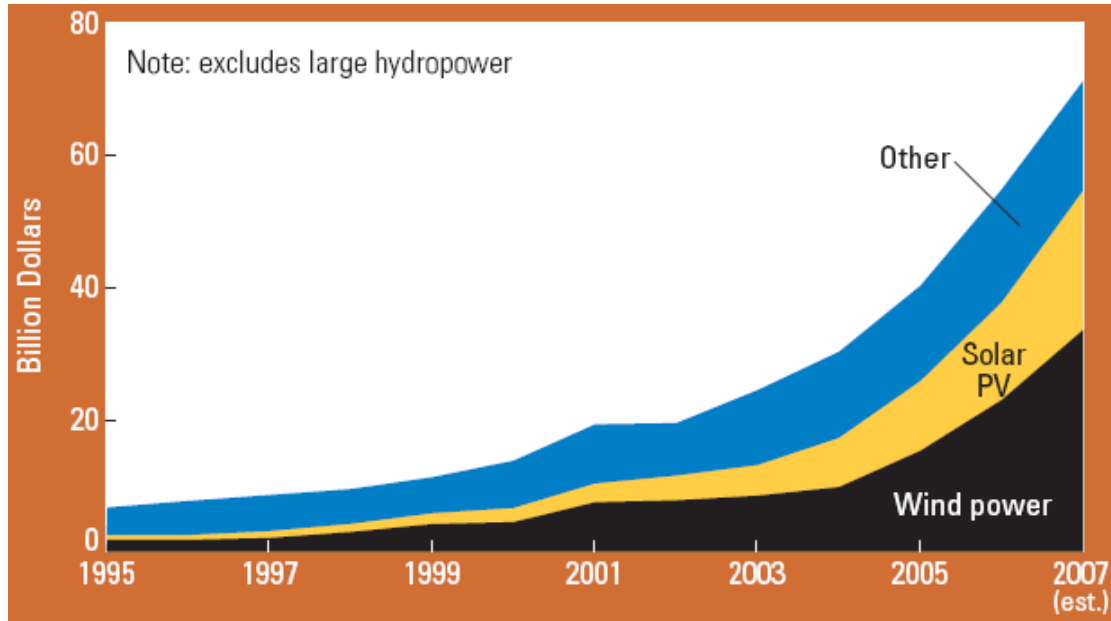


Fig 1-1. The growth of the annual investment in new renewable energy capacity [3]

However, there are still several limitations when using renewable energy, such as reliability, cost, etc. Most renewable energies rely much on weather, e.g., hydropower needs rain to supply flowing water, wind power needs wind to turn the blades, and solar power need clear sky, etc. Compared to conventional fossil fuels, it is more difficult to generate electricity from most renewable sources, and the costs can be much higher. To derive affordable and efficient renewable energy is one of the main renewable energy research topics.

1.1.2 Solar Energy

Solar energy is one of the most important renewable sources. The sun radiates an enormous amount of energy onto the earth's surface everyday, which is more than enough to provide the whole demand of the world [7]. Actually, most of the energy sources, including conventional fossil fuel energy and most renewables (such as wind, tides, biomass, etc.), originate from solar energy.

Solar energy technologies use the sun's energy to provide heat, light, hot water, electricity, and even cooling [8]. One of the important technologies is photovoltaic (PV), which converts sunlight directly into electricity by the photovoltaic effect.

The photovoltaic effect was first discovered in 1839 by French experimental physicist Edmund Becquerel when he experimented with an electrolytic cell made up of two metal electrodes exposed to light [9].

The first photovoltaic cell was made by American inventor Charles Fritts from selenium wafers in 1883. The first usable PV cell, using silicon with efficiency of 6%, was developed by Chapin et al in 1954 at the Bell laboratories. In 1958, PV cells were first used in the satellite Vanguard 1 to generate electricity from the sun.

Since early 1970s, more and more interest in PV electricity has been aroused due to its high potential as renewable energy converter, and PV has become an important form of power generation [7][10].

PV energy has the following main advantages [7][8][10][11]:

1) It is plentiful and sustainable. The sun provides 6000 times more than the energy consumed by humans.

2) It is clean and safe. PV will not cause environmental problems such as greenhouse effect, acid rain, deforestation and noise. Its use is pollution free; manufacturers of PV materials are committed to minimize pollution during production.

3) It is reliable. PV power generation has no moving parts and the maintenance costs are very low. When used as a distributed generation source, it can improve grid reliability and reduce the need for transmission lines.

4) PV devices have a very long life, up to 3 times longer than other renewable technologies [5].

The PV industry is growing very fast since 1990s. Fig 1-2 shows the worldwide production in photovoltaics from 1993 to 2006 [12]. PV production has been increasing at an average rate of nearly 50% each year since 2002.

Japan and Germany are currently leading the PV market [10]. By the end of 2004, Japan became the first country to install 1 Giga Watt of PV, and the Japanese government is planning to generate 10% electricity from PV by 2030 [13]. In Germany, the total electricity generation from photovoltaics was 3500 GWh in 2007, which is 4.0% of the total electricity generation from renewables, and 0.57% of the total electricity generation [14].

However, there are a few concerns when using PV energy.

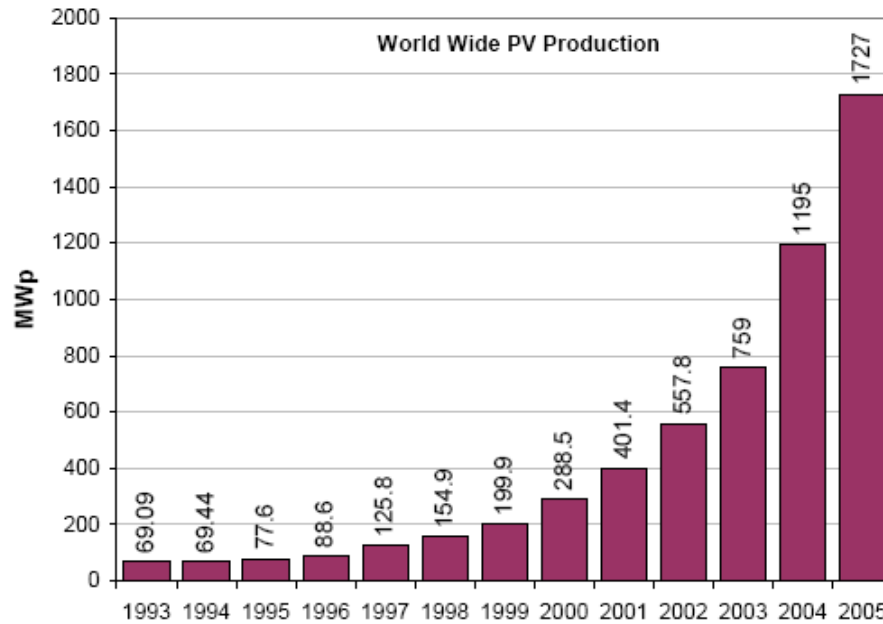


Fig 1-2. Worldwide PV production [12]

Firstly, PV energy relies on weather. It is obviously not available at night, and is less efficient under cloudy conditions. Therefore, its generation is variable and intermittent.

Secondly, the high cost is a major issue at the moment, and it is the greatest barrier to PV-generated electricity. Currently, at a large scale the cost of PV generated electricity is much higher than that generated by conventional means.

To reduce the cost of PV generated electricity to make it competitive with bulk electricity generation from conventional sources and to increase the PV system conversion efficiency are two major aims of the research works in PV technology [15]. PV technology is expected to become a significant part of the world's future energy supply.

1.1.3 Solar energy at the University of Leicester

Research work on renewable energy conversion systems including solar photovoltaic and wind turbine generators has been actively carried out in the University of Leicester since almost twenty years ago.

Two outdoor PV systems have been installed and are operating successfully at the University of Leicester.

The first one is an 11.5 kWp PV system (as shown in Fig 1-3) installed on the roof of the Concrete Laboratory next to the Engineering building at the end of 2004 [16]. This system consists of a PV array of 64 BP Solar Saturn 7 modules, 7 SMA Sunny Boy inverters with various power ratings, complete with sensors and data acquisition facilities. The PV modules can be interconnected in different configurations and appropriate numbers and sizes of inverters can be selected for optimized operation. This system has been used for demonstration as well as research purposes, particularly for analysis of the effect of local shading on PV system performance. The shading is due to a number of nearby buildings and a protected old oak tree (as can be seen in Fig 1-3).

The second PV system is a 38.1 kWp building integrated system installed on the newly refurbished and extended David Wilson Library in 2007 [17]. This system consists of 3 PV arrays installed in different locations, each adopting a different type of PV technology (mono-crystalline, poly-crystalline and thin-film amorphous). It is performing successfully, supplying clean and green electricity for the university.



Fig 1-3. Photo of the PV array on the roof of the Concrete Laboratory,
showing the shading from a local tree

Besides the outdoor PV systems, indoor research on simulated PV systems has been carried out. As part of an EPSRC-funded project with industrial backing, John Gow designed and built a PV system that adopted his maximum power point (MPP) algorithm, using a simulated PV source [18] in 1999. The research in this thesis is based on this system.

1.2 Photovoltaic Cells and Photovoltaic Systems

1.2.1 Photovoltaic Effect

The photovoltaic effect is a physical phenomenon of converting the energy carried by

optical electromagnetic radiation into electrical energy [11]. It was discovered by E. Becquerel in 1839, when he found that certain materials will produce an electric current when exposed to light [11][19].

Sunlight is composed of packets of energy, called photons. The photon is the basic unit of light and other electromagnetic radiation [20]. Photons contain various amount of energy corresponding to the different wavelengths of light. The energy can be expressed by the equation:

$$E = h \cdot \nu$$

Where h is Planck's constant and ν is the photon's frequency. As the wavelength of light increases, the photon energy of that light decreases.

When certain materials, such as semiconductors, are exposed to light, the photons within a certain energy band can be absorbed. Other photons may pass through the material or be reflected without being absorbed. Different semiconductors have different optical absorption coefficients [11].

When a photon is absorbed, the energy of the photon will be transferred to an electron of the material under illumination. When this energy is larger than the electron binding energy, the electron will be ejected from its ground energy state, and an electron-hole pair will be created.

PV cells are made to facilitate this effect, converting solar energy to electricity. Fig. 1-4 shows how a silicon based PV cell works. PV cells are made of various semiconductor materials, most commonly silicon. A typical PV cell is formed with a PN junction and

two electrical contact layers (front contact and rear contact). The front contact allows light to pass through and be absorbed in the semiconductor. When the PV cell is exposed under light, some photons are reflected or pass through the cell without being absorbed. The others are absorbed and hole-electron pairs are then generated. The holes and electrons are then separated by the electric field produced by the p-n junction. This results in a potential difference and a current flow (electricity) if the PV cell is connected to a load. [7][11][21][22].

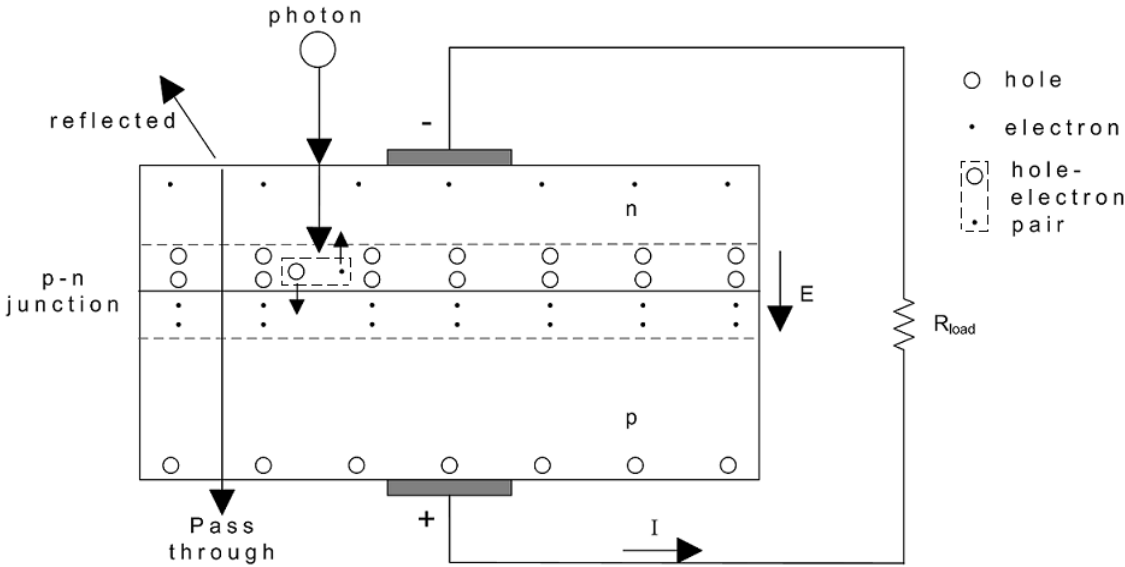


Fig 1-4. Structure and working mechanism of a PV cell

1.2.2 PV technologies

PV cells can be manufactured from different materials. There are two major PV technologies: wafer-based silicon technology and thin-film technology [7][11][12].

Current PV production is dominated by single junction silicon-wafer PV cells (known as first generation technology [21][22]). Crystalline silicon PV cells are more efficient than thin-film ones but more expensive to produce. They are most commonly used in medium to large electrical applications such as grid connected PV generators.

Mono-crystalline and poly-crystalline (or multi-crystalline) are two dominant silicon technologies. Mono-crystalline PV cells use pure semiconducting materials and have higher efficiency (24% in research laboratories and over 17% in industrial production [23][24]). Poly-crystalline PV cells are slightly less efficient but lower in cost than Mono-crystalline ones.

As the second generation PV cell technology, thin-film PV cells use very thin layers of semiconducting materials, so they can be manufactured in large quantity at low cost. However, the efficiency is lower. Currently, this technology prevails in small consumer applications such as watches, calculators and toys. The most established thin-film PV cells are made from amorphous silicon (α -Si). Other materials used in thin-film technology include Copper Indium Diselenide (CIS), Cadmium Telluride (CdTe) and other exotic combinations.

In addition to the above technologies, there are some other PV technologies. Organic cells have been reported in literatures but their efficiencies are currently very low (only 2.5% was achieved in [25]) compared to non-organic ones. Hybrid PV cells combine both mono-crystalline and thin-film silicon to produce cells with the best features of both technologies as proposed in [26]. Moreover, third generation PV technology try to

improve the electrical performance of the second generation while maintaining low production costs [21].

1.2.3 Terminal Characteristics of PV cells

Fig 1-5 shows two generally accepted electrical equivalent circuits derived from the physical mechanism of PV cells. The first contains two diodes to reflect diffusion and carrier recombination. The second is a simplified model providing an approximate characteristic for the description of the PV cell.

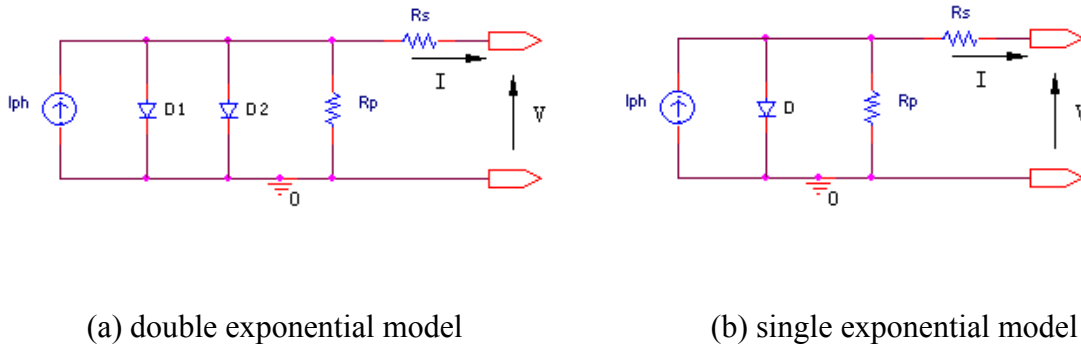


Fig 1-5. Equivalent circuits for a PV cell

The electrical terminal characteristic (I-V curve) of a typical silicon PV cell is shown in Fig 1-6. The double exponential equation (Eqn 1-1) and the single exponential equation (Eqn 1-2) have been evaluated and widely used to describe the characteristics of PV cells. [27][28][29]

$$I = I_{ph} - I_{S1} \left(e^{\frac{q(V+IR_S)}{kT}} - 1 \right) - I_{S2} \left(e^{\frac{q(V+IR_S)}{AkT}} - 1 \right) - \frac{V + IR_S}{R_p} \quad (1-1)^*$$

* Equation 1-1 refers to the current-voltage characteristic of the two diode equivalent circuit given in Fig 1-5 (a). Equation 1-2 refers to the case of a single diode equivalent circuit shown in Fig 1-5 (b).

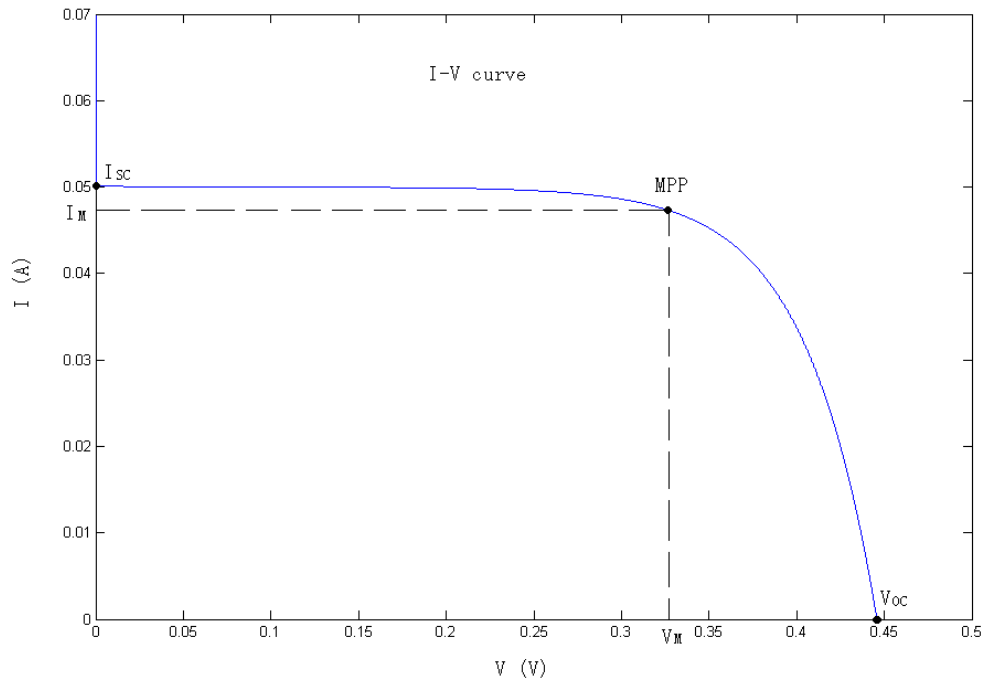


Fig 1-6. Typical I-V curve for a PV cell

$$I = I_{ph} - I_S \left(e^{\frac{q(V+IR_S)}{AkT}} - 1 \right) - \frac{V + IR_S}{R_p} \quad (1-2)^*$$

where

V – PV cell terminal voltage (V)

I – PV cell terminal current (A)

I_{ph} – photocurrent (A)

I_{S1} – saturation current due to diffusion mechanism (A)

I_{S2} – saturation current due to carrier recombination in space-charge region (A)

I_S – saturation current (A)

R_P – cell shunt resistance (Ω)

R_S – cell series resistance (Ω)

A – p-n junction ideality factor

q – electronic charge, $=1.6 \times 10^{-19} \text{ C}$

k – Boltzmann's constant, $=1.38 \times 10^{-23} \text{ J / K}$

T – junction temperature, K

There are four salient parameters that define the shape of the I-V curve.

Short-circuit current I_{SC} : $I_{SC} = I |_{(V=0)} = I_{ph}$

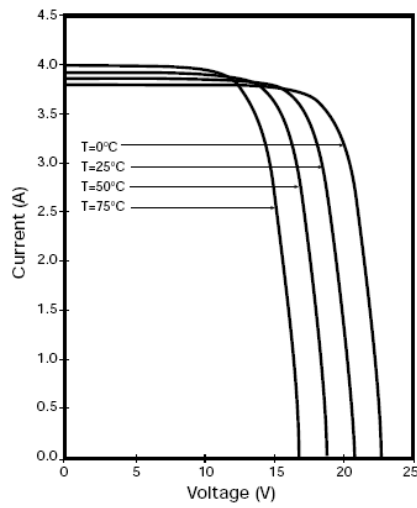
Open-circuit voltage V_{OC} : $V_{OC} = V |_{(I=0)}$

Maximum power point (MPP): $(I_M, V_M) | \frac{dP}{dV} = 0$, where the PV cell generates maximum power when supplying a load.

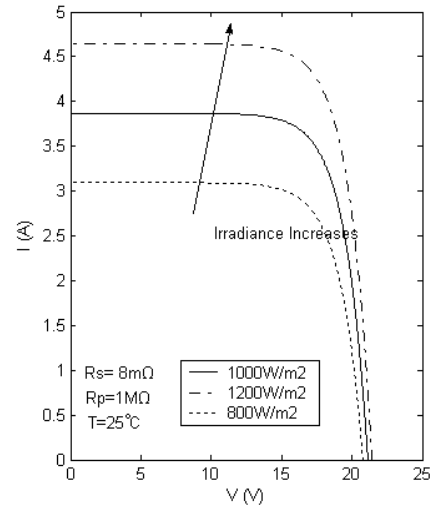
Fill Factor (FF): $FF = \frac{I_M \cdot V_M}{I_{SC} \cdot V_{OC}}$, which reflects the shape of the I-V curve.

There is extensive literature on the theoretical analysis and experimental evaluation of the effects of parameters such as temperature, irradiance level, cell series resistance and cell shunt resistance on the behaviour of PV cells [7][11][27][29][30]. The effect of these parameters on the I-V characteristics can be summarized as follows:

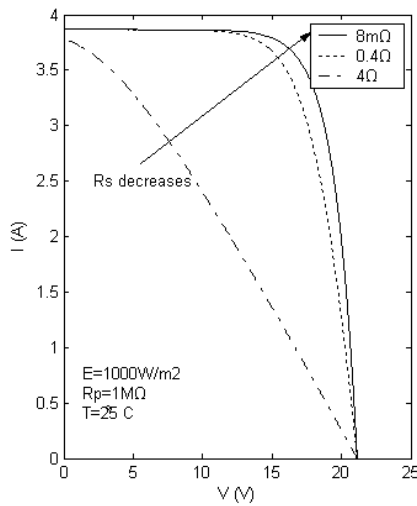
1) Effect of temperature: Temperature has a strong effect on the saturation current I_s while slightly affects I_{ph} . As a result, V_{OC} has a negative temperature coefficient of approximately $-2.3\text{mV}/^\circ\text{C}$ for silicon cells. Fig 1-7(a) shows a typical trend of this effect (from datasheet of BP Solar MSX60 PV panel).



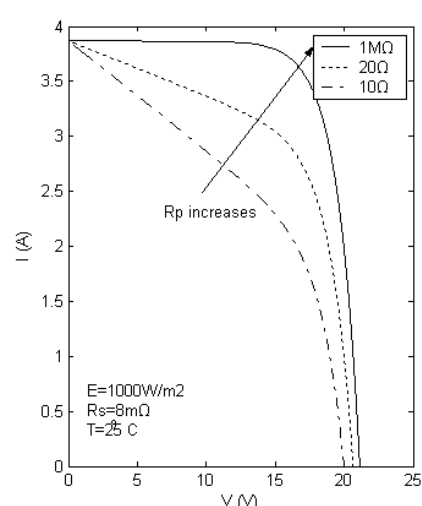
(a)



(b)



(c)



(d)

Fig 1-7. Typical effects of parameters on I-V curves

2) Effect of irradiance: I_{ph} is directly proportional to the irradiance while the voltage variation is much smaller as shown in Fig 1-7(b).

3) Effect of series resistance: A larger R_S reduces I_{SC} and FF with V_{OC} unaffected as illustrated in Fig 1-7(c).

4) Effect of shunt resistance: A smaller R_P reduces V_{OC} and FF without affecting I_{SC} as shown in Fig 1-7(d).

The above parameters have effects on the steady-state I-V characteristics. On the other hand, the capacitance of PV cells can also affect the dynamic I-V characteristics. The existence of PV capacitance can alter the dynamics of the current flow on changing illumination or changes in the operation point. This can potentially affect the MPP tracking capabilities of many MPP tracking algorithms leading to reduced power transfer. This will be explored in more detail in Chapter 3 of the thesis.

1.2.4 PV Systems

1.2.4.1 PV modules and PV arrays

Depending on the cell area, the output current from a single PV cell can be used directly. However, its output voltage is usually too small for most applications. Therefore, to produce useful DC voltage, a number of PV cells are connected in series and mounted in a support frame, which forms a PV module (or a PV panel).

To generate higher currents and/or voltages, PV modules can be connected in series and/or in parallel to form a PV array for higher power applications. Bypass and/or

blocking diodes are often used in a PV array to reduce power loss when one PV module generates less photocurrent.

Consider a PV array where the number of cells connected in series is N_S and that in parallel is N_P . Assuming that each cell has identical parameters, the electrical characteristic of the array can then be expressed as Eqn 1-3 or Eqn 1-4 [11][27], which is more useful in practical applications.

$$I = N_P \left[I_{ph} - I_{S1} \left(e^{\frac{q \left(\frac{V}{N_S} + \frac{I}{N_P} R_S \right)}{kT}} - 1 \right) - I_{S2} \left(e^{\frac{q \left(\frac{V}{N_S} + \frac{I}{N_P} R_S \right)}{AkT}} - 1 \right) - \frac{\frac{V}{N_S} + \frac{I}{N_P} R_S}{R_p} \right] \quad (1-3)$$

$$I = N_P \left[I_{ph} - I_S \left(e^{\frac{q \left(\frac{V}{N_S} + \frac{I}{N_P} R_S \right)}{AkT}} - 1 \right) - \frac{\frac{V}{N_S} + \frac{I}{N_P} R_S}{R_p} \right] \quad (1-4)$$

In this work, PV cells, strings, modules, panels or arrays will be generally called PV sources.

1.2.4.2 Partial shading of PV arrays

Ideally, PV modules should be built using identical panels and should not incur any shading. However, the occurrence of partially shaded conditions is not easily avoided because of clouds and obstacles such as trees and buildings (A typical partial shading example is shown in Fig 1-3).

Partial shading can not only lead to hot spots in PV modules [7][11][31], but is also one of the main causes for reduced energy yield in many PV applications [32].

A. The hot spot problem

When connecting PV cells/modules in series, if one of the PV cells/modules has a much lower photo current I_{ph} than others due to partial shading, dust or degradation, it operates as a load for other cells and is reversed biased. This cell/module will then dissipate energy rather than generate hence leading to a cell temperature rise. If the temperature is too high, the cell/module can be damaged and affect the whole PV module/array. The most common method to avoid this is to put a bypass diode across a PV string or modules (as shown in Fig 1-8) [11].

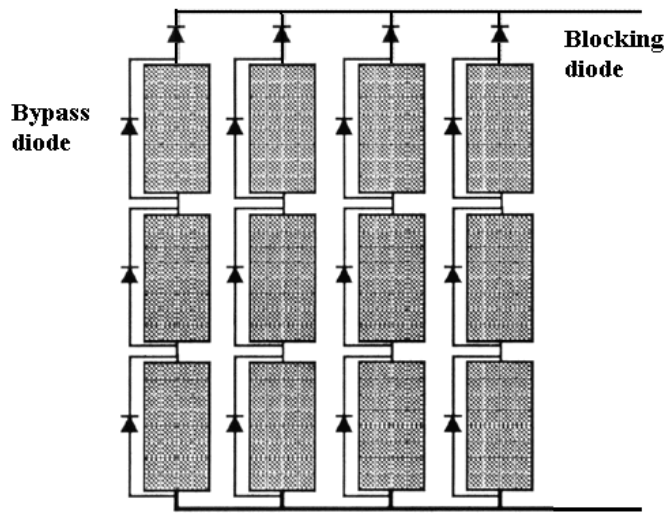


Fig 1-8. Bypass and blocking diodes in PV arrays

The number of bypass diodes per module is a compromise between avoiding the formation of hot spots and the costs for extra components. For today's crystalline silicon PV modules, the optimized number of cells in series per bypass diode is mostly commonly 18 [32].

Hot-spots can also be created when PV modules with different open circuit voltages are connected in parallel, e.g., when one of the PV modules in parallel is shaded. In this situation, the PV module with lower open circuit voltage may behave as a load and

consume power generated by others. This PV module can be damaged if the temperature is too high. To avoid this problem, blocking diodes are sometimes connected in series with PV modules as shown in Fig 1-8.

B. Power output loss due to shading

As described in the previous section, bypass diodes are usually used in PV modules to protect them from hot-spot damage. Because the shaded cell defines the current of the entire series string, even minor shading could cause a major reduction in power output of PV modules.

Fig 1-9 shows the simulation result of the electrical characteristics of a PV array under partial shading (dotted lines). The PV array consists of 4 BP Solar MSX60 PV panels all connected in series, and one of them is shaded. The irradiance on the shaded panel (@ $750\text{W}/\text{m}^2$) is 75% of the others (@ $1000\text{W}/\text{m}^2$). Under this partial shading condition, the P (V) characteristic exhibits multiple peaks, and the global maximum output power is 204 W, which is only 83.6% of the maximum power of the PV array under uniform full illumination (244 W, shown as the solid lines in Fig 1-9).

Similar experimental results are reported in [33]. A comparison experiment was carried out to investigate the effect of partial shading. Two identical PV modules each comprising 72 PV cells were used in the experiment, one of which has one cell intentionally shaded (one-cell shaded module). The one-cell shaded PV module caused significant losses in the whole PV system. Compared with the unshaded module, the maximum power output of the one-cell shaded module degraded by about 30% (from 21.48 W to 15.44 W). It may be more effective to completely remove the partially shaded

PV module from the PV system rather than to have it degrade the performance of the other unshaded PV modules.

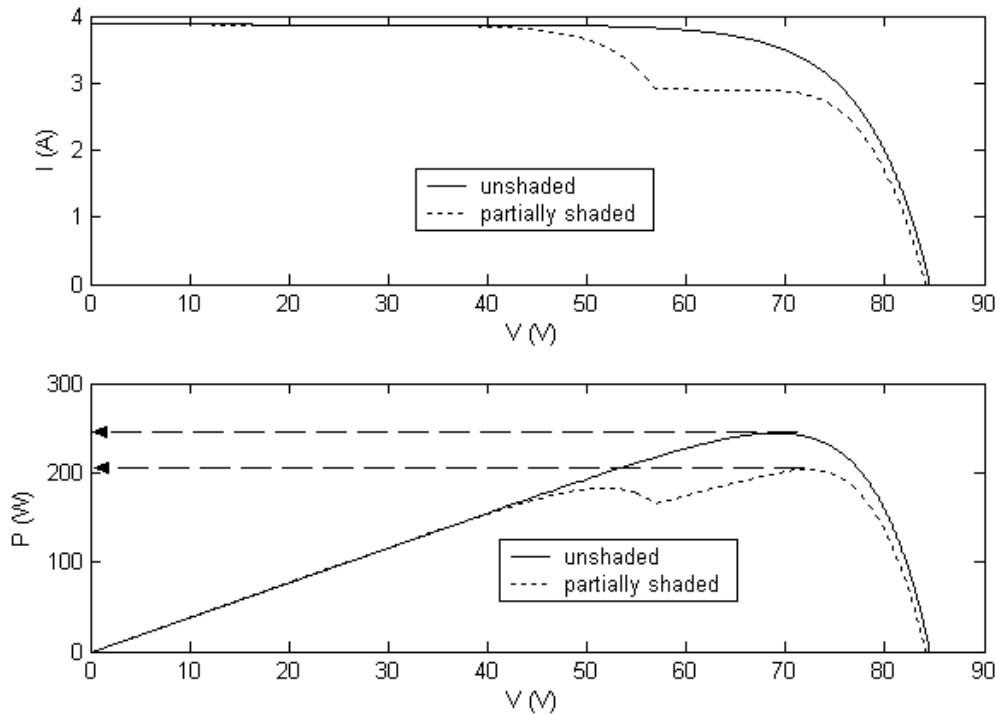


Fig 1-9. Electrical characteristics of a PV module with partial shading

As shown in Fig. 1-9, the $P(V)$ characteristic under partial shading conditions is more complex than the one without partial shading. It has more than one local maximum point. To date, MPP tracking schemes are not very efficient under partial shading conditions. This will be discussed in section 1.3.2.

1.2.4.3 PV system topologies

There are three types of PV systems [34]: stand-alone system, grid connected (also called grid interactive) system and hybrid systems.

For grid connected systems, the output of PV sources feeds power directly to the grid. Because the output of PV cells is DC, it needs to be converted into AC so that it can be connected to the grid. Different system structures have been developed and reported [35]-[38]. The approaches include single DC string with single DC-AC inverter, module integrated inverters, module integrated DC-DC converter with single inverter, string inverters, multi-string inverters, etc.

In [38], an efficient configuration suitable for medium to large scaled photovoltaic plant is described. Each PV module or string of modules has its own DC-DC converter with MPPT controller and feeds its power into a common DC link to be inverted into AC through a central inverter as illustrated in Fig 1-10. In this way, maximum power can be extracted from each PV module, therefore, the overall power yield from the whole PV system can be maximized.

1.3 Maximum Power Point Tracking Algorithms

As described in section 1.2.3 and 1.2.4, PV sources exhibit a maximum power point (MPP) in their steady-state characteristic. The MPP varies with changing conditions such as irradiance levels and temperature. To make best use of PV sources, it is essential to always operate at the MPP.

To evaluate an MPPT algorithm, there are a few aspects to consider, such as tracking speed, stability, simplicity and cost of implementation, and tracking efficiency. The tracking efficiency is defined as [39]:

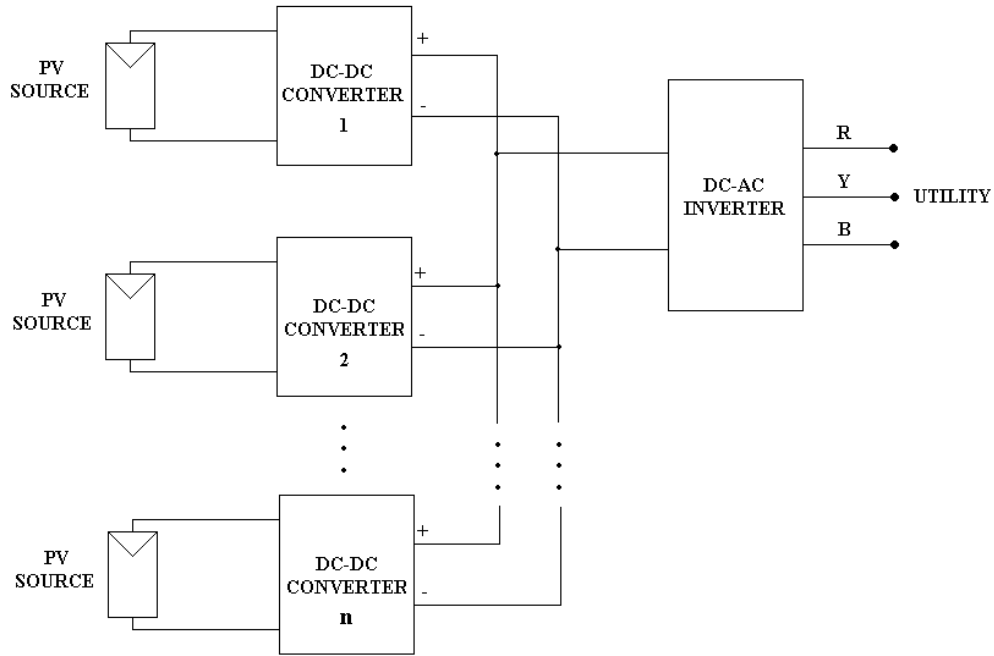


Fig 1-10. Block diagram of the PV system with module integrated DC-DC converters and single inverter

$$\eta_{MPPT} = \frac{\int_0^t P_{actual}(t) dt}{\int_0^t P_{max}(t) dt} \quad (1-5)$$

Where P_{max} is the theoretical maximum power that can be produced by a PV source under certain conditions and P_{actual} is the actual extracted power from the PV source under the control of the MPPT algorithm under test.

1.3.1 Conventional MPPT methods under uniform irradiance

Conventional MPP tracking (MPPT) methods can be classified into a number of categories [40].

The first category consists of constant voltage or current reference methods. The controller sets the voltage or current reference to an empirical ratio of the open circuit voltage or short circuit current. It is very simple and quick, but can't extract maximum power under all environmental conditions and has a low tracking efficiency [39].

The second category consists of the Perturbation and Observation (P&O) methods. P&O methods use the idea of hill climbing algorithms. They work well when the irradiance does not vary rapidly with time. And due to their simplicity and ease of implementation, they are the most widely applied methods in PV industry. However, their drawbacks are slow tracking speed and oscillations around MPPs [41]. To reduce or eliminate these drawbacks, P&O methods have been improved by using variable step-sizes [42]. Another problem with P&O method is that when the environmental conditions change rapidly, e.g., when the irradiance increases rapidly, the operating point may deviate from the MPP by tracking towards a wrong direction [41]. This is because the algorithms are not able to distinguish between changes caused by the perturbation or by the changing environmental conditions. Methods to overcome this problem have been proposed in [43][44].

The third category is the Incremental Conductance method (InCon) [41]. It is claimed that this method can track faster and has a better performance than the P&O methods, especially under rapidly changing environmental conditions.

There are also some other MPPT algorithms. For example, an MPPT method that senses only the converter's output voltage or current is presented in [45]. The PWM converter is modelled as a time- varied transformer or a loss-free resistor, so the input voltage or

current can be calculated from the output voltage or current. By analysing linear and non-linear loads, it was found that for loads with a non-negative incremental impedance, the output current and voltage increase monotonically as the output power increases. Thus maximum output current (or voltage) implies maximum output power. Therefore, the MPPT algorithm can be implemented based only on a single output parameter, which can simplify hardware design and control algorithm. With this method, it is the converter output power that is maximized rather than the PV array power. Thus the PV array may be operating slightly off the MPP, but the total efficiency is optimised.

The P&O and InCon MPPT methods are most commonly used in PV industry, therefore they will be studied in more detail and compared with other relevant MPPT algorithms in Chapter 2.

1.3.2 MPPT methods under partial shading conditions

Most of conventional MPPT methods assume that there is only one single maximum power point on the Power-Voltage characteristic of a PV source, However, when a PV array is under partial shading conditions, its characteristic may exhibit multiple maximum power points (see Fig. 1-9). These MPPT methods have limited reliability in dealing with the partial shading conditions [46].

Thirteen commercial inverters with MPP trackers were tested with real partially shaded PV arrays in [47]. All of these trackers have very high MPP tracking accuracy under stationary conditions. But when the P (V) curve exhibits two local maximum power points, only 7 out of 13 could track the global MPP. When P (V) curve has three local maxima, none of them was able to track the global MPP, while 10 out of 13 tracked the

second maximum power point. It causes up to 70% losses because the MPPT algorithms are unable to track the global MPP of the PV arrays.

Quite a few researchers [48]–[54] have worked on global MPP tracking schemes for PV systems operating under partial shading conditions.

Kobayashi et al. [48] proposed a two-stage MPP tracking scheme for a PV system under partial shading conditions. In the first stage, the operating point moves to the intersection of the I (V) curve and the load line $R_{pm}=V_{pm}/I_{pm}$, where V_{pm} is 80% of the open circuit voltage and I_{pm} is 90% of the short circuit current. In the second stage, the operating point moves to the MPP using conventional MPPT scheme. However, in the first stage, the operating point is not always close to the global MPP [49] [50], and it may miss the global MPP in second stage. Also, online open circuit voltage and short circuit current measurements require extra components in the PV system and increase the complexity of the control scheme. Although the measurements can be done within a short period (1ms), it will cause some power loss during the measurements.

Full range search based MPPT schemes have the advantage of easy implementation and high reliability under partial shading conditions [50]-[53].

There are two full range MPP scan methods: Power-Current curve scan [51] and Power-Voltage curve [50] scan. P (I) or P (V) curves are scanned periodically, in this way it can always find the global MPP. However, the scan interval is not based on any identified need, but is only chosen empirically. Any full range scan results in some power loss, therefore, unnecessary scans will actually reduce the total power yield.

A search based MPP tracker, designed to improve the PV system efficiency for a racing solar car, is described in [52]. The racing car is powered by a PV module and batteries. The MPP tracker includes a full range MPP searching and a conventional P&O MPPT scheme. The full range MPP searching is triggered when the operation conditions are changed, such as starting the car, system restart, the car entering shadow, etc. Also the full range MPP searching can be manually triggered by the driver. There is not much information on whether/how a judgment is made for the necessity of a full scan. And every full range MPP searching takes 3.8 seconds, which is quite long, and it may not be very suitable if the condition changes rapidly when driving the racing car.

An improved Fibonacci linear search algorithm has been proposed to track the global MPP under rapidly changing irradiance or partial shading conditions in [53]. For partial shading conditions, an equation of output power change rate is introduced for the detection of partial shading. If the output power change rate is greater than certain constant, the algorithm will be initialized to do a wide-range scan. However, this method only applies to abrupt changes of partial shading conditions. When the shading pattern changes slowly, e.g. the shade of a nearby building moves slowly during a day due to the slowly changing incident angle of the sunlight, this method will not be able to identify the change in power hence fail to track the global MPP.

A global MPP tracking scheme which only needs to scan part of the P (V) curve has been proposed [49] [54]. After some observations of the P (V) curves using the MATLAB model presented in [54], H. Patel et al. proposed an MPPT algorithm for PV systems operating under partial shading conditions in [49]. The authors observed that on either side of the global maximum power point, the power of local maxima decreases

monotonically. Based on this conclusion, a "global peak tracking subroutine" was proposed, which is called periodically in the main MPP tracking program. The subroutine searches the neighboring peaks of the current peak every 25 seconds, and if the power at one of the neighboring peaks is more than the current peak, the tracking algorithm will continue to search for the next peak in that direction until it comes to a peak that generates less power than the last one. It is claimed that the global MPP can be found without scanning the entire P (V) curve.

There are two drawbacks of this method. First of all, the conclusion obtained from the observations is not always true and this will be discussed in detail in section 4.1. Secondly, the search subroutine runs every 25 seconds even under uniform irradiance conditions, in which case, it has to scan the entire P (V) curve because there are no other local peaks.

In conclusion, because of the complexity of the PV electrical characteristics under partial shading conditions, a full range scan is necessary to find the global maximum power point. To reduce the number of unnecessary scans, judgment is required to detect partial shading conditions.

1.4 Existing Experimental Set Up

In the Power Electronics Laboratory of the Electrical Power and Power Electronics Group, an experimental set-up of a PV system with two DC-DC converters and a single DC-AC inverter exists, built by John Gow in 1999 [38]. The block diagram of the system is shown in Fig 1-11.

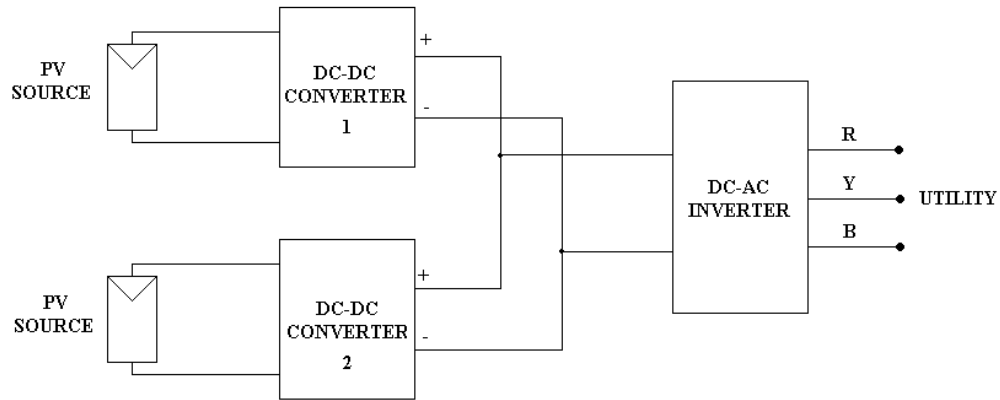


Fig 1-11. Block diagram of the existing PV system experimental set-up

The output of the PV source is emulated by a DC voltage source V_S in series with a resistance R_S as shown in Fig 1-12. This forms a typical Thevenin source that feeds the converter, which has an equivalent resistance of R_{load} . R_S consists of two equal sections of 0.95Ω . To simulate a sudden environmental change, a switch across one section can be opened or closed.

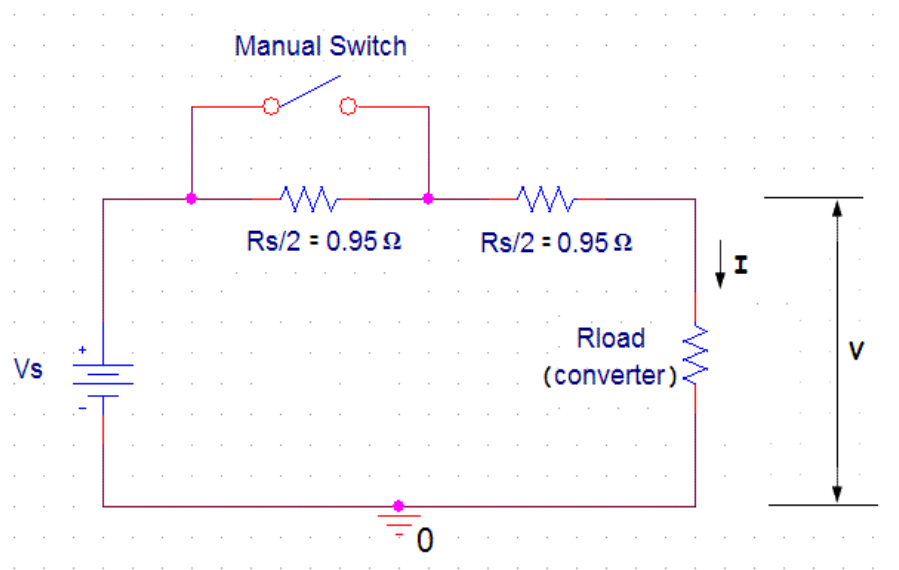


Fig 1-12. Emulated PV source

The grid-side inverter is an Alspa GD4000, which has the job of maintaining the DC link voltage at 650V nominal (adjustable between 600V and 750V) by absorbing the power from the DC/DC converter(s) and delivering it to the 3-phase grid. It is capable of controlling the power flow from the DC link as well as monitoring the grid to detect islanding operation.

In this configuration, each PV panel (or module or sub-array), which is operated at low voltage for safety reasons, is connected to an independent DC/DC converter with MPP tracker. The converters are parallel connected and feed the common DC link, so that shaded PV panels can continue to provide power at reduced levels under partial shading conditions. The requirements for these DC/DC converters are therefore: a) continuous input current, b) high boost ratio, c) galvanic isolation. A current-fed full bridge Boost converter with HF transformer satisfies all the above requirements. Moreover, this type of converter already provides a boost ratio of around 2, thus helping to reduce the turns ratio requirement for the transformer design. Therefore, a current-fed full bridge Boost converter with galvanic isolation shown in Fig 1-13 was selected as the DC-DC converter. The switches are SKM120B02 MOSFETs. The step up ratio for the transformer is chosen as $N1:N2=1:8.55$. Because the inverter will maintain a constant DC link voltage, the primary voltage of the transformer TX1 will also be kept constant, in accordance with the step down ratio. For example, if the output voltage is set to the nominal value 650V, the primary peak voltage of TX1 will be $650/8.55=76V$.

In the original set-up the MOSFETs are controlled by a Digital Signal Processor (DSP) based controller, which includes three subsystems: the control logic subsystem, the DSP subsystem and the analog/digital interface subsystem. The control logic subsystem for

bus decoding, timing and PWM generation is implemented through a Xilinx XC4003 Field Programmable Gate Array (FPGA). The DSP subsystem using a TMS320C50 provides the MPPT calculations and all the intelligent controls. The analog/digital interface subsystem contains three channels of ADC for sampling input and output voltages and current, and one channel of DAC to pass power feedforward information to the inverter. The MPPT algorithm used in the DC-DC converter is based on the intrinsic ripple of the input voltage and current as proposed and implemented by John Gow [18]. This algorithm is described in detail in Chapter 2.

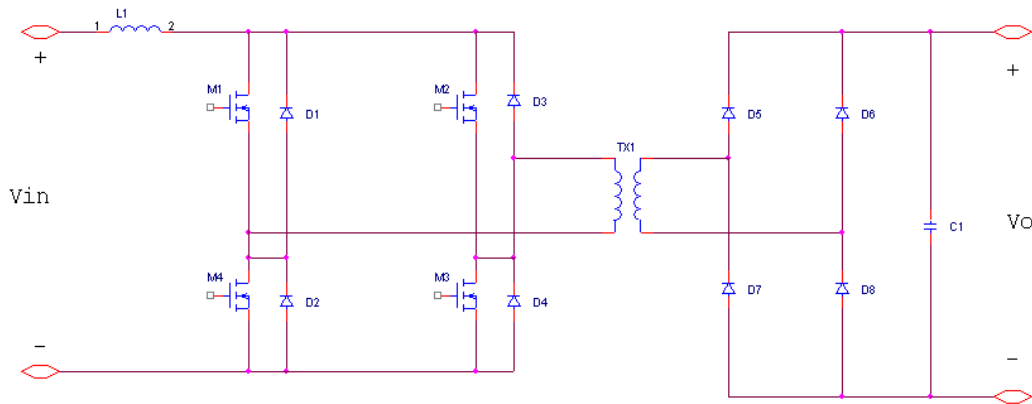


Fig 1-13. Current-fed Boost converter

1.5 Objective of Research and Structure of Thesis

The objective of this research is to design an intelligent controller for PV converters, to ensure fast, efficient and reliable tracking of maximum power point under all conditions. It can be divided into the following parts:

- 1) To investigate existing MPPT algorithms comparing their advantages and disadvantages.

- 2) To study the factors influencing the performance of MPPT algorithms and the consequent problems, especially PV dynamics due to PV capacitance and partially shaded operation.
- 3) To propose an intelligent algorithm that is capable of dealing with the above problems.
- 4) To experimentally realize the proposed controller and to test it.
- 5) To build a test facility that provides real and flexible control of test conditions.

The structure of the thesis is summarized below.

In chapter 2, the characteristics of PV sources are described and studied. Models of PV sources for generic use as well as for certain research use are established in Matlab. Using these models, existing MPPT algorithms are then modelled and studied in Matlab. The modelling described in this chapter provides the tools needed for the subsequent research.

In chapter 3, the PV dynamics due to the capacitance of PV cells and the resulting effect on MPPT algorithms are studied. The problem is addressed and suggestions to reduce or eliminate the effect are proposed.

Chapter 4 focuses on the partial shading problem. Through intensive study of PV characteristics, a novel method to identify the occurrence of partial shading and consequently to initiate a global scan for the true MPP has is presented.

In chapter 5, the design and construction of a solar emulator is described. This emulator will facilitate experimentation, providing flexible control and adjustment of the irradiance levels.

An experiment set-up with the improved MPPT controller using a faster and more powerful DSP is realized and described in chapter 6, complete with test results.

Finally, conclusions on this study and suggestions for future work are given in chapter 7.

Chapter 2. Basic Comparative Study of MPPT Algorithms

2.1 Introduction

Novelty and improvements are most likely based on profound knowledge of existing techniques. The intelligent MPPT control method presented in the thesis is also based on intensive investigation and comparative study of existing MPPT algorithms which will be described in details in this chapter.

There are several main categories of MPPT methods. The first most common one is constant voltage or current reference methods. It is very simple and quick, but can't extract maximum power due to environmental changes and is low efficient (90%) [39].

The second category is Perturbation and Observation (P&O) methods. P&O methods work well when the irradiance does not vary quickly with time. But they have drawbacks of slow tracking speed and oscillations around MPPs [41] [43]. When the environmental conditions change rapidly, e.g., when the irradiance increases rapidly, the operating point may drift away from the proper MPP [41]. This is because the algorithm is not able to distinguish between changes caused by the perturbation and by the environment.

The third one is the Incremental Conductance method (InCon) [41]. It involves determination of the incremental conductance which should be equal to the conductance of the PV source at the MPP. It is reported to be faster and have better performance than the P&O methods, especially under rapidly changing environmental conditions.

The fourth one utilized the Intrinsic Ripple (InRp) of the input current and voltage of DC/DC converters connected to PV sources as the perturbation [18]. By sampling twice within one cycle and comparing the power, the algorithm then determines the direction for the next step. It is a faster version of P&O methods but more prone to noise and more complex to implement.

There are also other MPPT methods. However, the P&O and InCon are two most commonly used categories, therefore, are the main objects under investigation. The InRp method is believed to be novel and was used in the existing experimental set up, therefore, it is also investigated. These three MPPT methods are modelled, simulated and compared with the aid of the simulation software MATLAB Simulink.

The modelling of PV sources is an important part of the whole MPPT model. Reliable PV models are needed for studying the operation of various MPPT methods. Furthermore, they are also needed in order to understand the characteristics of PV sources under special conditions such as partial shading conditions and PV dynamics and consequently to intelligently dealing with these conditions.

Therefore, the modelling of PV sources with different complexity will firstly be described in this chapter. Then will the simulation of MPPT algorithms.

2.2.1 Modelling of steady-state PV sources

2.2.1.1 PV model with only 1st quadrant characteristics

Fig 2-1 is widely accepted as a simple equivalent circuit for a PV cell [27-29]. The terminal characteristic for the circuit can be expressed as follows.

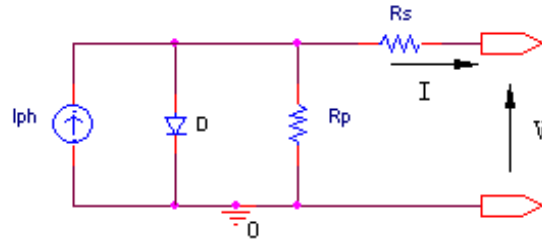


Fig 2-1 Single Diode PV cell model

$$I = I_{ph} - I_S \left(e^{\frac{q(V+IR_S)}{AkT}} - 1 \right) - \frac{V + IR_S}{R_p} \quad (2-1)$$

where the list of parameters have been defined in section 1.2.3.

Usually R_p is very large and R_s is very small, in which case it may be acceptable to ignore their existence. Then Eqn 2-1 can be simplified to

$$I = I_{ph} - I_S \left(e^{\frac{qV}{AkT}} - 1 \right) \quad (2-2)$$

For a large scale PV source (modules, panels, arrays, etc) with N_s PV cells in series and N_p strings in parallel, the terminal current can be expressed as:

$$I = N_p \left[I_{ph} - I_S \left(e^{\frac{qV}{N_s AkT}} - 1 \right) \right] \quad (2-3)$$

Provided that each cell has the same parameters, the terminal voltage can be rewritten from the above equation to:

$$V = \frac{N_s AkT}{q} \cdot \ln \left(\frac{I_{ph} - \frac{I}{N_p}}{I_S} + 1 \right) \quad (2-4)$$

Using this expression, the terminal voltage V can be approximately calculated from the known variables and parameters without iteration. So the simulation speed of this model will be very fast.

From Eqn 2-4, it looks like that V is proportional to the temperature T . However, in fact, other parameters especially the saturation current I_s are also strongly affected by T . So Eqn 2-4 does not fully describe the temperature dependency of V . In the simulation study described in later sections, the temperature change has not been considered and only the change in I_{ph} will be taken into account.

Based on expression 2-4, a simple PV source model can be built in MATLAB as shown in Fig 2-2. The MATLAB function has two input variables. One is the PV source terminal current I and the other is the photocurrent I_{ph} . This function will then calculate the terminal voltage V from Eqn 2-4 and use it as the output. Multiplying V and I yields the PV source output power P . V , I and P are connected to a scope to observe the waveforms simultaneously. The MATLAB function is given in Appendix 1.

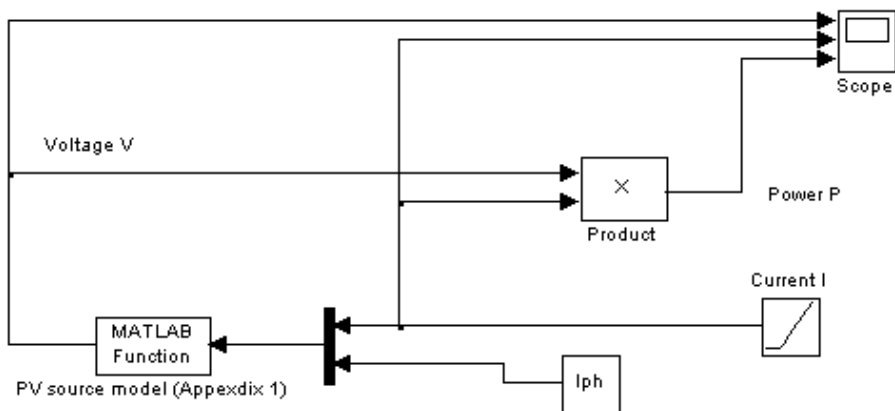


Fig 2-2. PV source model in Matlab Simulink

Fig 2-3 depicts the terminal characteristics for a MSX60 PV panel ($N_p=1$, $N_s=36$, $A=1.83568$, $I_s=5.79804*10^{-6}A$ and $T=298K$. These are the simulation parameters used throughout the thesis for a single PV panel of this model.) at different irradiance levels ($I_{ph}=1A, 2A, 3A$ and $3.87A$) using this model.

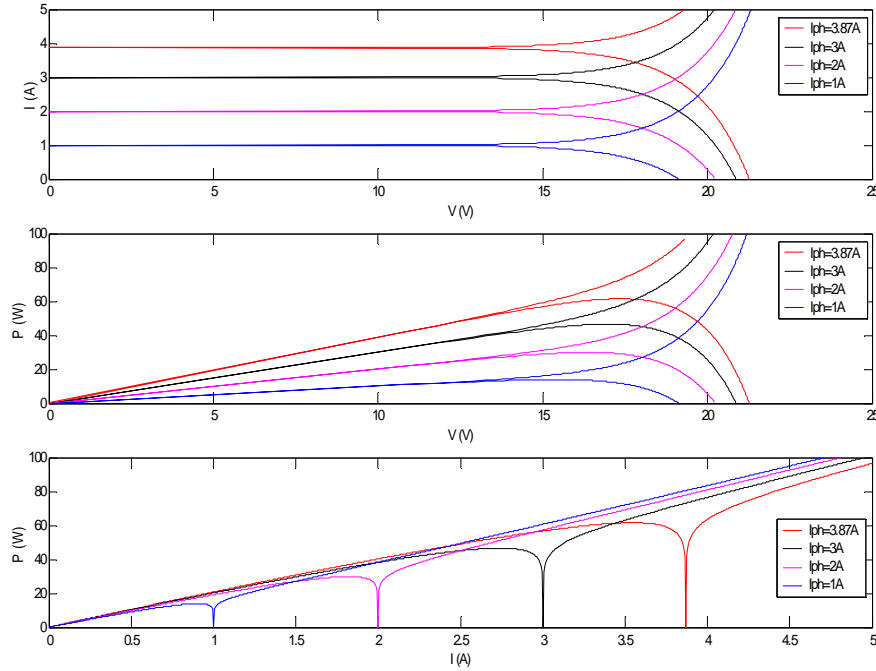


Fig 2-3. MSX60 PV panel terminal characteristics
From top to bottom: I-V, P-V and P-I curves

Bifurcation of the waveforms is noticed in Fig 2-3, which is obviously not true for real PV sources. This is because that when the terminal current I exceeds the short circuit

current, $\frac{I}{N_p}$ is greater than I_{ph} so that $(-\frac{I_{ph} - \frac{I}{N_p}}{I_s} + 1)$ becomes a negative number. In

MATLAB, the natural logarithm $\text{LOG}(X)$ will produce complex results if X is not positive. The observed bifurcations are a consequence of the MATLAB simulation and

the upward curves should be ignored. Alternatively, to correct this, a PV source model including 2nd quadrant characteristics was established as in the next section.

2.2.1.2 PV model including 2nd quadrant characteristics

Expressions including the 2nd quadrant characteristics have been proposed [55]. One of the ways can be expressed as in Eqn (2-5), which can avoid iteration and is easy to model.

$$I = [I_{ph} - I_s (e^{\frac{qV}{AkT}} - 1)] \cdot M(V) \quad (2-5)$$

where M(V) is the multiplication factor according to the following expressions:

$$M(V) = 1 \quad \text{if } V > 0;$$

$$M(V) = \frac{1}{1 - \left(\frac{V}{V_{br}}\right)^a} \quad \text{if } V < 0; \text{ (where, } a \text{ is the breakdown exponent)}$$

$$M(V) = \infty \quad \text{if } V = V_{br} \text{ (where, } V_{br} \text{ is the breakdown voltage)}$$

The MATLAB Simulink model is shown in Fig 2-4 and MATLAB function is in Appendix 2. Fig 2-5 is the simulated waveforms of the same PV panel model as in previous section including 2nd quadrant characteristics. It can be observed that operation in the 2nd quadrant can lead to very high power dissipation in the PV panel and must therefore be avoided. Bypass diodes are practically used to prevent overheating PV sources.

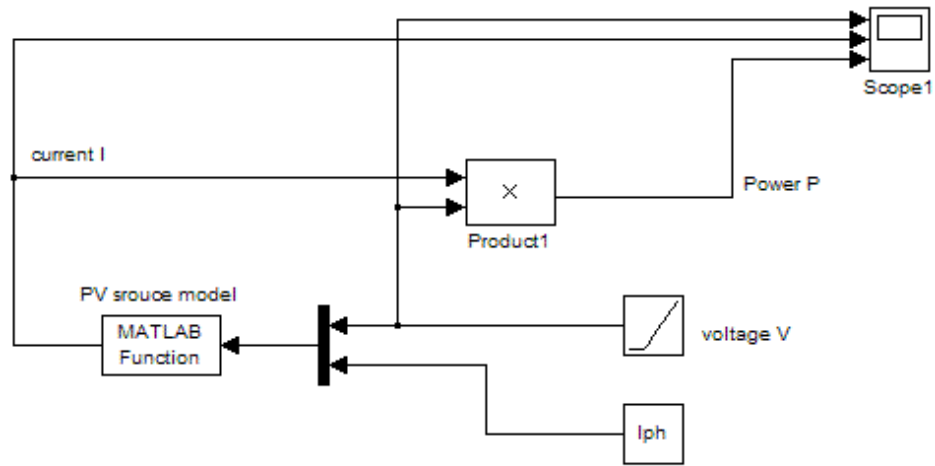


Fig 2-4. PV model including 2nd quadrant characteristics

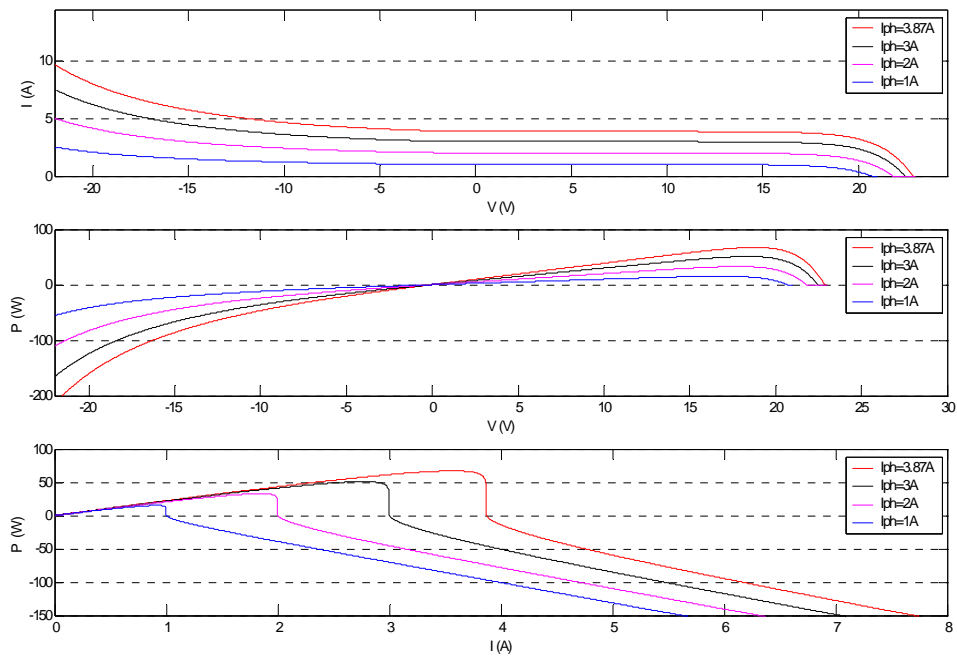


Fig 2-5. MSX60 PV panel terminal characteristics including 2nd quadrant considered

From top to bottom: I-V, P-V and P-I curves

2.2.1.3 PV model with bypass diodes

In practical applications, there will be great power loss when part of a PV string was shaded and may cause the hot spot problem. A bypass diode is connected in parallel to each string to deal with the problem. For an ideal bypass diode, the voltage across the shaded PV string will be 0. Therefore, the PV model could be modified as in Appendix 3. The ‘else’ condition performs as the bypass diode. The Simulink model is the same as in Fig 2-2. And the simulated characteristics were plotted in Fig 2-6.

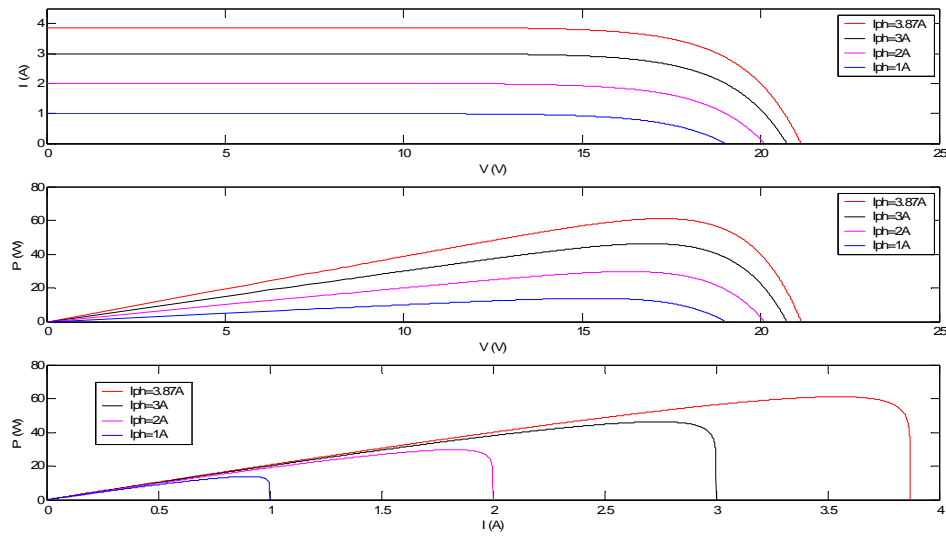


Fig 2-6. MSX60 PV panel terminal characteristics with bypass diodes

From top to bottom: I-V, P-V and P-I curves

This is a simple PV source model for practical use and will be used later for assessing the performance of MPPT algorithms.

2.2.1.4 Complete steady-state PV model

The above simple PV source model (will be referred to as the Basic PV Model) works alright for purposes such as understanding the principle of various MPPT algorithms.

However, in the real world, PV cells also exhibit internal resistance (series resistance R_s and parallel resistance R_p). The resistance has an effect on the open circuit voltage V_{OC} , the short circuit current I_{SC} and the shape of the PV characteristic curve (Fill Factor). This also will affect the PV output power. For purposes of more advanced and accurate research, an improved model including the internal resistances can be obtained as follows.

Let the subscription '0' indicate parameters for a single cell, then for a single cell,

$$I_0 = I_{ph0} - I_{S0} \left(e^{\frac{q(V_0 + I_0 R_{S0})}{AkT}} - 1 \right) - \frac{V_0 + I_0 R_{S0}}{R_{P0}} \quad (2-6)$$

Assuming all cells have identical parameters, for a PV source consisting of N_s cells connected in series and N_p cells in parallel, its terminal characteristic can be expressed as follows,

$$I = I_{ph} - I_S \left(e^{\frac{q(V + IR_S)}{AkT}} - 1 \right) - \frac{V + IR_S}{R_P} \quad (2-7)$$

It can be easily derived that:

$$R_S = \frac{N_S}{N_P} \cdot R_{S0} \quad (2-8)$$

$$R_P = \frac{N_S}{N_P} \cdot R_{P0} \quad (2-9)$$

Therefore, a complete steady-state model for a PV source including internal resistances can be obtained by connecting a resistor of value $(N_S/N_P)R_P$ in parallel to and a resistor of $(N_S/N_P)R_S$ in series with the Basic PV Model as illustrated in Fig 2-7. The complete steady-state model of a PV source with N_P paralleled strings of N_S series connected cells is then described as Eqn 2-10. And the corresponding model implemented in MATLAB is shown in Fig 2-8.

$$I = N_P \left[I_{ph} - I_S \left(e^{\frac{q \left(\frac{V}{N_S} + \frac{I}{N_P} R_S \right)}{AKT}} - 1 \right) - \frac{\frac{V}{N_S} + \frac{I}{N_P} R_S}{R_P} \right] \quad (2-10)$$

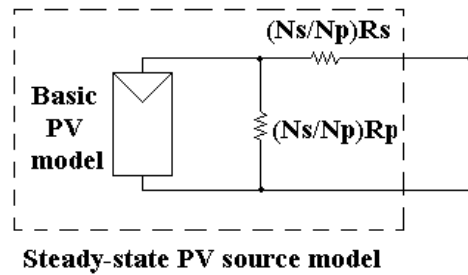


Fig 2-7. Complete steady-state PV model

The characteristics of a PV array of 2 parallel strings of 3 series connected MSX60 PV panels are simulated using the Basic and the Complete steady-state PV source models and are given in Fig 2-9 for comparison.

The list of simulation parameters is given as,

1) Common parameters:

$N_p=2$, $N_s=36*3=108$, $A=1.83568$, $I_s=5.79804*10^{-6}$ A and $T=298$ K.

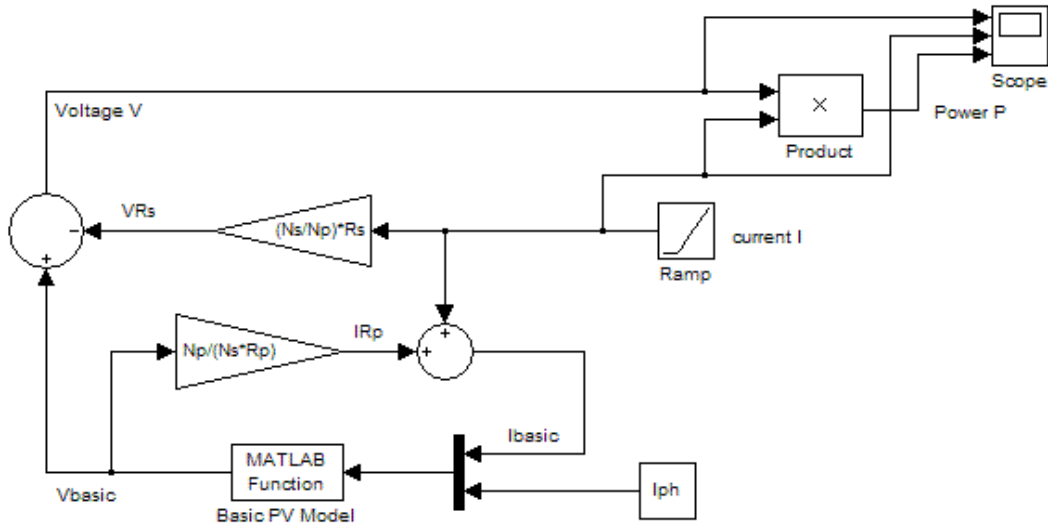


Fig 2-8. Complete steady-state PV model in MATLAB

2) Different parameters:

	Fig 2-9 (a)	Fig 2-9 (b)
R_S (Ω)	0.8	0.008
R_P (Ω)	1k	1M

It can be seen that the complete model has a smaller Fill Factor (FF, which is defined as

$$FF = \frac{I_M \cdot V_M}{I_{SC} \cdot V_{OC}}, \text{ see section 1.2.3). Also the effective output power is reduced in the}$$

Complete PV Model because there is energy consumption in both R_S and R_P .

However, the parameters in Fig 2-9 (b) are more realistic. And it can be observed that the discrepancy in characteristics between the Basic Model and the Complete Model is tiny

hence can be neglected. Therefore, the Basic PV Model instead of the Complete Model will be used in the later work for ease of modeling and faster speed.

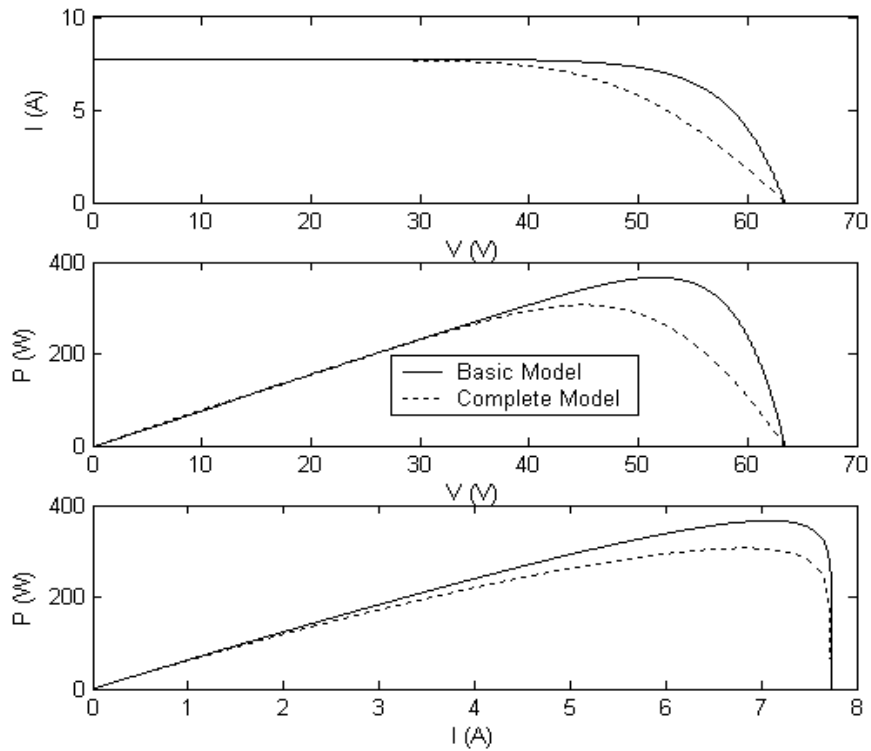


Fig 2-9. Simulated characteristics of PV source models
solid lines- the Basic model **dotted lines -** the Complete model

2.2.2 Modelling of Multiple PV Sources under Non-Uniform Conditions

In practical applications, PV cells are often interconnected to form modules, arrays, etc. In such PV applications, there are possibilities of multiple local maxima instead of just one maximum power point in the PV terminal characteristics. These can result from partial shading due to clouds or buildings, or variations caused in manufacturing or aging process.

According to a recent report, 13 commercial inverters with MPP trackers were tested under partial shading conditions, resulting in three local maxima power points [47]. The tests indicated that none of them was able to find the true MPP, 10 of which operated at a local maxima with 10% power loss and 3 at another point with 71% power loss.

It can be seen that failure to find the true MPP under partial shading conditions can cause substantial power losses. Before trying to come up with any novel solutions, a model to simulate such conditions is needed. This can be realised in MATLAB as shown in Fig 2-10, where the PV source is divided into three modules PV1, PV2 and PV3 each with a bypass diode (the Basic PV Model is used).. Different irradiance levels can be simulated by setting different values of the photocurrents (I_{ph}) for the three modules. The number of modules (i.e. the number of local maxima) can be easily modified according to different purposes of study.

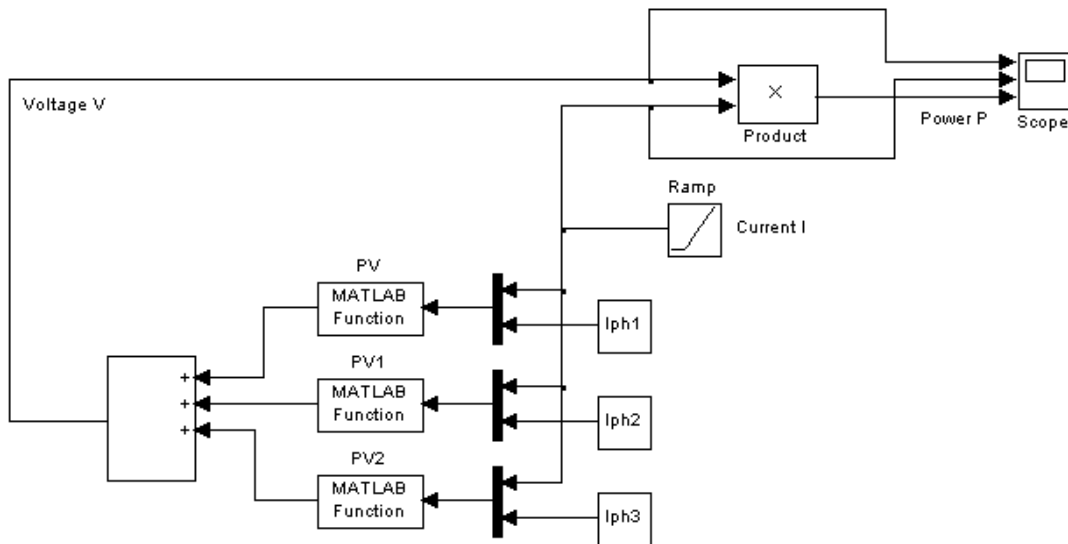


Fig 2-10. Steady-state PV model to simulate partial shading conditions

An example of the simulated characteristics of a partial shading condition with three local maxima is shown in Fig 2-11, in which $I_{ph1} = 1A$, $I_{ph2} = 3A$, $I_{ph3} = 4A$. Normally MPPT algorithms starting from the open circuit will find the local maxima at around 127.6V (302W) rather than the global MPP at about 101.5V (422.8W), causing a reduction of approx. 30% in yield.

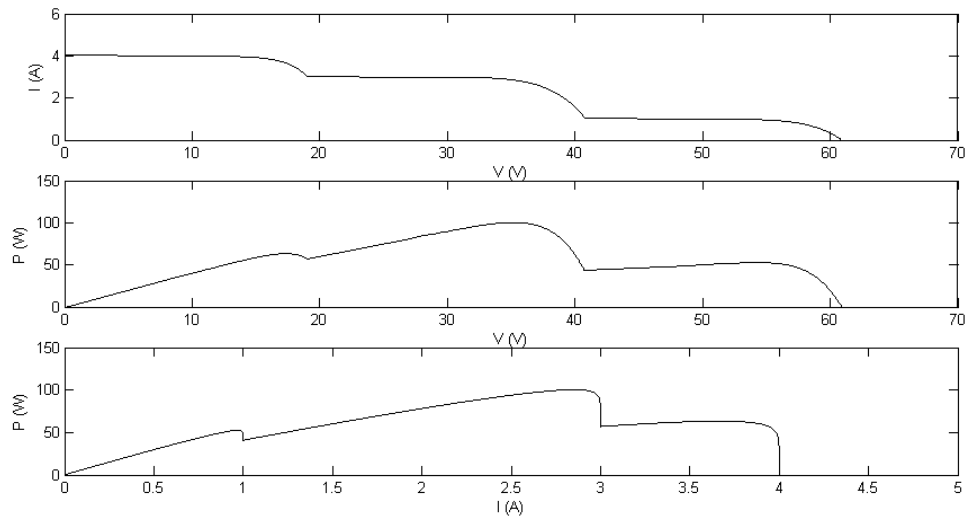


Fig 2-11. Simulated characteristics under partial shading conditions

2.3 Simulation of MPPT Algorithms

Fig 2-12 shows the circuit diagram of the system used for modeling MPPT algorithms. The output of a PV source is fed into a Boost converter. The output of the Boost converter is then connected to a DC link with a constant voltage V_{out} . The switch of the Boost converter is controlled by MPPT controller applied with different MPPT algorithms. This system is modelled using MATLAB Simulink as shown in Fig 2-13. The Basic PV model is used in the “PV Matlab function”. The values of the parameters for the PV model can be found in Section 2.1.1.1.

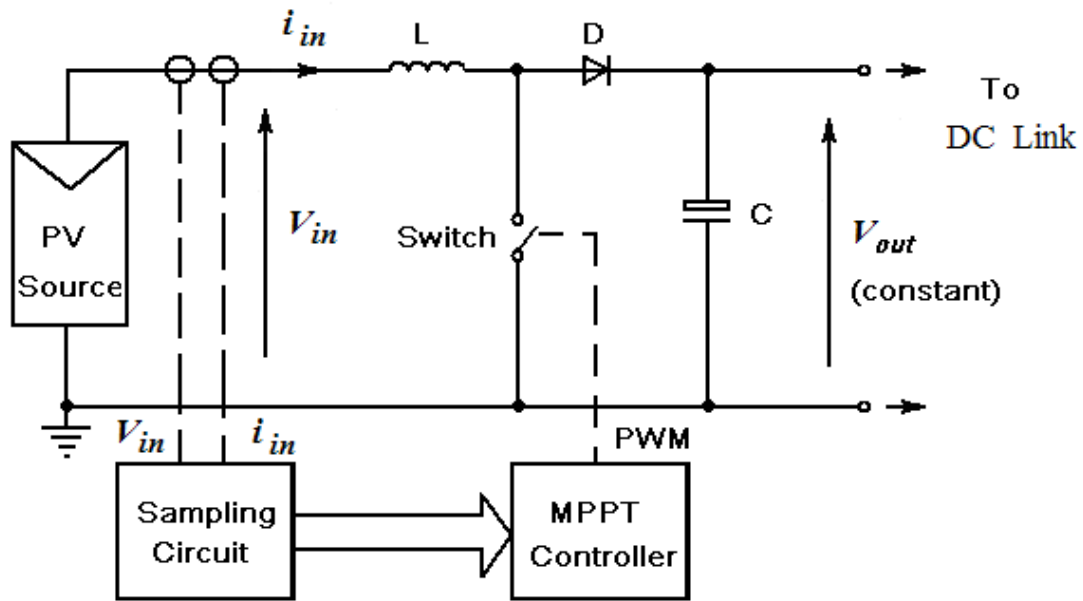


Fig 2-12. Circuit diagram of the PV system

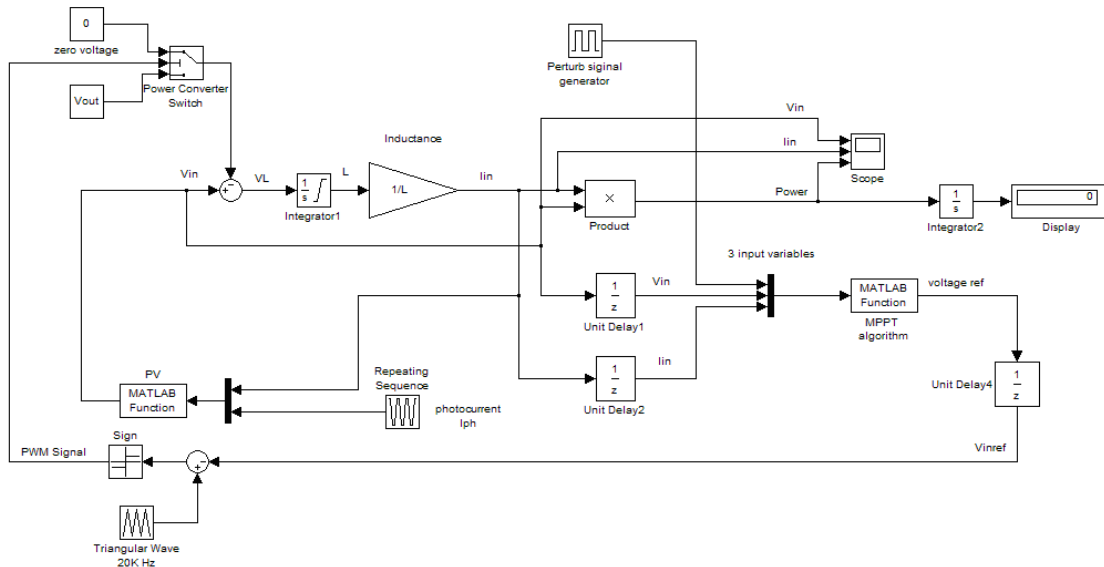


Fig 2-13. PV system Simulink model with MPPT algorithms

To test and compare the implemented models with different MPPT algorithms, a pattern of varied irradiance has been created as shown in Fig 2-14. The irradiance drops

continuously from the initial standard full intensity ($I_{sc}=3.87A@STC$) to half the level and then increases back to full intensity level.

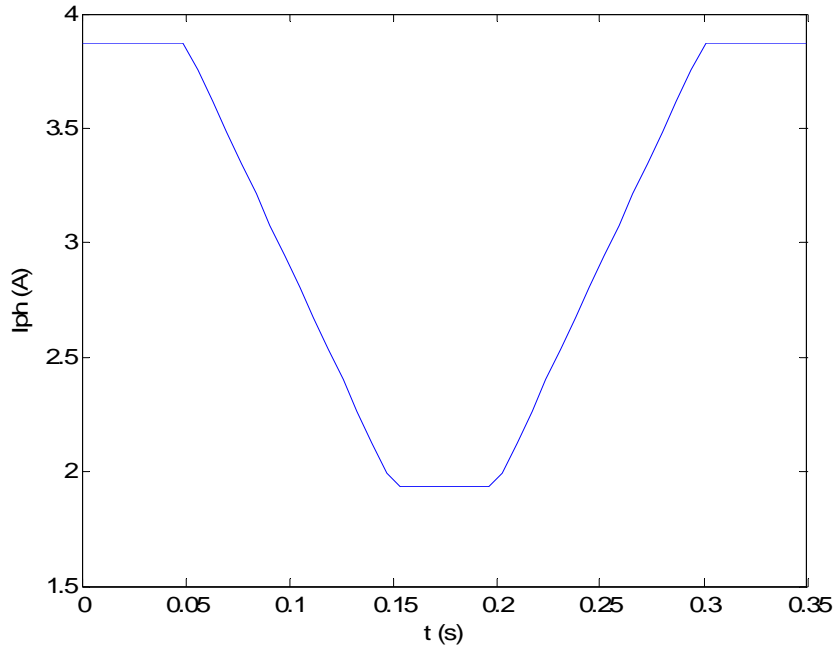


Fig 2-14. The I_{ph} (irradiance) pattern for testing MPPT algorithms

2.3.1 Perturbation & Observation Methods

Perturbation & Observation (P&O) methods are widely used in MPPT. Its principle is to introduce a perturbation to the operation voltage and see whether the power increases or decreases. If the power increases, that means the perturbation is the right direction to get closer to the MPP, so the algorithm will continue in the same direction. Fig 2-15 demonstrates the flow chart [41]. The MPPT algorithm used in Fig 2-13 is “P&O MPPT algorithm” as listed in Appendix 4.

Fig 2-16 shows a simulated transient tracking process of the implemented P&O method. It can be noticed that the voltage ripple is greater when the irradiance level (E)

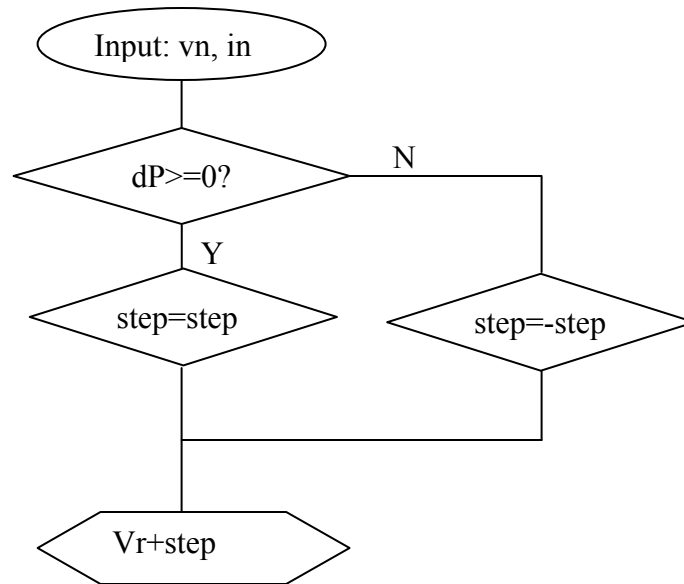


Fig 2-15. Flow chart of P&O MPPT algorithm

continuously increases than when it decreases. This is because then E continuously increases, even a step further away from the MPP may result in an increase in power, therefore, the algorithm will continue to perturb in the same direction. On the contrary, when E continuously decreases, even a correct step closer to MPP may result in a power decrease, so the next perturbation will change its direction. Therefore, it takes more steps in the same direction before the perturbation changes its direction when E continuously increases. When the continuous change is also very fast, the operation point may deviate far away from the maximum power point. This is a major disadvantage of the P&O methods as reported in [41].

2.3.2 Incremental Conductance Methods

The P&O methods have two major disadvantages [41]. In steady-state there is always a small power variation around the MPP due to perturbation, and therefore some power

loss will be incurred. The other disadvantage is that under rapidly changing environment, the operating point may deviate from the proper MPP gradually as already shown in 2.3.1.

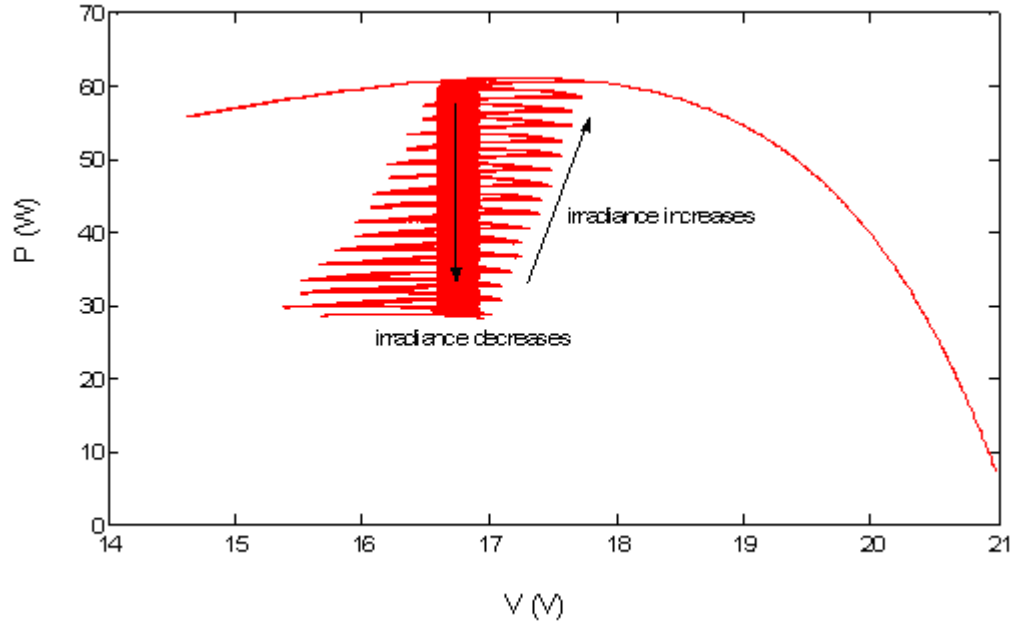


Fig 2-16. The simulated transient tracking of the P&O method

The Incremental Conductance Method (InCon) was proposed [41] to avoid the above problems.

The InCon method is derived from the fact that at MPP,

$$\frac{dP}{dV} = \frac{d(VI)}{dV} = I + V \frac{dI}{dV} = 0 \quad (2-11)$$

By rearranging the above equation, the following condition for the MPP is given by

$$-\frac{I}{V} = \frac{dI}{dV} \quad (2-12)$$

This equation can be physically interpreted as that at MPP the opposite of a PV source's conductance shall be equal to its incremental conductance.

On the basis of the above derivation, the flow chart of the InCon method is as shown in Fig 2-17 and the algorithm was implemented in the same Matlab model circuit as in Fig 2-13, except that function program is replaced by “InCon MPPT algorithm” as listed in Appendix 5.

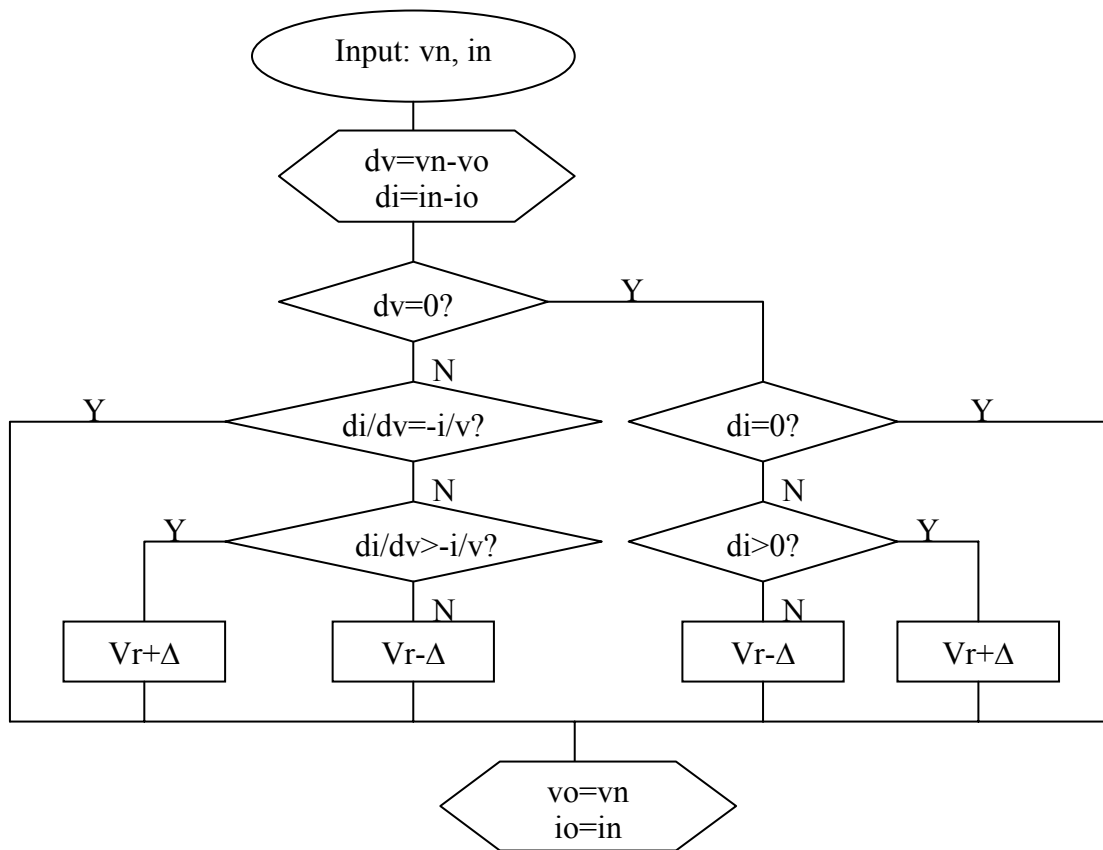


Fig 2-17 Flow chart of the Incremental Conductance MPPT algorithm

The InCon method is simulated with the same pattern of varying irradiance. Fig 2-18 shows the transient tracking process. It can be observed that InCon method may drift away from MPP too, although is slightly better than the P&O methods. As can be seen from the flowchart, the algorithm only enters the right branch, which is to avoid drifting away from MPP under rapidly changing irradiance, when the operating voltage does not change (or at least with very small variation in practice).

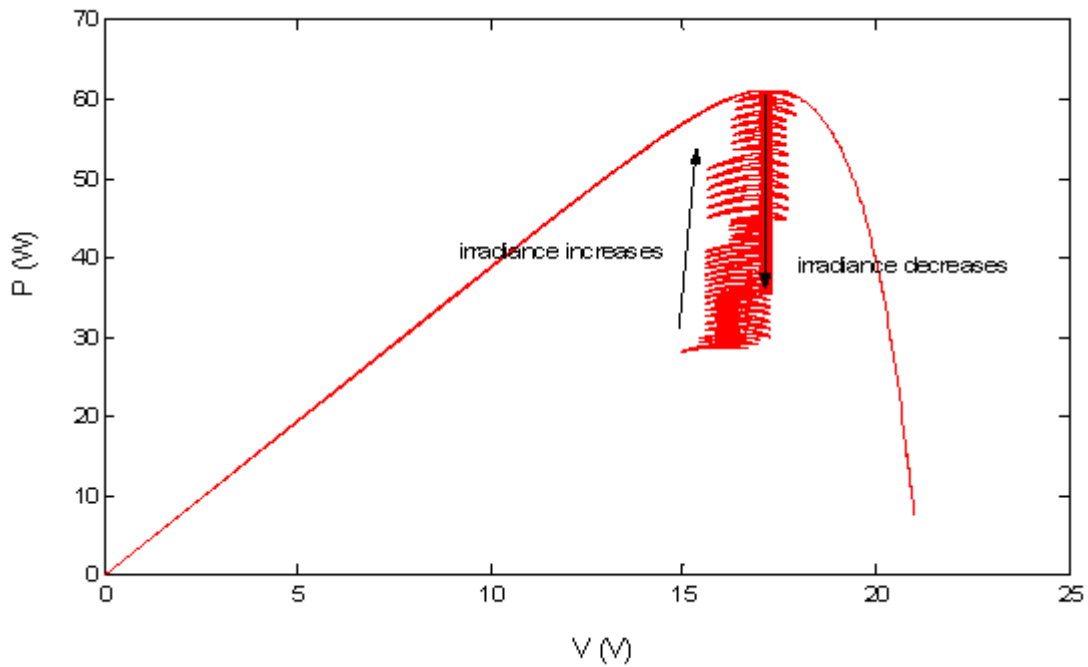


Fig 2-18. The simulated transient tracking of the InCon method

2.3.3 An MPPT Algorithm Based on Intrinsic Ripple

A very fast MPPT algorithm based on intrinsic ripple (InRp) was described in [18]. Due to the existence of the input inductor L_1 of the Boost converter, the input current I_{in} will ramp up and down every switching period. The average value of the current determines the operating point (OP). Fig 2-19 shows a typical PV characteristics curve. During each period, two samples of the input current I_{in} and voltage V_{in} at switching are taken, shown as P1 and P2 in Fig 2-19. The power is calculated by multiplying I_{in} and V_{in} . Around the MPP, the curve is similar to a parabola. Therefore, if the OP is at MPP, P1 and P2 should be at the same power level. If the power level of P2 is greater than P1, the OP is below MPP. And vice versa. By calculating the difference in the power of the two sampled points,

both the sign and the slope of the curve can be obtained. By integrating the tracking error, that is, to solve the following equation, the duty cycle can be calculated.

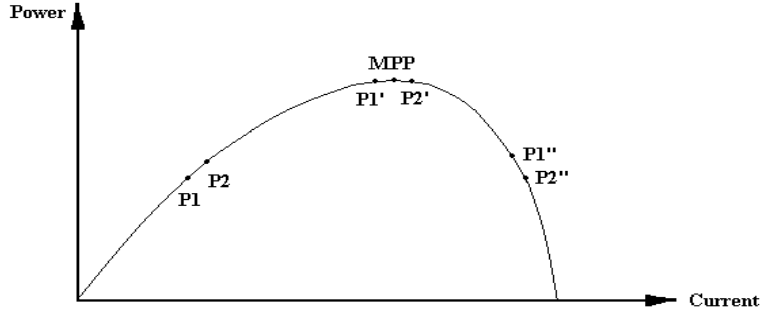


Fig 2-19. PV characteristics curve

$$d = K_e \cdot \int \left(\frac{dP}{dI_{in}} \right) \cdot dt = K_e \cdot \int \left(\frac{P_2 - P_1}{I_2 - I_1} \right) \cdot dt \quad (2-13)$$

The InR_p MPPT algorithm (see Appendix 6) is modelled as shown in Fig 2-20. The difference to Fig 2-13 is that there is no external perturbation signal but utilizing the intrinsic switching ripple as perturbation. The simulated tracking process is plotted in Fig 2-21.

2.4 Comparison of MPPT Algorithms and Conclusions

In this chapter, generic models of PV sources have been established in MATLAB. The PV source can be PV cells, modules or arrays. The model includes series resistance and parallel resistance. The model can also consist of multiple PV sources under different irradiance levels for partial shading study.

Three major MPPT methods have also been modelled and simulated in Matlab with the same irradiance pattern. Firstly it can be found from the simulated results that P&O is most prone to drifting away from MPP under rapidly and continuously changing environment. InCon methods perform better at this aspect but still may deviate from the MPP.

Secondly, the power extracted from the PV panel over the irradiance varying period of 350ms has been integrated and averaged, as shown in Table 2-1.

Table 2-1. Simulated power yield of P&O, InCon and InRp MPPT methods

	Step size (P&O/InCon) or K_e (InRp)	Total Energy (J)	P_{av} (W)
P&O	0.1V	16.33	46.66
InCon	0.5V	16.34	46.69
InRp	1	16.52	47.20

From the above simulated results, InRp MPPT method has the highest tracking efficiency (see 1.3) while P&O and InCon methods have similar tracking efficiencies that are slightly lower than the InRp method.

There are a few drawbacks of the InCon and InRp methods. First of all, they require calculation of derivatives and divisions, which increases the complexity and cost of the controller. Secondly, the InRp method requires two sampling points within one period, which makes it more prone to noise caused by the converter, the inverter and the

environment; therefore, demand extra complexity of sampling, filtering and noise reduction (EMC), etc.

On the other hand, P&O methods are easy and low-cost to implement and are found to have comparable tracking efficiency (see Table 2-1). This conclusion is also verified by both simulation and experiment results presented in [39]. It was indicated that the P&O methods with optimized parameters have a high overall MPP tracking efficiency (99.3%) which is very close to that of the InCon method. Therefore, the P&O MPPT methods are selected in developing the intelligent control algorithm proposed in this work.

Chapter 3. Effect of PV Dynamics on MPPT Algorithms

3.1 Introduction

PV cells exhibit capacitance. The existence and effect of the capacitance in PV cells have been noticed and investigated for different purposes and under different conditions, mainly for studying loss mechanisms or flash characterization of PV cells [56-60]. In the latter case the PV dynamics will cause a shift in the characteristic curves. However, it has so far not been reported that the presence of this capacitance may cause MPP tracking algorithms to deviate from the true MPP. To study this effect, some knowledge on PV capacitance has been obtained and a dynamic PV model has been established in MATLAB, which will be discussed in detail below.

Depending on the operating conditions, the capacitance of PV cells may vary. Higher capacitance is found to be at voltages around and greater than the MPP. This is mainly due to the diffusion capacitance which is related to the lifetime of the minority carriers. This capacitance depends exponentially on the bias voltage [59] as described in Eqn 3-1.

$$C_{diff} = \frac{q}{kT} \cdot \tau \cdot I_S \cdot e^{\frac{qV}{kT}} = C_0 \cdot e^{(b \frac{qV}{kT})} \quad (3-1)$$

where,

C_{diff} – diffusion capacitance

– minority carrier lifetime

C_0 – base capacitance

b – fitted parameter

3.2 Modelling of PV Dynamics due to Capacitance of PV Cells

3.2.1 Experimental Test

Experiments have been carried out under illuminated conditions to show the existence and the effect of cell capacitance and to establish its size range. The tests were conducted using a BP Solarex MSX60 PV panel, consisting of 36 polycrystalline series connected PV cells, under a constant irradiance of about $400\text{W}/\text{m}^2$. A variable resistor acted as a load.

MPP tracking is in fact a process of adjusting the equivalent resistance of the converter (i.e. load) to match the internal resistance of the PV source at MPP. Therefore by applying step changes in the load resistance of the PV panel, the MPPT process can be emulated. Fig 3-1 shows the resulting waveforms for step changes of the load from 5Ω to 6Ω . Overshoots and undershoots can be observed, which clearly indicates the presence of capacitance. In principle it is possible to find the value of the prevailing cell capacitance from these waveforms.

However, a simpler way to work out the size of the capacitance is using a good quality component analyzer. The values of the capacitance of the panel were measured using the Wayne Kerr Precision component analyzer 6440A at different operating points on a certain characteristic curve (i.e. irradiance was constant). The characteristic and the corresponding trend line as shown in Fig 3-2 are drawn from the measured data. It can be seen that the capacitance measured by the component analyzer changes exponentially

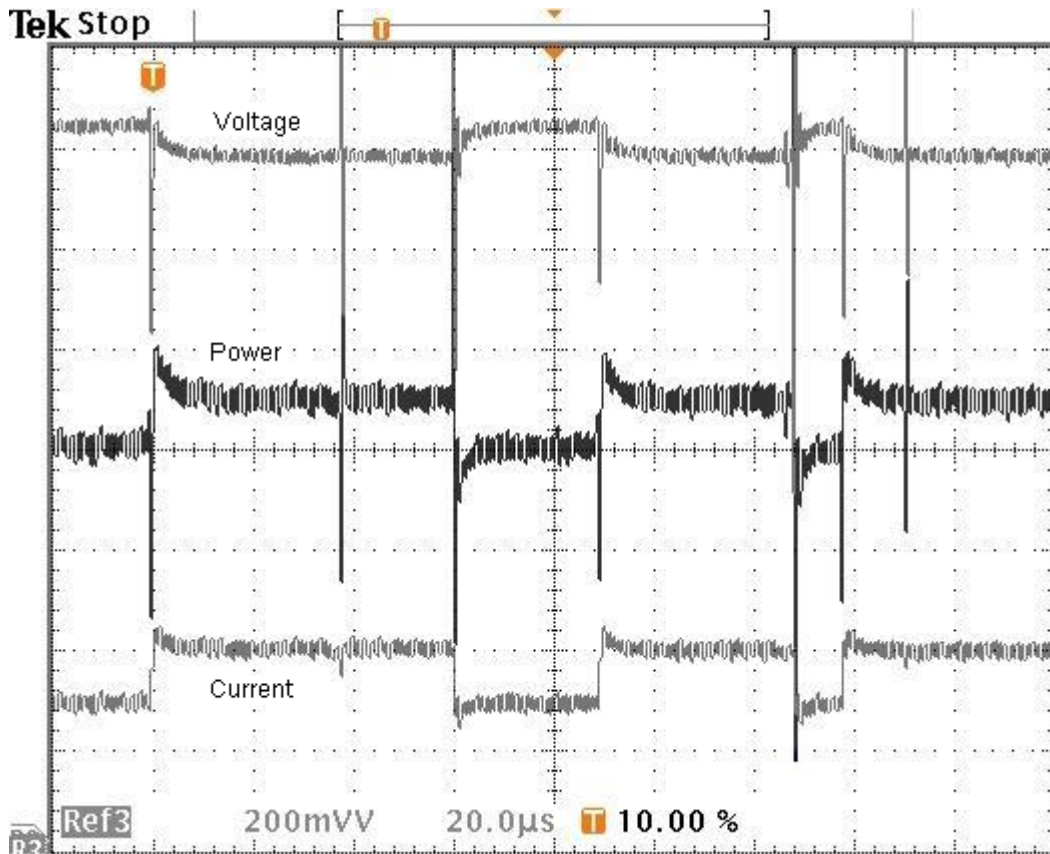


Fig 3-1. Experiment waveforms of the PV output voltage, current and power for step changes between two values of load resistance around MPP

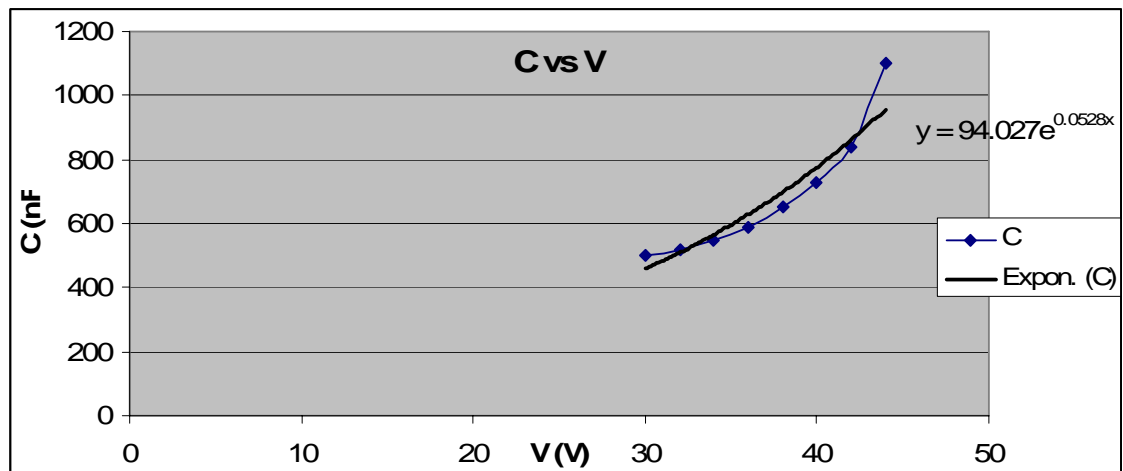


Fig 3-2. Experiment result of the dependence of the PV capacitance on the voltage

with the voltage, which agrees well with the theory. It was also measured that the capacitance for this panel around the MPP is in the range of several hundred nF. Subsequently the MATLAB modelling of the dynamics for this PV panel uses the value of 500 nF.

3.2.2 MATLAB Modelling

The capacitance can be modelled as a capacitor in parallel with the steady-state PV source model as described in 2.2.1. The equivalent circuit is then as shown in Fig 3-3. The value of the capacitor can be expressed as a function, a lookup table or a constant for ease of simulation.

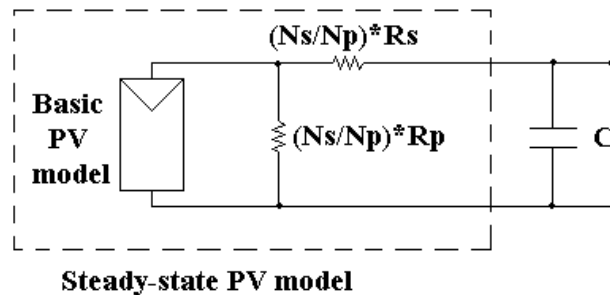


Fig 3-3. Equivalent circuit of a PV source including the capacitance

The equivalent circuit of a PV source including the dynamics due to its capacitance C can then be modelled in Matlab as shown in Fig 3-4.

Using the data from the experiment, simulations are run in MATLAB/Simulink with the same step changes in the load resistance connected to the output of the model. The resulting waveforms for step changes around MPP are shown in Fig 3-5. It can be seen that the simulated waveforms are very similar to those obtained from the experiment (Fig

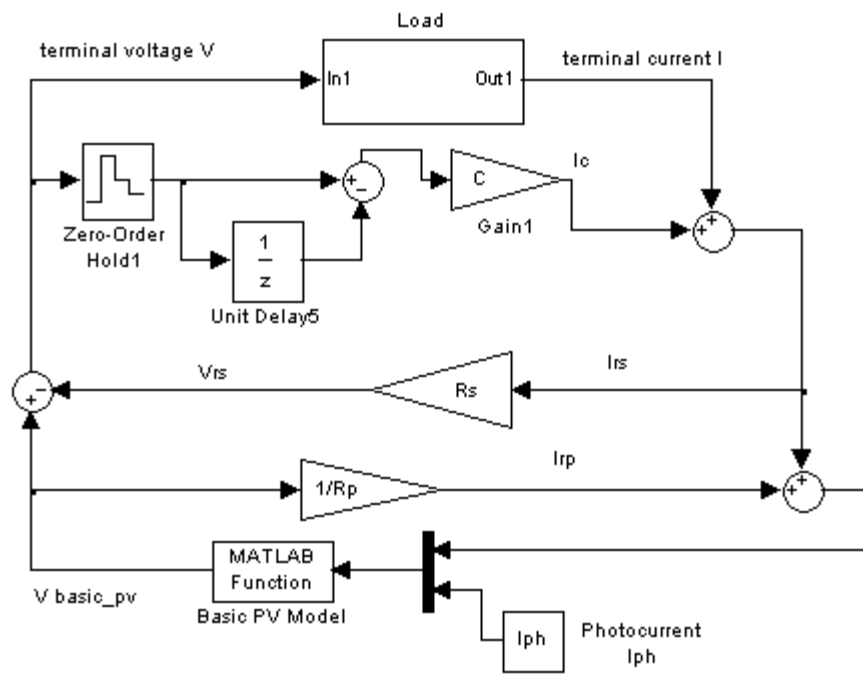


Fig 3-4. Dynamic PV model in MATLAB

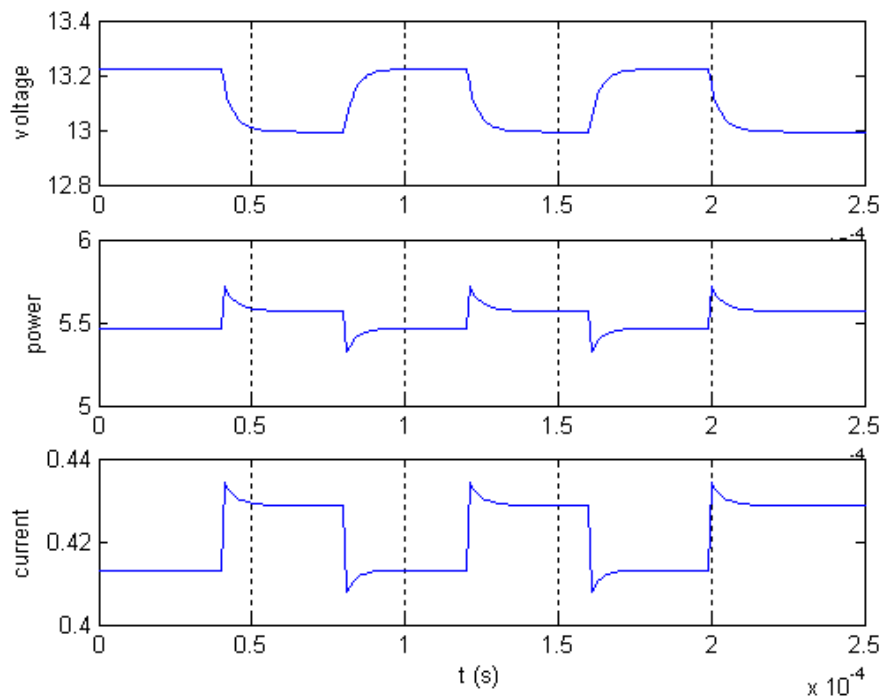


Fig 3-5. Simulated waveforms of the PV output with step changes

3-1). This validates the PV source model for studying PV dynamics, which will further be used to simulate the effect of PV dynamics on MPPT algorithms.

Various complicated methods to measure the PV capacitance have been proposed, such as the small signal method. However, the results in this section have shown that a good quality component analyzer can do the job equally well, which is fast and convenient.

3.3 Effects of PV Dynamics on Operation of MPPT Algorithms

Depending on the step size of the change of the load and the operating frequency, the overshoot duration time differs and can be in the range from tens to hundreds of microseconds.

For example, for a typical BP Solar SMX60 PV panel, the voltage at the MPP is 17.1V, and the current at the MPP is 3.5A. The equivalent resistance at the MPP can then be worked out as approx. 5Ω. The capacitance of panel has been established as around 500nF around the MPP. Therefore, the time constant is

$$\tau = R \cdot C = 5 \times 500n = 2.5\mu s$$

The PV capacitance increases with additional parallel connected PV cells/panels, hence the time constant will be even larger.

For the DC-DC converter used in the work, the switching frequency is 20 kHz, which is a normal switching speed. The switching period is 50 μs. For faster switching converters, the period is even shorter.

Therefore, the time constant can be large enough to have effects on the accuracy and stability of fast MPPT algorithms.

The change in the stored energy in the capacitance causes the dynamic characteristic of a PV source to deviate from the steady-state curve. When the MPPT algorithm decides to decrease the bias voltage, the capacitor discharges and the dynamic curve (power v.s. voltage) is actually above the steady-state one. In contrast, increasing the bias voltage will result in dynamic operation below the steady-state curve.

As illustrated in Fig 3-6, when bias voltage decreases, the capacitance is discharged so that there is a short dynamic increase in the power after which the system settles on the steady-state curve. Similarly, when the bias voltage increases, the dynamic power is temporarily below the steady-state level.

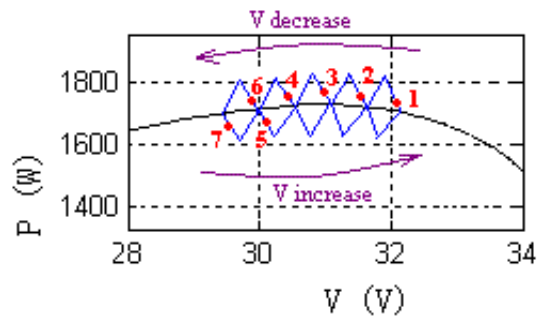


Fig 3-6. The effect of the PV dynamics

For the P & O method, assume that the current sampling point is point 1 and a decision is made to decrease the reference voltage. The next sampling point is point 2. An increase in power is detected and thus the operation point is moved further left and is sampled again at point 3 and 4. A power decrease is then detected and thus the algorithm decides to change the direction of perturbation and it samples again at point 5. Now a power

decrease is detected and the direction of perturbation is again reversed. In this way, the operating point will keep moving left as in most cases a power decrease is detected when trying to move back to the right. If the PV capacitance was independent of the bias voltage, then the OP would drift away from the MPP and end up at the short circuit point ($V=0$). But since the capacitance decreases with the bias voltage this process is finally halted and the cycle is repeated in the opposite direction. However, the incorrect decision around the MPP certainly will cause a loss in power thus lowering the total efficiency the system.

In practical applications, switch-mode circuits are generally used to convert the PV power as well as to track the MPP. In that case, converter dynamics also exist within each switching period due to the PV capacitance.

Using the Matlab model, this effect can be demonstrated as follows. The black curve in Fig 3-7 shows the steady-state P-I characteristic of the PV source.

The red and blue curves are dynamic waveforms with same current ripple but at different operating points. Points A/A' and B/B' are the switching points. From A to B, the current ramps up along the upper curve with the higher power level; from B to A the current ramps down along the lower curve with a lower power level. And as shown in the lower figure, red OP has a higher average power (closer to the MPP).

For the P & O method, if the sampling is around the point where the current starts to ramp up (A/A'), a higher power is detected at the higher current level (blue). Thus the MPPT algorithm will continue operation at this current level, which has actually a lower

average power level. In contrast, if sampling is performed at B/B' the correct current level is found.

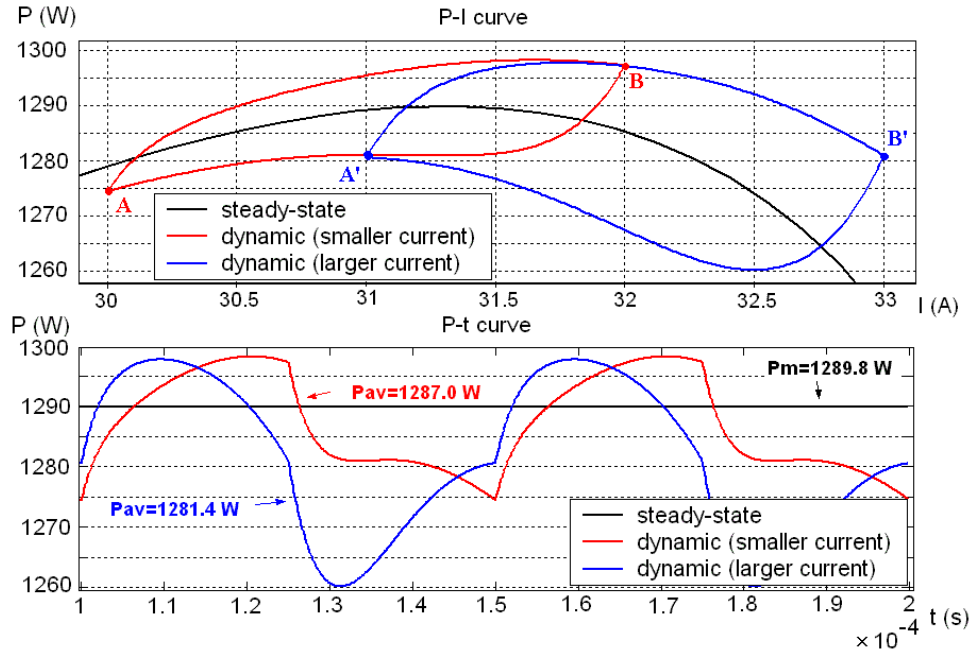


Fig 3-7. Dynamics at different Operation Points

The InR_p method seeks an OP with the smallest difference in power between the two switching points within one cycle. Thus the algorithm will choose the OP with higher current level (blue), which is again not the right decision.

It can therefore be seen that the combination of dynamic effects and sampling instance can lead to incorrect operation of MPPT algorithms. Operating at a point away from the true MPP will lead to a loss in generated power.

3.4 Conclusions

The effect of PV dynamics due to the capacitance of PV cells on MPPT algorithms has been brought to attention in this work. It has been shown that the energy stored in the

capacitance of PV cells may confuse MPPT algorithms if fast sampling and tracking are used. With certain MPPT algorithms, the PV system will underestimate the power it can extract (hence a loss in power) and may even move its operation point away from the true MPP. This effect will be enhanced where PV modules/panels are paralleled on a large scale to reduce the influence of partial shading. A similar effect can occur in voltage-sourced inverters when a large capacitor is placed at the input of the inverter to eliminate voltage ripples from the AC side. It has also been shown that the sampling timing within a converter cycle can affect the correct operation of MPPT algorithms.

In conclusion, dynamic effects due to the capacitance of PV cells and inverters should be taken into account when designing fast tracking MPPT algorithms. The timing of sampling is also important. It is therefore suggested that sampling and tracking speed shall not be so high that MPP tracking is affected by the time constant associated with the PV capacitance. And it is also suggested that data be sampled at the end of each switching to allow the dynamic effect to settle and that averaging or filtering shall be adopted in the sampling.

A further investigation should be carried out to find a way to identify and compensate for the PV capacitance if very fast tracking is required.

Also it has been established by simulation and experiments that a good quality component analyzer can be used for measuring the PV capacitance under illumination.

Chapter 4. Novel MPPT Method to Identify Partial Shading

4.1 Introduction

As mentioned in Chapter 1, when multiple PV panels each with a bypass diode are connected in series, they are liable to exhibit multiple local maxima under partial shading conditions. Partial shading can occur due to clouds or buildings, or variations caused in manufacturing or aging process.

When this happens, there are great chances that MPPT algorithms will fail to find the global MPP, hence cause substantial power loss. According to [47], 13 commercial inverters with MPP trackers were tested under partial shading conditions with three local maxima power points. The test results showed that none of the trackers was able to find the global MPP; 10 of them operated at a local maxima power point with 10% power loss, and 3 at another point with 71% power loss.

Methods to solve this problem have been proposed [48] [50]. However, they are all based on the idea of doing a wider range of scan repeatedly after some fixed period. That period is not based on an identified need and is usually set arbitrarily. Any scan will result in some power loss, and unnecessary scans will therefore actually reduce the PV yield.

In [54], a novel MPPT algorithm was proposed based on the observation that there was only one global maximum power point, on either side of which the power of local maxima monotonically decreases. While this conclusion may be true for most cases, it does not always hold as will be shown here.

For a non-uniformly illuminated PV cell, the equivalent irradiance level is the average result integrated over the area. For example, when one half of a PV cell (with cell area of A) is exposed to an irradiance level of E while the other half is completely shaded, the equivalent irradiance level is

$$\bar{E} = \frac{E \cdot \frac{A}{2} + 0 \cdot \frac{A}{2}}{A} = \frac{E}{2}$$

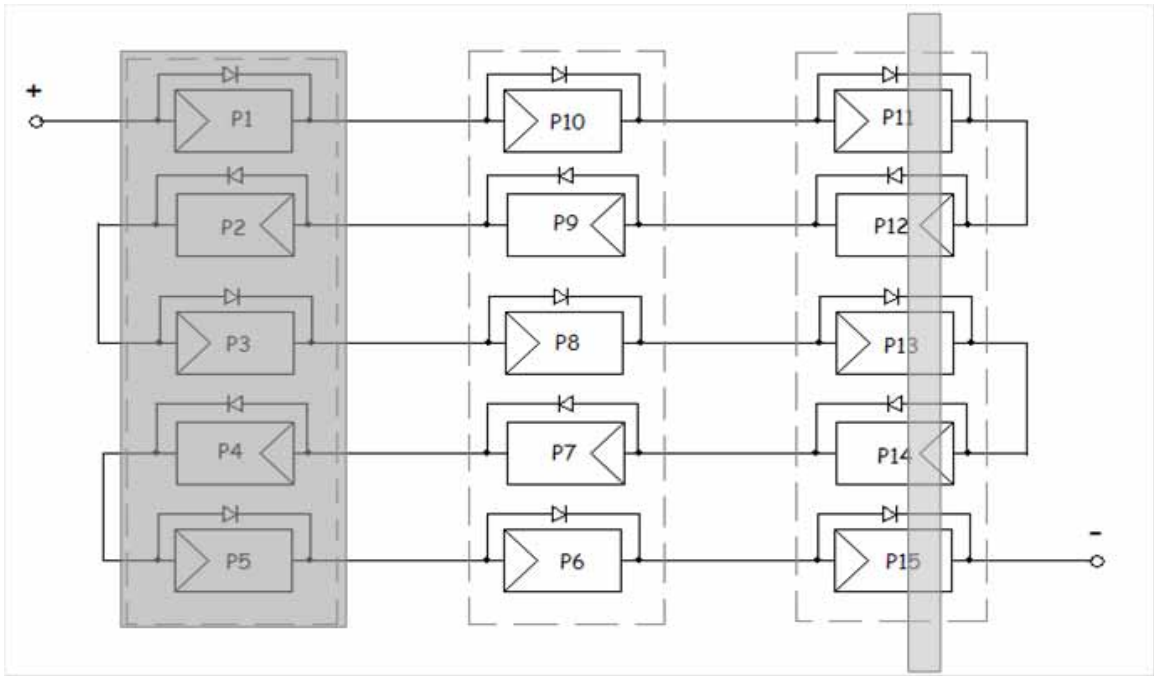
This can be treated as a PV cell with an area of A and an irradiance level of E/2, or as a PV cell with an area of A/2 and an irradiance level of E. In the same way, for N_p PV cells or panels connected in parallel under the same irradiance level, it can be treated as a single PV cell or panel with an equivalent area of N_p times.

Fig 4-1 shows an array of 15 PV panels experiencing two different shading patterns. The 15 panels are all connected in series and they are physically installed as a 3×5 array.

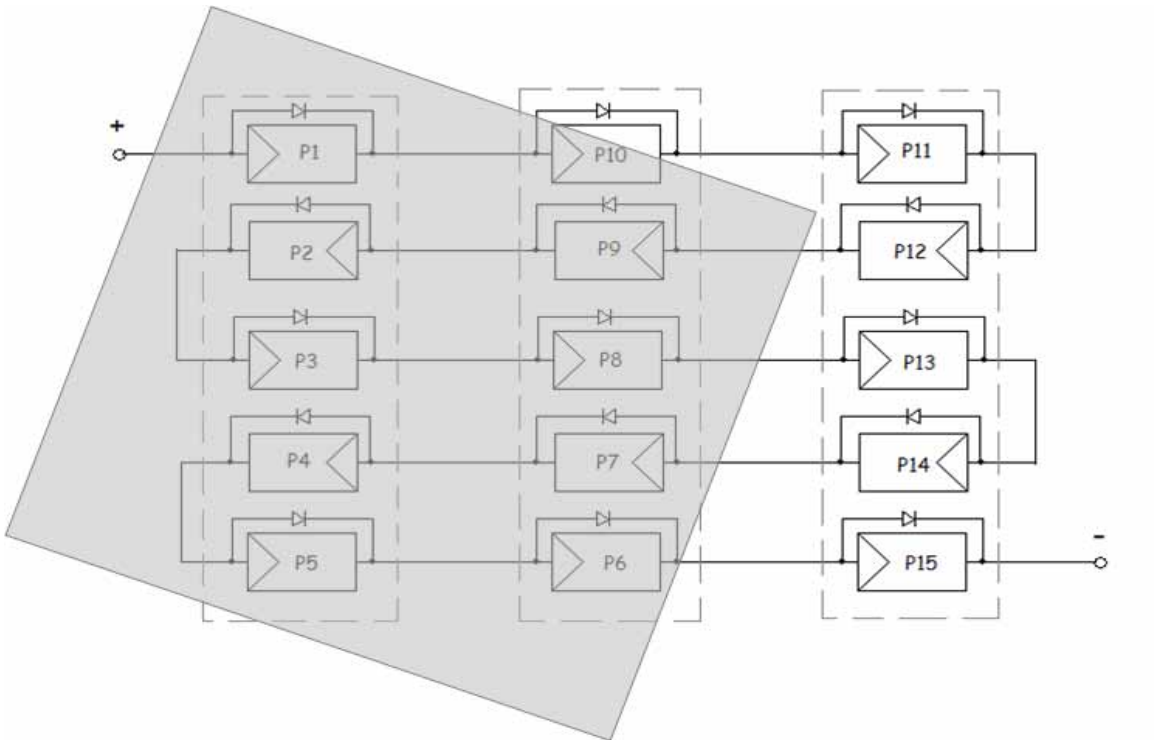
Shading pattern A: The PV panels numbered as P6-P10 are fully illuminated with irradiance level E; the panels P1-P5 are shaded by a nearby building to an irradiance level of $\frac{E}{4}$; the panels P11-P15 are partly shaded by a flag pole, which causes the equivalent

irradiance to be $\frac{3E}{4}$.

Shading pattern B: With the incident angle of the sun changed, the panels P1-P9 and part of the panel P10 are shaded by the nearby building; and the flag pole is no longer in the way so panels P11-P15 receive full irradiance E. In this situation, P1-9 receive an



(A)



(B)

Fig 4-1. two different shading patterns for an array of 15 PV panels

irradiance of $\frac{E}{4}$ while P10 equivalently receives $\frac{E}{2}$.

Fig 4-2 shows the Matlab simulated characteristics of the total output power P over the terminal voltage V . The conclusion in [54] holds for shading pattern A (solid line, 5 panels with $I_{ph}=1A$, 5 panels with $I_{ph}=3A$, and 5 panels with $I_{ph}=4A$.) but does not for pattern B (dashed line, 9 panels with $I_{ph}=1A$, 1 panels with $I_{ph}=2A$, and 5 panels with $I_{ph}=4A$.). It can be seen that for pattern B the power of the local MPP in the middle is less than the one on its either side. An experiment result as shown later in Fig 5-25 in Chapter 5 provides another example when the conclusion in [54] does not hold. In fact, the power of a local MPP is determined by the equivalent irradiance level as well as the number of series-connected panels with the same irradiance level. Therefore, the distribution of local MPPs can be versatile rather than increases in power until the global MPP and then decreases (from short circuit to open circuit).

In addition, in cases that two or more local maxima having same or similar maximum power (like the case in Fig 4-2 B), whether to operate at an operation point with smaller current or smaller voltage is a question as well.

So how to identify the occurrence of partial shading and how to determine the timing to do a global scan would be a valuable study. In this chapter, the characteristics of PV panels without and with partial shading are studied. By comparing the patterns, a novel method for identifying the presence of partial shading is proposed, which can be used to determine the need to do a scan for any global MPP. It has been implemented and the experiment results will be presented in Chapter 6.

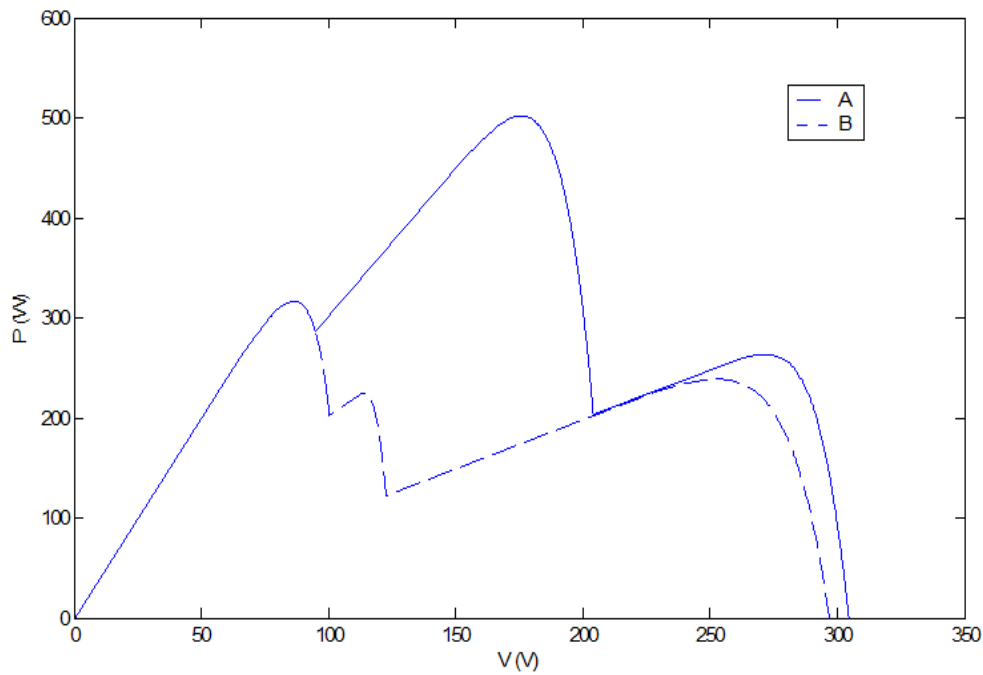


Fig 4-2. Output characteristics of the PV string

4.2 PV Characteristics without Partial Shading

For the purpose of identifying partial shading, it is essential to understand the intrinsic characteristics of PV panels with and without partial shading hence the difference between the two situations. In this section, the trajectory of the MPP at different irradiance levels without partial shading will be derived.

As described in Chapter 2, a simple form of the terminal characteristic for a PV panel can be expressed as:

$$I = I_{ph} - I_s \left(e^{\frac{qV}{AkT}} - 1 \right) \quad (4-1)$$

For the simplicity of derivation, let $C = \frac{AkT}{q}$, so that Eqn (4-1) can be rewritten as:

$$I = I_{ph} - I_S (e^{\frac{V}{C}} - 1) \quad (4-2)$$

The output power of the PV panel can be expressed as:

$$\begin{aligned} P &= I \cdot V \\ &= I_{ph} \cdot V - I_S (e^{\frac{V}{C}} - 1) \cdot V \end{aligned} \quad (4-3)$$

The derivative of this function with respect to V is then found as:

$$\begin{aligned} \frac{dP}{dV} &= I_{ph} - I_S (e^{\frac{V}{C}} - 1) - \frac{I_S}{C} \cdot e^{\frac{V}{C}} \cdot V \\ &= I_{ph} - I_S (1 + \frac{V}{C}) \cdot e^{\frac{V}{C}} + I_S \end{aligned} \quad (4-4)$$

At the MPP, $\frac{dP}{dV} = 0$, therefore,

$$\begin{aligned} I_{ph} - I_S (1 + \frac{V}{C}) \cdot e^{\frac{V}{C}} + I_S &= 0 \\ \Rightarrow I_{ph} &= I_S (1 + \frac{V_M}{C}) \cdot e^{\frac{V_M}{C}} - I_S \\ &= I_S [(1 + \frac{V_M}{C}) \cdot e^{\frac{V_M}{C}} - 1] \end{aligned} \quad (4-5)$$

where, V_M is the terminal voltage at maximum power.

By combining Eqn (4-3) and Eqn (4-5), the relation between the maximum power P_M and the voltage at MPP can then be derived as:

$$\begin{aligned}
 P_M &= I_{ph} \cdot V_M - I_S \left(e^{\frac{V_M}{C}} - 1 \right) \cdot V_M \\
 &= I_S \left[\left(1 + \frac{V_M}{C} \right) \cdot e^{\frac{V_M}{C}} - 1 \right] \cdot V_M - I_S \cdot V_M \cdot \left(e^{\frac{V_M}{C}} - 1 \right) \\
 &= \frac{I_S}{C} \cdot V_M^2 \cdot e^{\frac{V_M}{C}} \\
 &= \frac{q \cdot I_S}{AkT} \cdot V_M^2 \cdot e^{\frac{q \cdot V_M}{AkT}}
 \end{aligned} \tag{4-6}$$

For a PV array with N_s identical panels connected in series, the trajectory of the MPP can then be expressed as:

$$P_M = \frac{q \cdot I_S}{AkT \cdot N_s} \cdot V_M^2 \cdot e^{\frac{q \cdot V_M}{AkT \cdot N_s}} \tag{4-7}$$

Fig 4-3 shows the derived trajectory of the MPP for 15 panels in series as well as the simulated P-V characteristics using the Matlab models established in Chapter 2. This trajectory will be referred to as the **standard MPP trajectory** in the following sections.

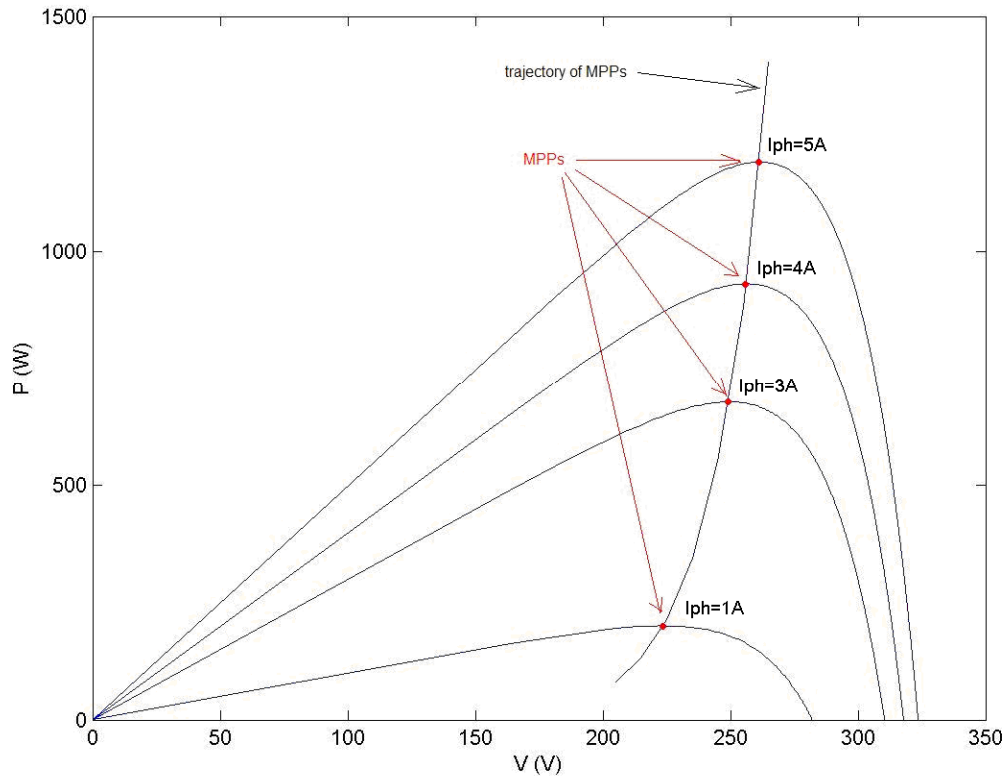


Fig 4-3. The standard MPP trajectory

4.3 PV Characteristics under Partial Shading Conditions and Identification of Partial Shading

Partial shading can occur due to passing clouds, shading from nearby obstructions such as buildings or flag poles, cell/panel mismatch, etc. Therefore, the affected areas and degrees of shading can be quite different.

PV characteristics with various shading patterns have been simulated using the Matlab model in Chapter 2 and compared with the standard MPP trajectories. Fig 4-4 shows the simulated characteristics of an array of 15 series-connected PV panels as configured in

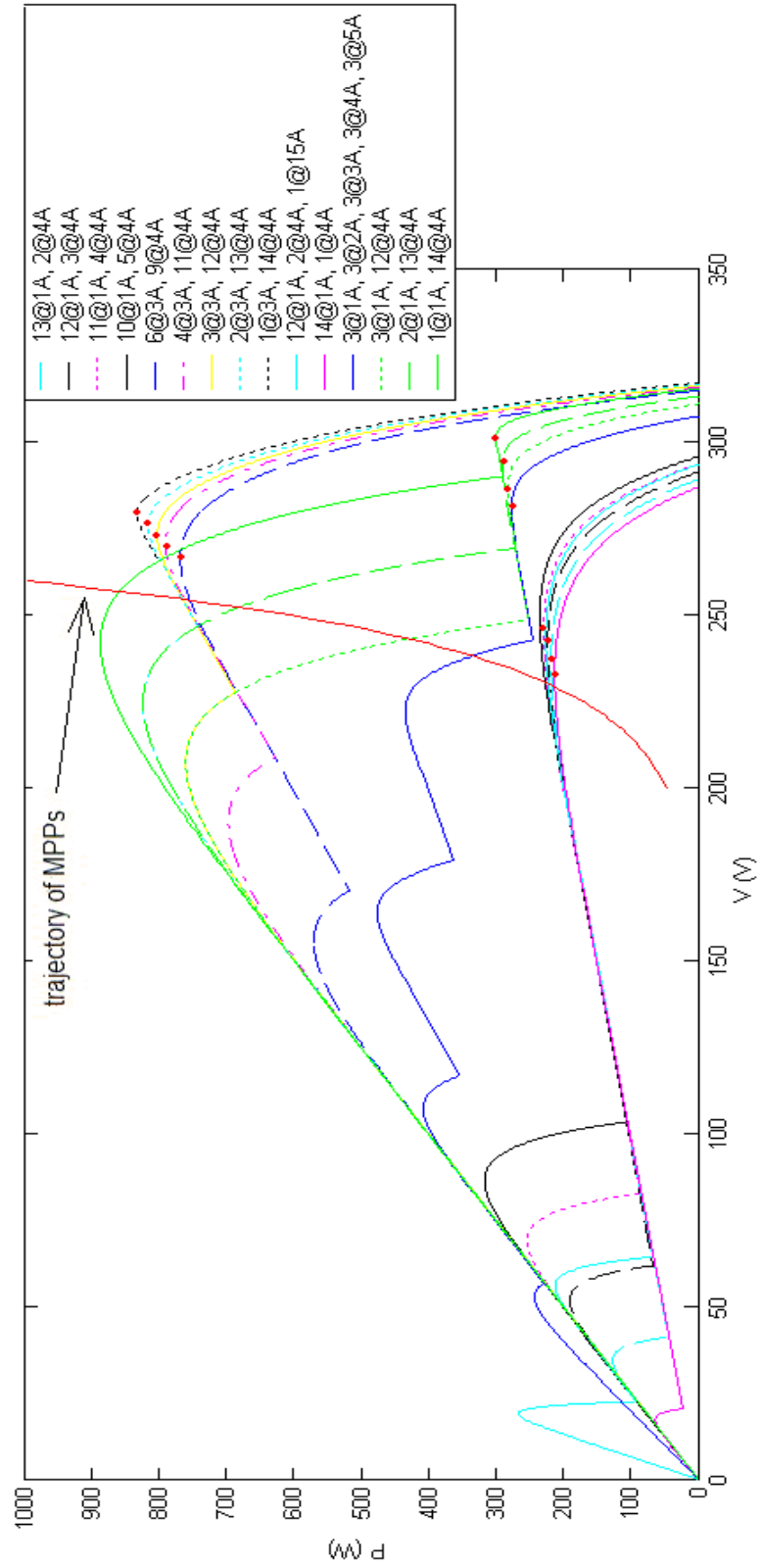


Fig 4-4. PV characteristics under partial shading

Fig 4-1 under various shading patterns, which is complex enough to reveal an interesting rule pertaining to the pattern under partial shading.

From Fig 4-4, it can be observed that the first local maximum power point (marked as red dots) that MPPT algorithms will find when starting from OC will always be located to the right of the standard MPP trajectory when partial shading is present. These local MPPs will be referred to as $MPPs_{(OC)}$.

The second observation that can be made from Fig 4-4 is that those $MPPs_{(OC)}$ all deviate from the standard MPP trajectory to a different extent depending on the pattern of partial shading. Further investigation of this effect is carried out by calculating the voltage deviation ΔV_M of the $MPPs_{(OC)}$ from the standard MPP trajectory as listed in Table 4-1.

Table 4-1 Calculated $MPP_{(OC)}$ voltage deviation ΔV_M from the standard MPP trajectory

Line style	cyan dashed	black dashed	magenta dotted	black solid	cyan solid	blue dashed	magenta dash-dotted	yellow solid	black dotted
ΔV_M	<3%	5%	6%	8.6%	6%	5%	6%	7%	9%
Global MPP?	Y	Y	N	N	N	Y	Y	Y	N
Best OP?	Y	Y	Y	? [†]	Y	Y	Y	Y	N

[†] This judgment will need to be based on the voltage range of the converter in use.

The term Best OP in the above table stands for “Best Operation Point”. It is not always the OP that has the highest output power (i.e., the Global MPP), but a best OP determined on the power yield as well as the working conditions for the converters. Take the cyan solid line as an example, the furthest left hand side OP has a higher output power than the $MPP_{S(OC)}$. However, its voltage is too low for most of the converter’s operating range. Therefore, it is not the Best OP.

There are a few conclusions that can be drawn from Fig4-4 and Table 4-1:

- 1) The presence of partial shading makes the $MPP_{(OC)}$ to deviate to the right hand side of the standard MPP trajectory. This observation can be used to identify the occurrence of partial shading.
- 2) The larger the power of other local maxima is, the larger is the deviation ΔV_M . This can be used to determine whether there exist significant local maxima other than the $MPP_{(OC)}$.
- 3) The further left the other local maxima are located, the smaller impact they have on ΔV_M . This observation is very useful because even when the global MPP is not the $MPP_{(OC)}$, it is not worth moving the operation point from $MPP_{(OC)}$ to the global MPP. The cyan solid line is a very good example of this situation. The voltage of the global MPP is very low. Firstly, lower operating voltage means higher operating current hence higher cable losses. Secondly, most converters have a limited operating voltage range and they cannot perform at very low voltages. For the Boost converter used in this work, a low PV terminal voltage means large duty cycle.

By comparing the data in Table 4-1 and Fig 4-4, it is reasonable to suggest that a global scan of MPPs is started only when the deviation ΔV_M is more than 8%.

4.4 A Novel MPPT Algorithm Adopting Partial Shading Identification

A novel MPPT algorithm to greatly increase tracking efficiency especially under partial shading conditions is therefore a combination of a conventional MPPT method (e.g., a P&O method) and a partial shading identifier. The flow chart is shown in Fig 4-5. After finding a local MPP, the algorithm will then carry out a judgment if any partial shading has occurred or not.

The partial shading identifier is based on the above observations. By comparing the voltage deviation from the standard MPP trajectory, it decides if there is a need for a global scan. If the operating point is on the left hand side of the standard MPP trajectory (negative deviation), there is surely partial shading occurring hence a global scan will be initiated. If the OP is on the right hand side of the standard MPP trajectory (positive deviation) and the deviation is more than certain range (8% suggested), a global scan will also be started; otherwise, it will be regarded that there is no or at least not significant partial shading, therefore, there is no need to waste energy to carry out global scans.

There are two possible ways to establish the standard MPP trajectory. One is pre-stored data from manufacturers. However, there will be variations among different PV panels due to manufacturing process, especially after some time's use, there will be degradation. Moreover, the characteristics of PV panels depend strongly on the operating temperature. Therefore, it is suggested to use the second way: self-adaption. Initially manufacturers'

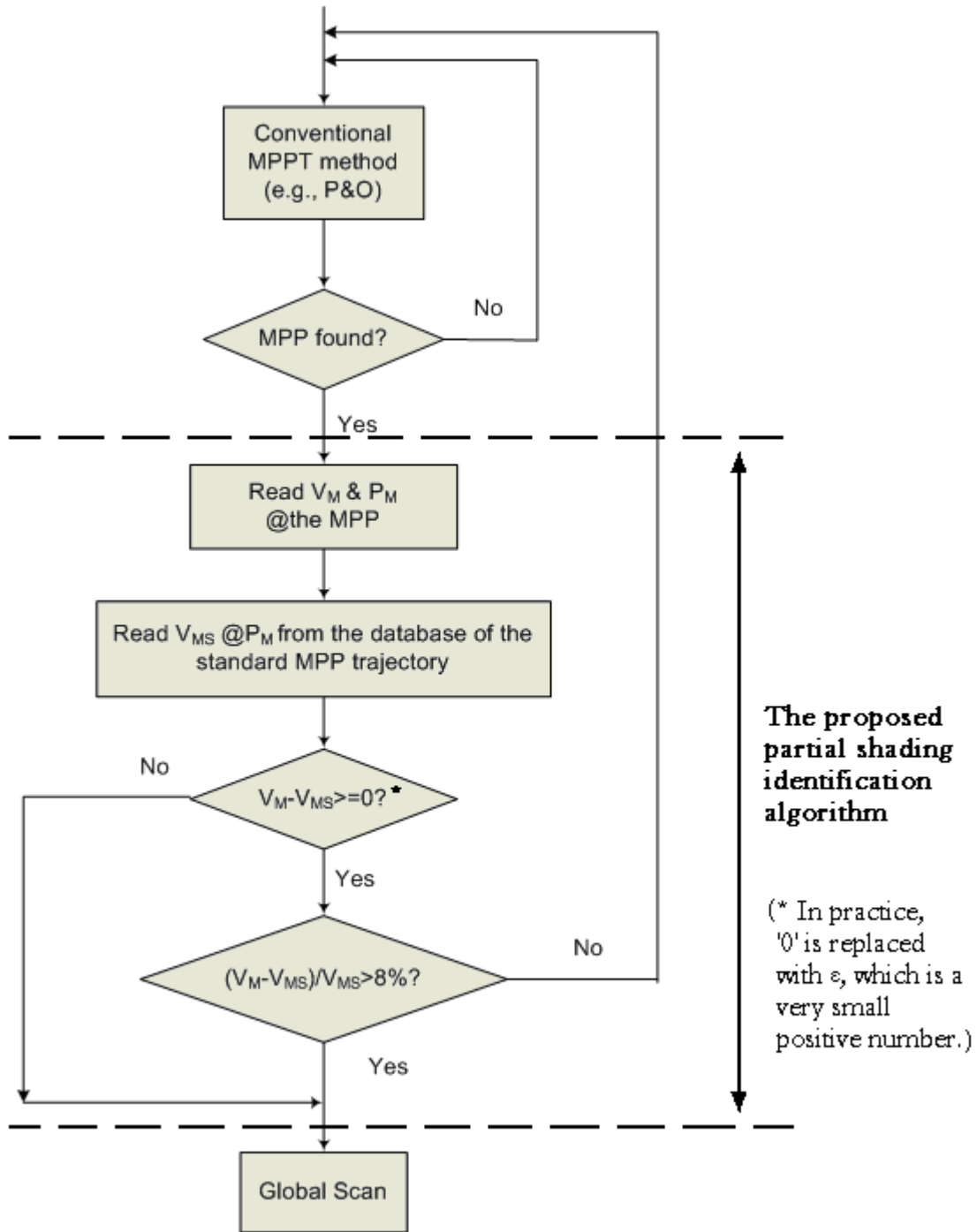


Fig 4-5. Flowchart of the proposed MPPT algorithm with partial shading identification

date will be used for the standard MPP trajectory. Then the database can be calibrated every certain time, e.g., annually. Also the temperature dependence of the trajectory can

be monitored and updated in the database. The temperature may be measured by attaching a thermometer to the PV panels or be estimated by calculating from the power level.

4.5 Conclusions

It is found in this chapter that there is a trajectory linking the maximum power P_M and the operating voltage at P_M under uniform illumination. By calculating the voltage deviation of a local maximum power point found by any conventional MPPT algorithm from the standard MPP trajectory, whether or not there is partial shading occurrence can be identified. With the effective partial shading identifier, global MPP can always be found under partial shading conditions so that the tracking efficiency can be greatly improved. In the meantime, when there is no significant partial shading, there will be no unnecessary periodical global scans which waste energy. Therefore, the proposed MPPT algorithm can significantly increase the MPP tracking efficiency.

Chapter 5. Design and Construction of a Solar Emulator

5.1 Introduction

5.1.1 Why a Solar Emulator Is Needed

In the experimental set-up, described in Section 1.4, the output of a PV source was emulated in the form of a typical Thevenin source - a DC voltage source V_S in series with a resistance R_S as re-drawn in Fig 5-1. This then feeds the converter, which has an equivalent resistance of R_{load} . R_S consists of two equal sections of 0.95Ω , one of which has a switch across it so that a sudden environmental change can be simulated by opening

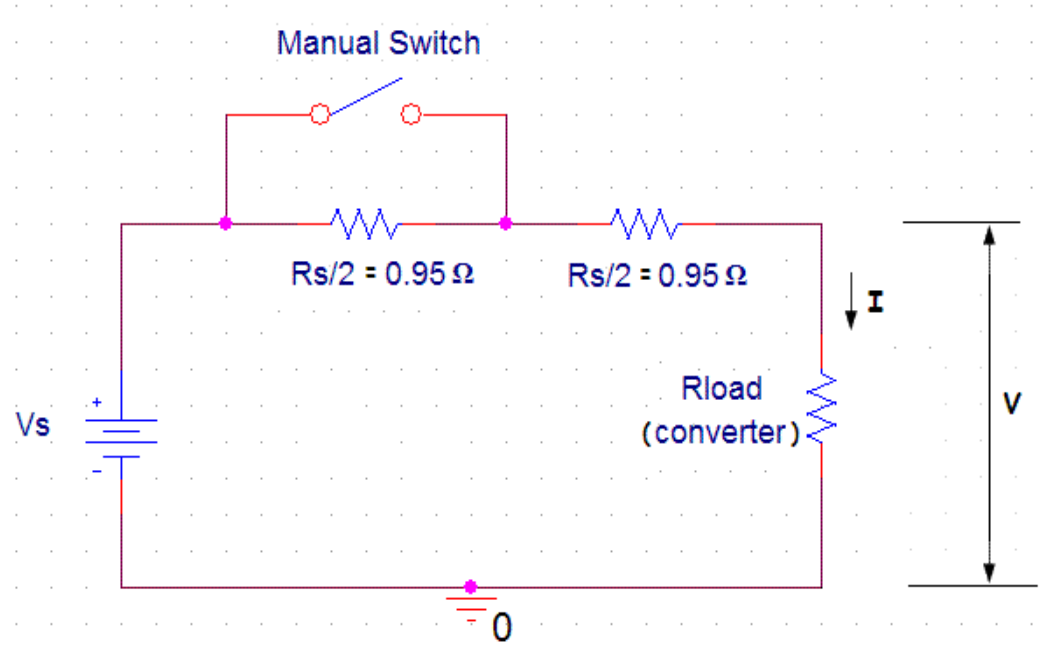


Fig 5-1. Original PV source emulator

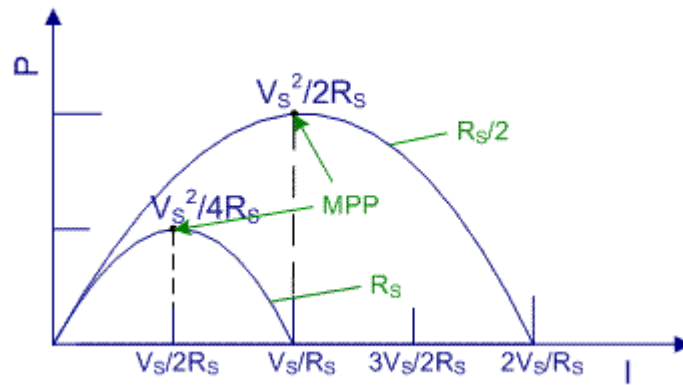
or closing the switch.

Fig 5-2 demonstrates the P (I) characteristics of a Thevenin source (a) and a real PV source (b). It can be seen that they both exhibit a maximum power point (MPP) within their operating range. Changing R_S has a similar effect as the change of irradiance E on the P (I) characteristics. Therefore, a Thevenin source with switchable series resistance can be used to study and test certain Maximum Power Point Tracking (MPPT) algorithms such as hill climbing methods.

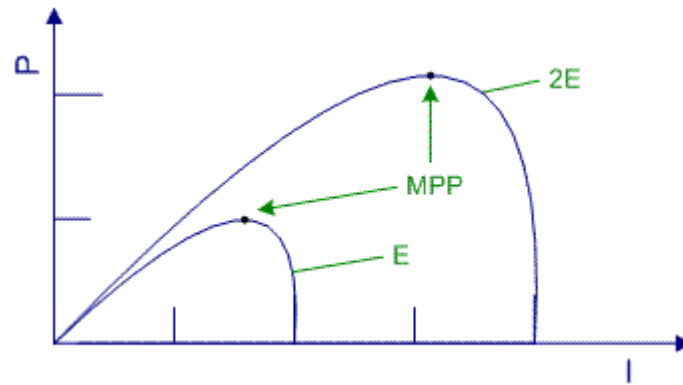
However, there are a number of limitations to this approach. Firstly, a Thevenin source is a good approximation only around the MPP. Also, having only changes in R_S does not reflect the actual characteristics of a PV source. For a real PV source, V_S changes together with R_S , under the effect of irradiance and temperature. Therefore, a Thevenin source can not be used for more complicated or more specific study purposes.

Furthermore, the scope of the present study includes the effect of PV dynamics due to PV cell capacitance on MPPT algorithms (see Chapter 3). It also includes the detection of occurrence of partial shading and the development of methods to control the converters to work at the global maximum power point under partial shading conditions (see Chapter 4). The existing PV source emulator in the form of a simple Thevenin source is unable to emulate such situations. Therefore, a more practical PV source emulator is needed to verify the true performance of MPPT algorithms and other aspects of intelligent control.

One possible implementation of a PV source emulator is the use of multiple DC power supplies with a feedback circuit and fast switches so that the output voltage-current curves follow a typical PV source characteristic. The fast switches are needed because



(a) Thevenin Source



(b) Real PV source

Fig 5-2. P-I characteristics

power supplies usually have a large capacitance at the output, which means that the output voltage can not change quickly. However, with such an emulator it would be difficult to emulate partial shading conditions which cause multiple local maxima in the PV characteristic.

Another way to create a PV source emulator is to illuminate a real PV panel with a solar emulator (sometimes called a solar simulator), as shown in Fig 5-3. The solar emulator is a device composed of a collection of light bulbs arranged such that the irradiance level over a PV panel is uniformly distributed. The light source can be divided into several (say 3) groups. Each group of bulbs is powered by a separate DC power supply and illuminates a sub-section area of the PV panel. In this way, a PV source with multiple local maxima can be emulated by supplying each group at a different voltage. In addition, this kind of solar emulator can be used to carry out tests on different PV panels as long as they are within its dimensional capacity. For example, it can be used to investigate how the capacitance and the characteristics of an amorphous silicon PV panel changes under partial shading conditions. Finally, because a real PV panel is used in the PV emulator, it will exhibit real dynamics due to its real internal capacitance. Therefore, realistic test results can be obtained.

Because of the above advantages, the PV source emulator in the form of a solar emulator using a real PV panel was adopted and designed to facilitate the research work. The aim of the solar emulator is to emulate sun light so that the test conditions are practical, controllable and repeatable.

As shown in Fig 5-3, the PV system now consists of the following parts: a solar emulator, a PV panel, a DC/DC converter, a grid-connected inverter, and the grid. The PV panel under illumination from the solar emulator feeds power into the DC/DC converter. Here, the DC/DC converter is a current-fed full bridge Boost converter with HF transformer and MPPT controller, feeding a common DC link with a grid-connected DC/AC inverter [18]. The inverter then delivers the generated power to the grid.

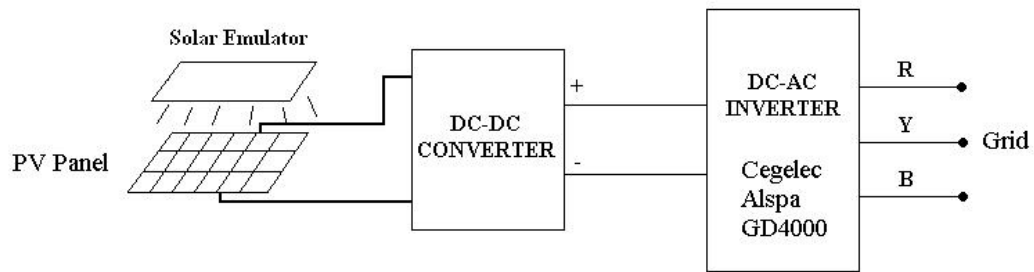


Fig 5-3. Block diagram of the PV system

5.1.2 Spectral Sensitivity of PV cells

5.1.2.1 Solar spectrum

Sunlight covers a wide spectrum from ultraviolet ($\sim 10\text{nm}$) to the far infra-red ($\sim 1,000\ \mu\text{m}$). Its spectrum varies with time and location. To allow evaluation and comparison of the performance of different photovoltaic devices, standard spectra have been developed, as shown in Fig 5-4 [61-63].

The standard spectrum for outer space is called Air Mass Zero (AM0). It has an integrated irradiance level of $1366.1\ \text{W/m}^2$ and is used in space applications.

There are two standard spectra for the sunlight at the Earth's surface (sea level): AM1.5 Direct (AM1.5D) and AM1.5 Global (AM1.5G).

AM1.5D defines a standard direct normal spectral irradiance which includes direct radiation only. It has an integrated irradiance level of $900\ \text{W/m}^2$ and is used in solar concentrator applications.

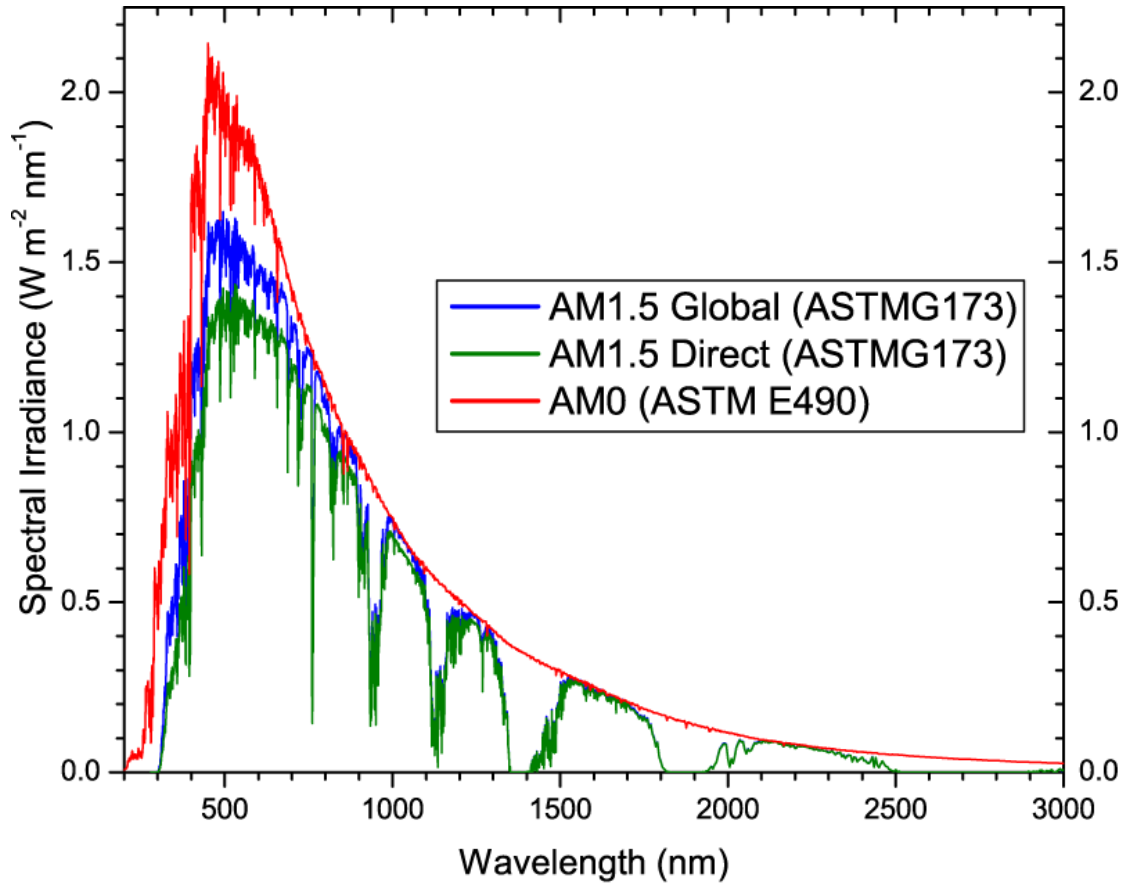


Fig 5-4. Standard Solar Spectra [61]

AM1.5G defines a standard total spectral irradiance which includes both direct and diffuse radiation. It has an integrated irradiance level of 1000 W/m^2 and is widely used in flat plate PV applications. Therefore, AM1.5G is the standard spectrum applicable for the scope of this work. And as shown in Fig 5-4 the spectral irradiance peaks in the visible range (360nm-830nm).

5.1.2.2 Spectral Sensitivity of PV cells

A PV cell consists certain semiconductor materials, hence has a certain band gap energy E_G . For silicon the band gap E_G is equal to 1.1 eV, which corresponds to a wavelength of 1122 nm.

A PV cell responds differently to different wavelengths of light. Fig 5-5 shows the typical absorption coefficient α of semiconductors [11]. It can be seen that α decreases with the wavelength, i.e., it increases with photon energy. Photons with energy less than E_G will not be absorbed.

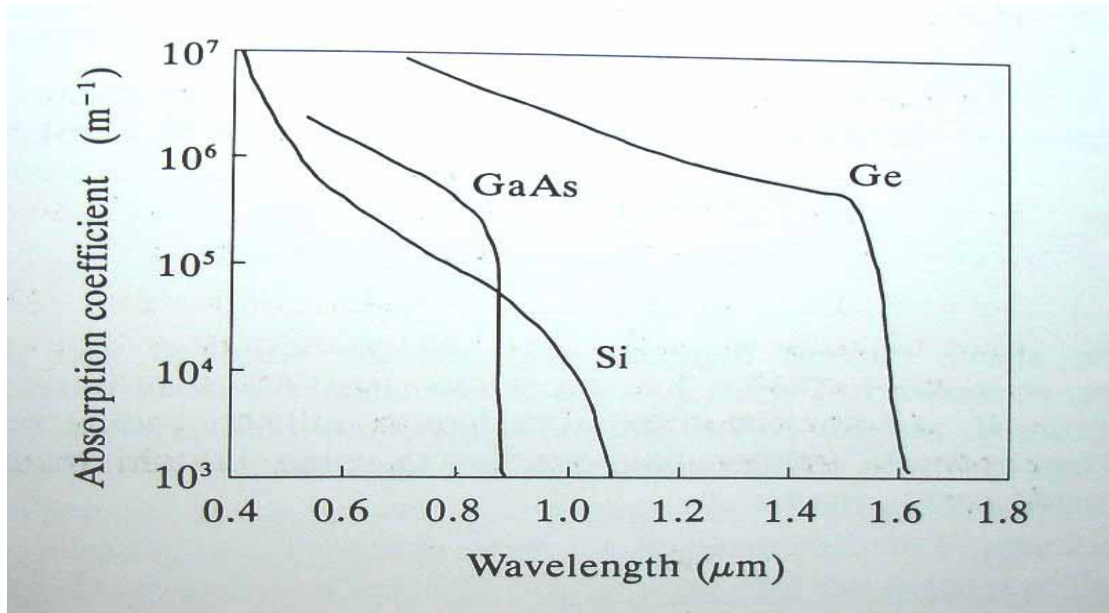


Fig 5-5. Absorption Coefficient of typical semiconductors [11]

To form a hole-electron pair, only the energy of E_G per photon is used. Photons with shorter wavelength (i.e. with higher energy) will have excess energy which will be transformed into heat [64].

Hence, the absorption coefficient as well as the heat loss decreases with wavelength. Therefore, there will be an optimum wavelength for the overall sensitivity of a PV cell.

The overall sensitivity of a PV cell is described by the Spectral Responsivity (or Relative Spectral Sensitivity), which can be defined as:

$$\text{Spectral Responsivity} = \frac{I}{P} \quad (\text{in A/W}) \quad (5-1)$$

where I is the produced current, and P is the power of the incident beam [65].

Fig 5-6 shows the Relative Spectral Sensitivity for an amorphous silicon cell and a crystalline PV cell [66] [67]. It can be seen that a typical a-Si PV cell uses only the visible light band (at a lower efficiency). However, a conventional mono-Si PV cell works over a much wider range (approximately 300nm-1200nm), including infra-red. And its sensitivity peaks in the infrared region (~900nm).

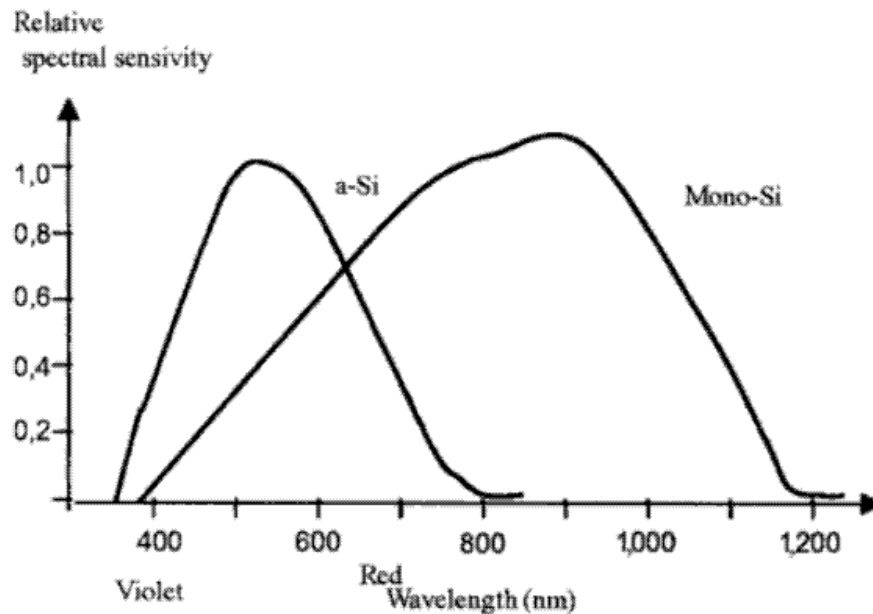


Fig 5-6. Spectral sensitivity of an amorphous silicon cell and a crystalline PV cell [67]

5.1.3 Standards for Solar Simulators

Solar simulators are classified in terms of spectral match, non-uniformity and temporal instability according to International Electrotechnical Commission (IEC) standard 60904-9 (Photovoltaic devices - Part 9: Solar simulator performance requirements). The classification is shown in Table 5-1 [68].

Table 5-1 IEC Classification of Solar Simulators

	Class A	Class B	Class C
Spectral Match	75%-125%	60%-140%	40%-200%
Non-Uniformity	$\leq \pm 2\%$	$\leq \pm 5\%$	$\leq \pm 10\%$

For larger solar simulators (test plane $> 30\text{cm} \times 30\text{cm}$), the non-uniformity is allowed to be greater. The solar emulator is not used for precise calibration or test, but to provide controllable irradiance levels for the PV panel. Therefore, for the application in this work the degree of spectral match is less important as long as the light spectrum of the solar emulator is similar to that of the sun over the range of interest (sensitivity range of PV cells).

The solar emulator used in this work was constructed so that the performance of MPPT algorithms can be tested under varying irradiance levels as well as under partial shading conditions. Only the relative irradiance levels illuminating the sub-sections of the PV panel is of interest, as long as the light within each sub-section is uniformly distributed. Therefore, the level of uniformity is the most important aspect in the design of the solar emulator to facilitate a comparative study of MPPT algorithms.

5.1.4 Existing Commercial Solar Simulators

There are manufacturers who construct and sell commercial solar simulators to PV cell/panel manufacturers as well as research labs/institutions, such as AstraNet, Spectrolab, Newport and Wacom, etc. Such solar simulators are divided into two types: steady-state (continuous) and pulsed.

Commercial steady-state solar simulators are usually very large apparatus, but only illuminate a small area (a few square inches). They are very expensive (many thousands of pounds) and are normally used in laboratories to test prototype PV cells/materials.

For large area testing, (long) pulsed solar simulators are used. For illuminating the same area, the manufacturing costs are only a fraction of the costs of steady-state solar simulators. However, for a large area (such as the size of a PV panel) they are still very costly (thousands of pounds or more) and they can only be operated for very short period (pulse duration up to hundreds of ms). Pulsed solar simulators are mainly used in characterization test of PV cells/panels [69].

As for the solar emulator needed in this work, it needs to be suitable for continuous operation and cover a large area (one or more PV panels). A commercial solar simulator which can achieve both requirements will be too expensive to be affordable by a university.

Most of the commercial solar simulators use Xenon arc lamps as the light source, because Xenon lamps have a close spectral match to the natural sunlight. The output spectrum of a typical Xenon arc lamp is compared in Fig 5-7 with that of the sunlight [70]. Note that

the Xenon spectrum contains intense spectral spikes in the IR range and extends further to the UV side than the sunlight. Therefore, spectral filtering is required to obtain a close match to the spectrum of sunlight.

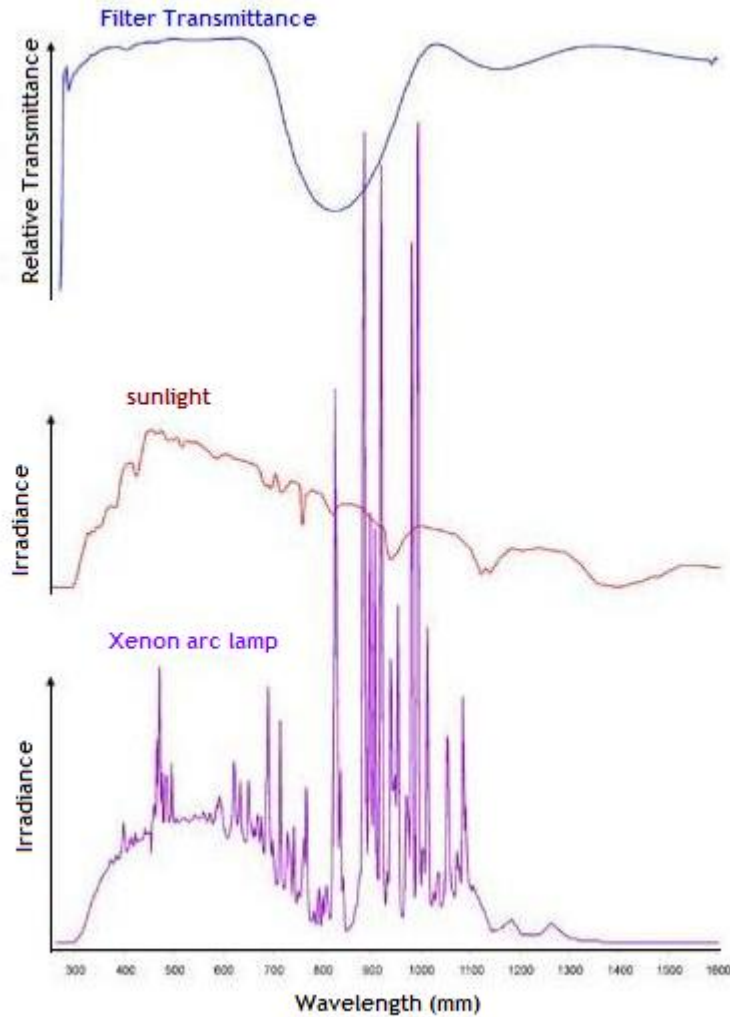


Fig 5-7. Spectrum of a Xenon lamp compared with that of the sunlight [70]

Secondly, there is usually only one Xenon lamp in a solar simulator, so a special optical design must be adopted to produce a uniform illumination over its test plane. The optical design is very complex and requires extensive knowledge of optics. Therefore, it is not an

easy task for university researchers in the field of power electronics to design a solar simulator using Xenon lamps.

Finally, Xenon lamps require very high start up voltages and they are inherently unstable to operate. So a special power supply circuit is needed for start-up as well as for regulating the operation conditions, which further increases the complexity and cost of the solar simulator system.

Therefore, considering the design complexity and cost, a Xenon lamp may not be the best choice for the planned solar emulator.

5.1.5 Design Requirements for the Solar Emulator

When designing the solar emulator for the intended use, there are certain requirements some of which may differ from those for commercial solar simulators.

It must:

- 1) Have the same or similar spectrum as that of the sun, at least over the range of interest where peak sensitivity of PV cells is achieved. Since the object of interest is the illumination of PV cells within a PV panel, a similar spectral characteristic as described in 5.1.2.2 is desirable.
- 2) Be suitable for continuous operation in steady-state.
- 3) Have an output capability of irradiance level up to 1000W/m^2 as required for the standard test condition (STC).

- 4) Have a test plane area large enough to accommodate at least one PV panel.
- 5) Have a uniform distribution of light across the whole area of the PV panel. If light is not uniformly distributed, it is equivalent to a partial shading condition, which will cause distortion of the I-V characteristics and may result in unintended multiple local maxima.
- 6) Maintain temperature within a certain range. It is best to maintain the PV cell temperature at STC (25°C). However, since PV panels normally operate in the range of 40-60°C outdoor in the sun, a temperature no higher than this range is acceptable.
- 7) Be capable of emulating partial shading conditions. Test results for 13 commercial inverters with MPP tracking are reported in [47]. When there were only two local maxima, seven of them were still able to find the global MPP. However, when there were three local maxima, none managed to do this. Therefore, the solar emulator needs to be divided into at least three sub-sections with adjustable levels of illumination so that the output of the PV panel will have multiple (at least 3) maxima.
- 8) Be affordable. As stated earlier commercial solar simulators are very expensive (thousands of pounds) to purchase, especially when a larger area must be illuminated. And it would cost even more to include extra features, such as the ability to create partial shading conditions. The cost to construct a solar emulator tailored to researchers' special needs have to be within the (limited) budget of university research.
- 9) Have a reasonable power consumption. It should be reasonably efficient with manageable heat dissipation and affordable power supply level.

5.2 Facilities to Test Lamp Characteristics

5.2.1 Radiometric and Photometric Quantities [71]

Radiometric quantities measure the electromagnetic radiation energy of any wavelength; instead, photometric (luminous) quantities are related to the sensitivity range of the human eye, i.e., the visible light (360nm-830nm).

Common radiometric quantities include:

- Radiant Energy Q_e (J), which defines radiant electromagnetic energy
- Radiant flux Φ_e (W), which defines radiant electromagnetic power
- Irradiance E_e (W/m^2) (also called radiant flux density), which defines power density (radiometric flux per unit area) received by a detector (such as PV cells/panels, etc.)

Common photometric quantities include:

- Luminous flux Φ_v (lumen, lm), which defines the power of visible light in relation to the sensitivity of normal human eyes.
- Illuminance E_v (lux, lx) (also called illumination), which defines photometric flux per unit area. In history, the unit foot-candle (fc) was also used, which is defined as lm/ft^2 .

- Luminous intensity I_v (candela, cd), which is defined as lumen per solid angle[‡] (lm/sr). It is widely used to indicate how bright a lamp is.

There is a conversion factor between radiometric and photometric units, which is called the Spectral Luminous Efficacy of Radiant Flux $K(\lambda)$. It is defined as the quotient of the luminous flux at a given wavelength by the radiant flux at the same wavelength [73], i.e.,

$$K(\lambda) = \frac{\Phi_{v\lambda}}{\Phi_{e\lambda}}, \quad (\text{unit: lm/W}) \quad (5-2)$$

Fig 5-8 depicts the spectral luminous efficacies of two standard observers: photopic and scotopic. These two responses correspond to those of human eyes under high (daytime) and low (nighttime) illumination, respectively.

From the above definitions and Fig 5-8, it can be derived that luminous flux Φ_v can be calculated as

$$\Phi_v = \int_0^\infty \Phi_v(\lambda) \cdot d\lambda = \int_{360nm}^{830nm} K(\lambda) \cdot \Phi_e(\lambda) \cdot d\lambda \quad (5-3)$$

Firstly, the solar emulator is aimed to illuminate the object PV panel at an irradiance level of 1000W/m^2 , which is a radiometric value. Therefore, candidates of lamps as light source for the solar emulator should be capable to radiate 1000W/m^2 to an object with a feasible distance to the lamps. Secondly, the illumination needs to be uniformly distributed over the whole area of the PV panel. Therefore, the radiometric intensity

[‡] Steradian (sr) is the SI unit of solid angle. 1sr is defined as the solid angle subtended at the center of a sphere of radius r by a portion of the surface of the sphere having an area r^2 [72].

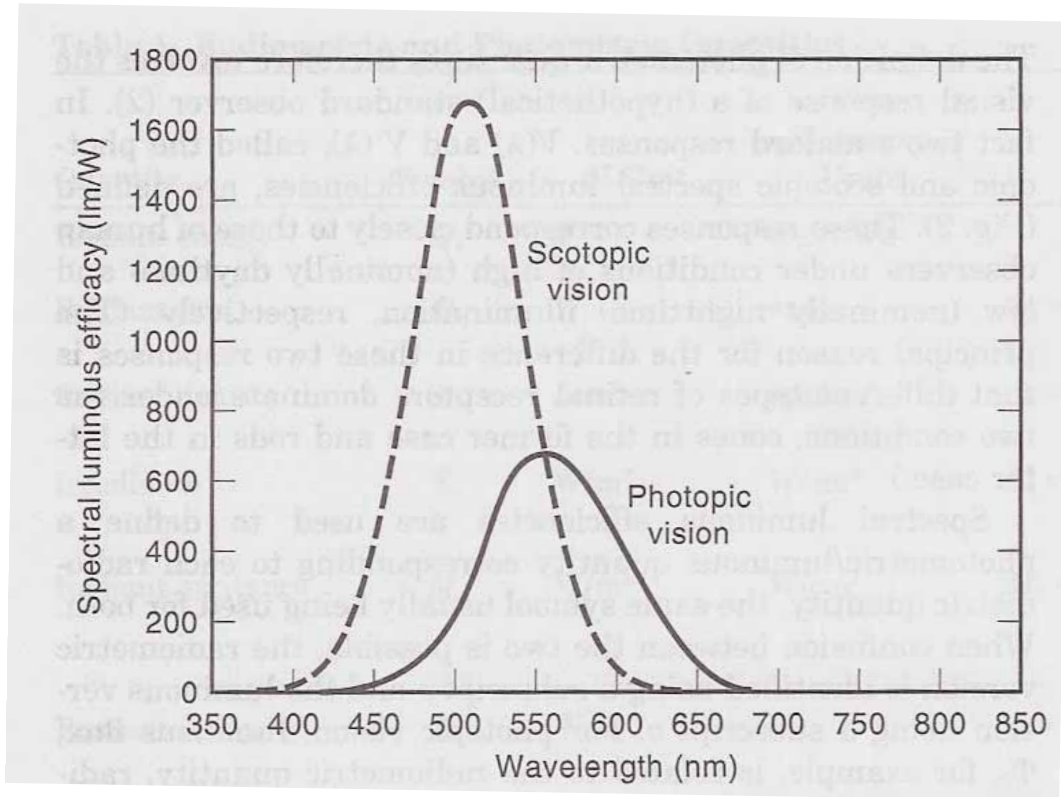


Fig 5-8. Spectral luminous efficacies:

Photopic $K(\lambda)$ – solid line, and Scotopic $K'(\lambda)$ – dashed line [73]

distribution curve of the lamps is needed for the optical calculation and design of the light source.

However, it was found that available datasheets of various lamps, such as halogen lamps, usually only give lamp characteristics in photometric quantities, such as luminous flux (in lumen) and luminous intensity (in candela). Fig 5-9 shows a candlepower distribution curve (or radiation pattern) of a halogen lamp, which only provides information in photometric quantities.

In conclusion, photometric quantities are measured within visible light range and with respect to the sensitivity of human eyes. The sensitivity of human eyes and PV cells to different wavelengths is different. Therefore, photometric quantities available in lamp

datasheets can provide a certain reference of irradiance levels, but they cannot truly reflect the irradiance levels, at least not over the full sensitivity range of PV cells (approximately 300nm-1200nm), which is wider than the visible light wavelength band. Obviously, an effective radiometric measuring device is needed for initial test of a lamp's radiometric characteristics as well as for testing the irradiance levels after the solar emulator is constructed.

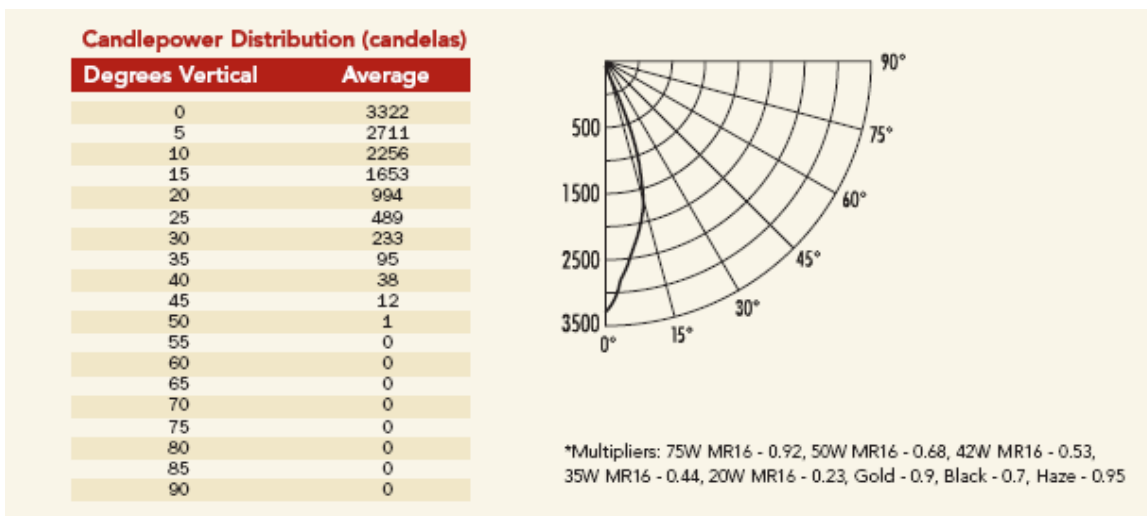


Fig 5-9. A candlepower distribution curve of a halogen lamp [74]

5.2.2 Irradiance Measuring Device

An ageing Kipp & Zonen CM5 pyranometer was the only available radiometric device available for use in the research laboratory. However, it was recently calibrated against a new Kipp & Zonen CM3 pyranometer using a large 500W halogen floodlight.

Initially, the CM5 pyranometer was used to measure the irradiance produced by the lamps. However, it is a thermal device and has a wider sensitivity band of wavelengths than a standard silicon PV cell. And its working area is large in size and it integrates light

incident to a large sensitive area. Therefore, it is not suitable for precise measurement for small illuminated areas, for example when measuring the distribution characteristics of one lamp. Also, the response is slow. And the whole device is physically large in size. Therefore, it is unsuitable for detailed measurement of the irradiance distribution once the solar emulator is constructed, especially when a PV panel is in place.

A photodiode operating in the photovoltaic mode (i.e. with no bias voltage applied) works exactly the same as a PV cell. Therefore it will be ideal as an irradiance measuring device, because it has the same spectral sensitivity as PV cells.

The BP 104S photodiode is adopted, which has a spectral sensitivity range of 400-1100nm. Its photosensitive area is very small (2.2mm by 2.2mm) and the thickness is only 1.2mm. An irradiance measuring device was constructed using the photodiode as the sensor. The device consists of two parts: a detector board (shown in Fig 5-10) and an amplifier board. The photodiode was mounted in the centre of the 20mm by 20mm

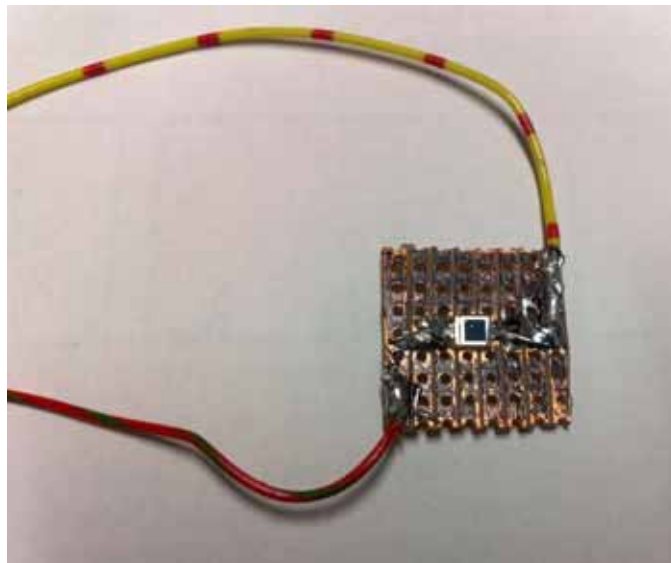


Fig 5-10. Detector board with a photodiode BP 104S in the centre

detector board. This forms a tiny detector with small thickness (approx. 2.5mm). Therefore, the detector board can be placed at any point of the illuminated surface under test.

The output current of the photodiode is very low, hence it needs to be amplified for accurate measurements. The detector was therefore connected to a separate amplifier board. The power supply and amplification circuit are shown in Fig 5-11. The resistor R_f can be adjusted for calibration of the photodiode against the CM5 Pyranometer.

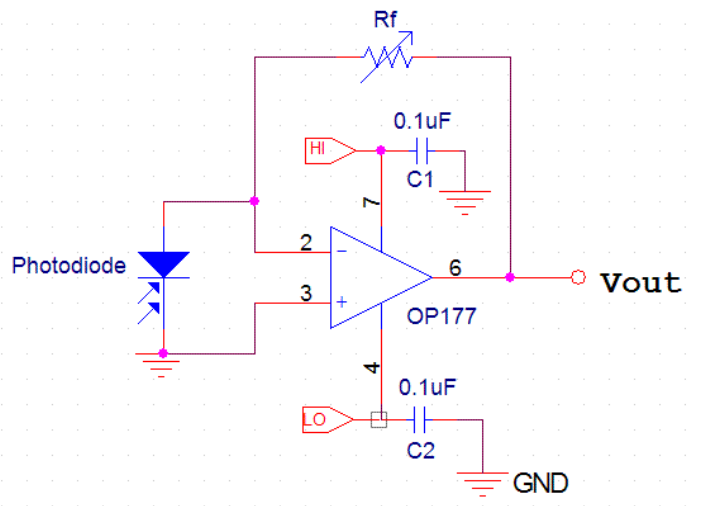


Fig 5-11. Amplification circuit of the photodiode detector

5.3 Design of a Solar Emulator Using Power LEDs

Power LED bulbs are far more efficient than halogen ones, therefore, investigations were first carried out on power LEDs. Luxeon LED emitters manufactured by Philips Lumileds are the brightest LEDs that could be found during the period of this work. They have the following advantages that make them good candidates for a solar emulator:

- a) high flux per LED;
- b) more energy efficient than incandescent and most halogen lamps, and heatsinks can be installed at the back of the bulbs so that less cooling is required;
- c) DC operated so that no AC fluctuation from the mains;
- d) cool beam, safe to touch;
- e) instant response (less than 100ns);
- f) fully dimmable.

Table 5-2 lists three of the brightest white Luxeon LED types and their most relevant specifications.

Table 5-2: Specifications of three bright white Luxeon LEDs [74]

Product	III emitter white	K2 emitter white	K2 emitter white
Part number	LXHL-PW09	LXK2-PW14-U00	LXK2-PW14-V00
Typical Lumens	80	100	120
Min Radiometric Power (mW)	355	875	1050
Max Radiometric Power (mW)	435	1050	1225

When designing the solar emulator using K2 emitters, 1000mW of radiometric power was used as the typical value. Therefore, to obtain the standard condition of 1000 W/m², the area illuminated by a K2 LED would be 10⁻³m², which means a radius of 17.84mm.

For the convenience of designing, an LED bulb is regarded as a point light source. As illustrated in Fig 5-12, the distance between the bulb and the illuminated surface is h . The radius of the illuminated area is r ($r=17.84\text{mm}$) and the angle of the light is α . The distance h can be calculated as below.

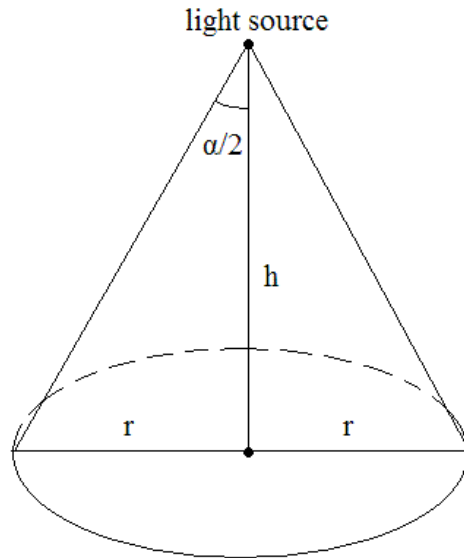


Fig 5-12. Illustration of illumination

$$\tan\left(\frac{\alpha}{2}\right) = \frac{r}{h} \Rightarrow h = \frac{r}{\tan\left(\frac{\alpha}{2}\right)} \quad (5-4)$$

The viewing angle[§] of Luxeon K2 white LEDs is 140° . It makes the light so widely spread that high irradiance level can be achieved only when the LEDs are very close to the illuminated surface. Therefore, it is necessary to combine an LED with an optical lens which focuses the light. The available angles of available optic lenses for K2 LEDs are

[§] Viewing angle is the off-axis angle from the bulb centerline where the luminous intensity is $\frac{1}{2}$ of the peak value[75].

listed in Table 5-3 [76] [77], which also shows the calculated distance between the LED and the illuminated surface for each option.

Table 5-3: Available optics angles and calculated distance

α (°)	4	6	10	12	17	20	24	27	30	50
h(mm)	511	340	204	170	120	101	84	74	67	38

It can be seen from Table 5-3 that there is a wide range of distances to choose from for the solar emulator. Considering the factors to be taken into account when designing the emulator, such as irradiance uniformity and temperature control, with the available distance range, it would be feasible to build a solar emulator with the K2 LED bulbs.

There are different sizes of PV panels available in the research laboratory. The smallest one is a Solarex MSX60 which has a size of 0.55m². The required quantity of LEDs to illuminate the area is $0.55/10^{-3}=550$ at least. Taking into account the overlap of light, approximately 1000 LEDs would be needed to construct such a solar emulator. The costs of the LEDs alone will be nearly £3000. Counting in the cost for the optic lenses, heat sinks, other components and labour, the total cost would be far beyond the available budget.

Furthermore, as shown in Fig 5-13, the spectral characteristic of white Luxeon LEDs has a peak of power emission at about 430nm and a trough at about 475nm. And the power emission drops to a low level after 650nm. This characteristic does not agree well with

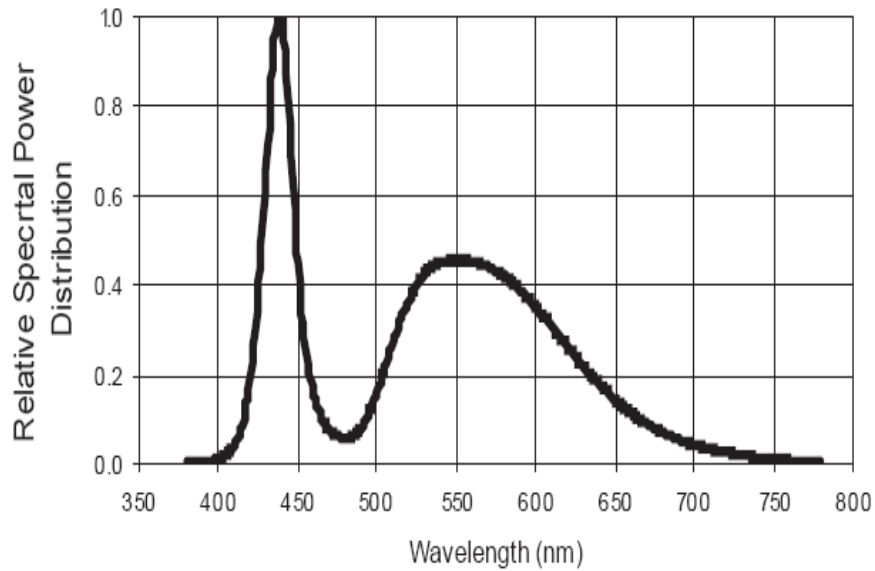


Fig 5-13. Spectral characteristics of a typical K2 white LED bulb [76]

that of the sun light (see Fig 5-4). For an improved spectral match, it would be necessary to use a mix of different coloured LEDs and/or filtering lenses, which greatly increases the complexity of the design.

Therefore, further investigation has concentrated on the use of halogen lamps.

5.4 Design of a Solar Emulator Using Halogen Lamps

5.4.1 Selecting the Lamp Type

Compared to power LEDs, halogen lamps are less efficient but much cheaper and offer at present more choices in models, wattage and optical characteristics.

Fig 5-14 shows an example of the spectral characteristics of sunlight and a halogen lamp [78]. Considering the sensitivity range of PV cells, halogen lamps can be a good alternative to sunlight as a light source to illuminate PV panels.

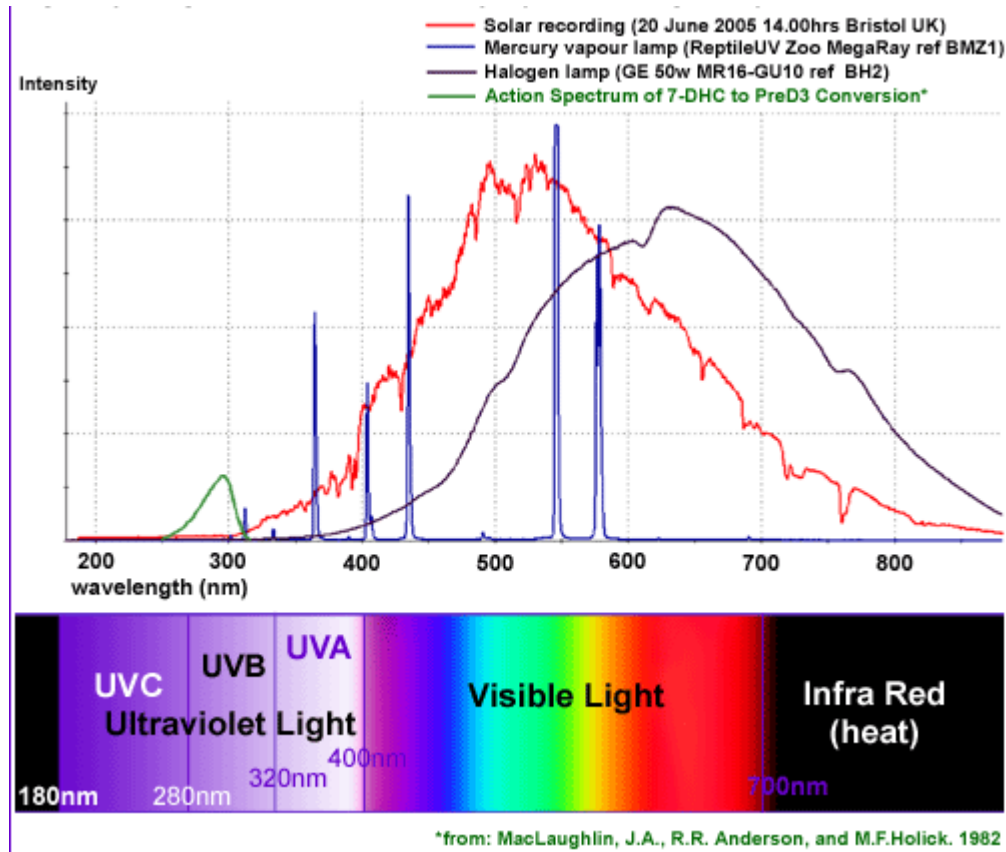


Fig 5-14. Spectral characteristics of sunlight and a halogen lamp [79]

The construction of a solar emulator using halogen lamps has been reported in [79]. However, few details on the design or the characteristics were given, for example, the uniformity of the light distribution and the ability to simulate partial shading conditions. For the present research, the latter is very important. Therefore, it was felt that the design of a solar emulator fulfilling all the requirements set out in section 5.1.5 would be a valuable contribution to the PV research.

Available datasheets of halogen lamps from various manufacturers provide only lamp characteristics in photometric quantities. As mentioned in section 5.2.1, photometric quantities are related to irradiance levels under certain conditions. Therefore, these

quantities were used in the first instance as a reference for selecting the type of halogen lamps.

After comparing luminous intensity, efficiency and price of various halogen lamps, Osram Decostar IRC lamps were chosen for further investigation. This category of lamps has an infrared reflective coating (IRC), so that less heat is emitted and a high working temperature is easier to maintain. As a consequence, IRC lamps consume up to 45% less energy than standard dichroic lamps of the same brightness [80].

First, an existing GE star lamp (1350cd) was used to establish the approximate conversion factor from photometric to radiometric quantities for halogen lamps. When this lamp was placed at a height h (see Fig 5-15) of 172mm, an irradiance level of $1000\text{W}/\text{m}^2$ at the centre O ($\alpha=0^\circ$) of the illuminated area was achieved. For light sources with the same spectral characteristics, it can be assumed that radiant flux $\Phi_e \propto I_v$.

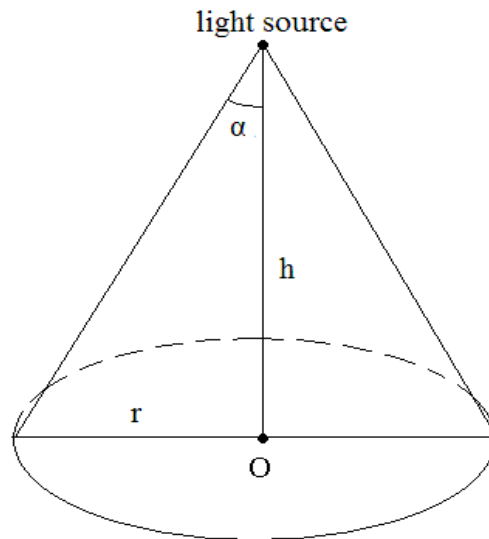


Fig 5-15. Illustration of illumination

Therefore the irradiance $E_e \propto \frac{I_v}{h^2} \Rightarrow h \propto \sqrt{\frac{I_v}{E_e}}$. This means that to achieve an irradiance of 1000W/m^2 at the illuminated centre O using a halogen lamp of luminous intensity I_v (in cd), the required height h (in mm) can be estimated as

$$h = 172 \cdot \sqrt{\frac{I_v}{1350}} \quad (5-5)$$

A generic program was developed in Matlab (see Appendix 7) to calculate the irradiance distribution pattern of halogen lamps for different angles α and height h .

The program opens a file containing the data of the photometric distribution of a lamp (see Appendix 7 for an example of the data for the Osram IRC 50W 24° lamps). The data was extracted from freeware called DIALux [81] for light layout calculation. A typical example of the light distribution is shown in Fig 5-16. The data is calibrated for an irradiance E_e of 1000W/m^2 at $\alpha=0^\circ$ with h calculated using Equation 5-5.

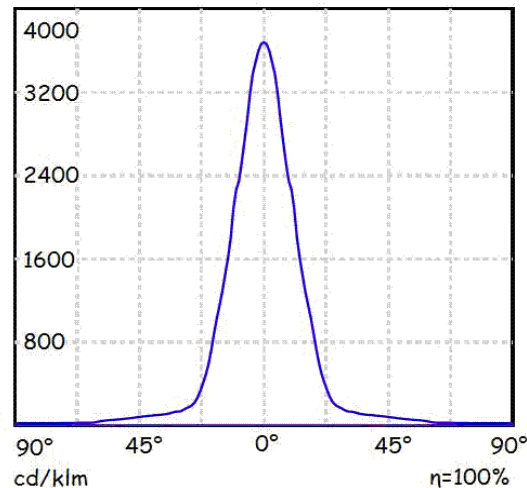


Fig 5-16. Light distribution of two an Osram Decostar IRC lamp, 50W 24° [82]

The Matlab program then defines an array of lamps, with an area much larger than that of the illuminated plane of interest so that the array of the lamps can be regarded as infinite in all directions.

For any user defined illuminated area with a height of h below the array of lamps and a distance of d between the centers of two adjacent lamps, the Matlab program calculates the irradiance of each illuminated point (very small area) using the calibrated light distribution data. The program then returns the average, maximum and minimum irradiance intensity, maximum deviation from the average intensity, and other results of interest. It also produces a 3D plot (as shown in Fig 5-17) to illustrate the light distribution pattern.

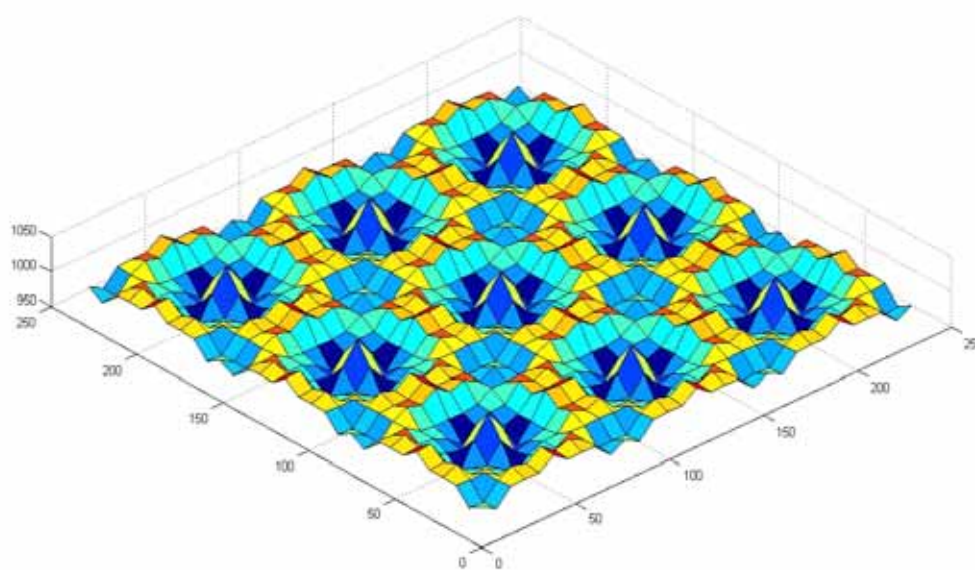


Fig 5-17. Plot of the irradiance distribution

The Matlab program was applied to all available Osram IRC lamps with different beam angles and power ratings. After comparing the total number of lamps needed to

illuminate a certain area (representing the cost and the power consumption), the 50W 24° lamp was selected for constructing the solar emulator. The operating voltage for this lamp is 12VDC.

5.4.2 Testing the Lamp Characteristics

The photodiode detector described in section 5.2.2 was used to measure the irradiance distribution of the selected halogen lamps. It was found that the measured irradiance distribution differs from the luminous intensity provided by the manufacturer, as shown in Fig 5-18 (where the irradiance E has been scaled to the same level as the luminous intensity I for ease of comparison). It shows that photometric and radiometric quantities are not the same as explained in section 5.2.1.

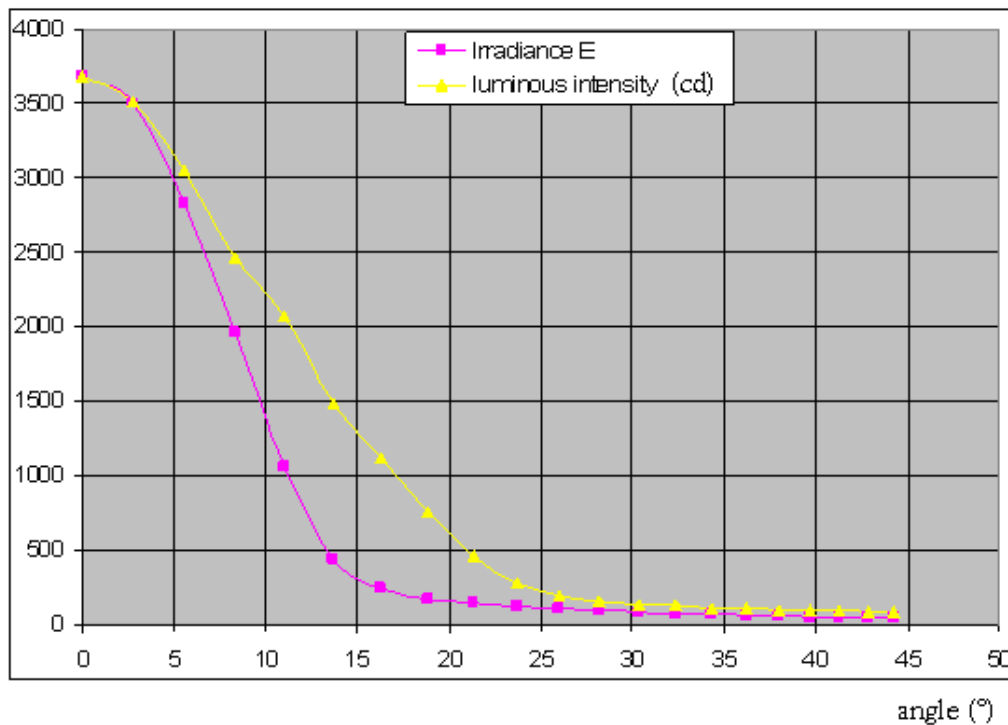


Fig 5-18. Manufacturer's luminous intensity distribution and measured irradiance distribution

The photometric intensity data of the manufacturer was therefore replaced by the measured radiometric distribution data in the Matlab program, and used to calculate the irradiance distribution for the design of the solar emulator.

5.5 Construction and Testing

5.5.1 Mechanical and Electrical Design of the Solar Emulator

5.5.1.1 Mechanical design

- Uniformity and the use of mirrors

Using the Matlab program described in Section 5.4.1, the irradiance distribution of groups of lamps was calculated for different height h and distance d between lamps. It was found that for $h=510\text{mm}$ and $d=80\text{mm}$ the average irradiance was $E_{av}=826.6\text{W/m}^2$ with a maximum deviation of only 1%.

It should be noticed that the above calculation was based on the condition when the array of lamps is infinite or at least much larger than the illuminated area of interest, i.e. the PV panel under test. If this condition is not met, the uniformity of the illuminated area of interest would not be obtained, especially around the edges.

The use of mirrors at the edges of the PV panel under test makes it possible to simulate an infinite array of lamps if the reflection of the mirrors is 100%, whilst keeping the actual array of lamps to the same size as the illuminated area (therefore making the size of the whole solar emulator as small as possible).

As illustrated in Fig 5-19, the mirrors Ma and Mb are placed at $d/2$ ($=40\text{mm}$) away from the lamps. A1 and A2 are the symmetrical images of the lamps L1 and L2 respectively about the left mirror Ma. A1' and A2' are the images of the previous images about the right mirror Mb. In this way, these images carry on forming images about the two mirrors, creating an effective infinite row of lamps for the area between the mirrors.

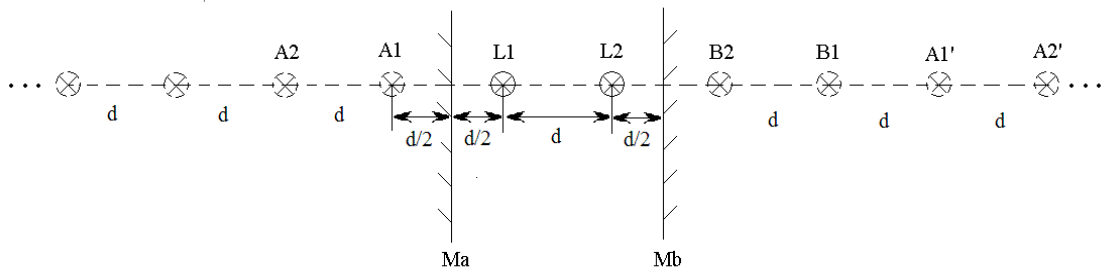


Fig 5-19: Imaging of lamps

As mentioned in 5.1.5, for the purpose of partial shading study, the PV panel under test needs to be divided into three sub-sections illuminated by three separately powered sub-arrays of lamps respectively. The irradiance distribution within each sub-section needs to be uniform and unaffected by the lamps for the other two sub-sections. Use of mirrors again to divide sub-sections can also solve this problem effectively. When mirrors are placed at $d/2$ ($=40\text{mm}$) from adjacent lamps, an infinite array of lamps for the sub-section can be emulated. In this way, the enclosed sub-section of the PV panel can be illuminated uniformly, independent of the other two groups of lamps.

The mirrors need to have a very good reflection and be able to operate under at elevated temperatures. MIRO-SUN Weatherproof high reflective aluminum sheets, manufactured by Alanod, were selected for the mirrors [82]. They are very reflective with a total light

reflection $\geq 93\%$. They are very thin (0.5mm) and the surface is not susceptible to degradation by heat from the lamps.

A number of polycrystalline Solarex MXS60 PV panels are available for use in the laboratory. Their dimensions are 1105mm by 503mm and the dimensions of the silicon area (with only PV cells) are approximately 1040mm by 464mm. To uniformly illuminate such an area, an array of 13 by 6 lamps is needed, i.e. 78 in total. The cost for 78 lamps plus lamp holders is less than £400.

Taking into account the power rating of available power supplies, the lamps were divided into the following three sub-arrays: 5×6 , 3×6 , and 5×6 lamps. Four mirrors are placed on the interior walls of the solar emulator (see Fig 5-20), and two mirrors are placed to divide the sub-sections (see Fig 5-21).

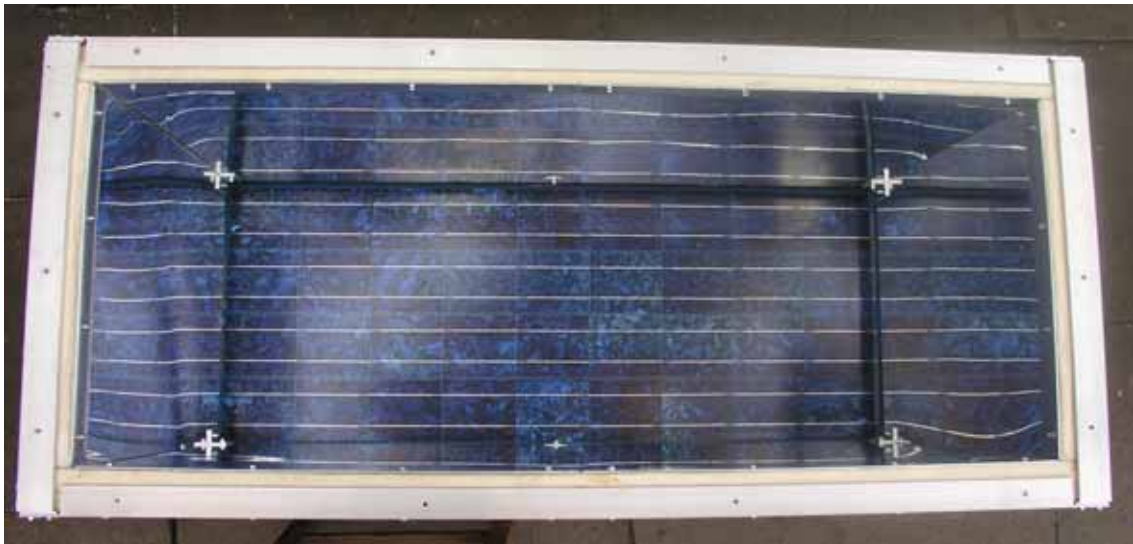


Fig 5-20: Interior of the frame of the solar emulator



Fig 5-21: The array of lamps and mirror dividers

- Temperature control

When all 78 lamps are at full power, they consume a total power of 3.9kW. However, 1000W/m² irradiance over an area of 0.56m² is expected, i.e., a radiometric output of only 556W. Therefore, there will be a lot of heat produced within the emulator and heat extraction becomes a major issue.

Fans are installed on the top of the solar emulator to extract excessive heat so as to maintain the operation temperature of the illuminated PV panel under certain value.

The selection of the fans for heat extraction is based on the heat flow equation:

$$Q = m \cdot C_p \cdot \Delta T \quad (5-6)$$

where Q is the dissipated heat, m is the mass flow rate through the fans, C_p is heat capacitance of air (4.1~4.2kJ/kg·K), and ΔT is the permitted temperature rise.

The mass flow rate can thus be calculated as

$$m = \frac{Q}{C_p \cdot \Delta T} = \frac{5kW}{4.19kJ/(kg \cdot K) \times (40 - 20)K} = 0.06kg/s \quad (5-7)$$

With an air density ρ of approximately 1.15kg/m³, the air flow rate \dot{q} is then found as

$$\dot{q} = \frac{m}{\rho} = \frac{0.06kg/s}{1.15kg/m^3} = 50l/s \quad (5-8)$$

Papst axial fans of type 4312MV were selected for the following reasons: 1) flow rate per fan of 29.7l/s, i.e. only two are required; 2) low noise (40dB); 3) variable speed operation with temperature sensors; 4) maximum operation temperature of 65°C.

As shown in Fig 5-22, two 4312MV fans were installed in the top of the solar emulator to extract the heat from the lamps; a third one is placed underneath the PV panel to reduce its temperature. The frame of the solar emulator was constructed using aluminium angles and sheets to reduce the weight. The lamp holders were installed onto a metal mesh so that hot air can rise through it and is then extracted by the top fans. To stop the mesh from sagging due to the weight of the lamps, reinforcement bars made from aluminium angles were installed lengthwise on top of the mesh. A similar reinforcement has been provided at the bottom frame of the emulator so that it can support the weight of the PV panel under test. Fireboards were placed inside the solar emulator to ensure safe heat

insulation. The underside of the emulator is left open and gaps between the sides and the PV panel are provided to promote the flow of cooling air.



Fig 5-22. Photo of the solar emulator assembly

5.5.1.2 Electrical design

Taking into account the power rating of available power supplies, the lamps were divided into three sub-arrays. From left to right, there are 5×6 (A), 3×6 (B), and 5×6 (C) lamps for the sub-arrays. They are powered by two 3kW ($300\text{V} \times 10\text{A}$) DC power supplies and a 1kW ($20\text{V} \times 50\text{A} \sim 60\text{V} \times 18\text{A}$) unit.

For sub-arrays A and C, two adjacent lamps are connected in parallel and 15 pairs are then connected in series. Therefore, when operating at full power, the terminal voltage of each sub-array will be 180V and the total current 8.3A.

For sub-array B, 9 lamps are in parallel forming a group, and two of such groups are then connected in series. When operating at full power, the terminal voltage of this sub-array will be 24V and the total current 37.5A.

The wires from each lamp holder were extended and marshaled to a terminal box which is mounted at the back the solar emulator as shown in Fig 5-23. Each wire was carefully labeled so that the connection of lamps can be changed at the terminal box in the future.



Fig 5-23. Wiring and the terminal box

5.5.2 Testing the Solar Emulator

5.5.2.1 Test of the irradiance distribution

The irradiance level at the PV panel was measured when all the lamps were operating at full power. It was found that the achievable irradiance level was much higher than

expected $1000\text{W}/\text{m}^2$. The discrepancy was mainly because the calculation using the Matlab program was based on the radiometric data measured by the CM5 pyranometer under a single halogen lamp. The irradiance distribution of a single lamp is not uniform; moreover the sensor area of the pyranometer is relatively large. Therefore, the obtained radiometric distribution data of the lamp is not very true. The photodiode irradiance detector was then re-calibrated against the CM5 pyranometer, the result of which is $4.4556\text{V}=1000\text{W}/\text{m}^2$ for the photodiode detector.

Using the photodiode detector, the irradiance distribution was obtained as shown in Fig 5-24. The power supplies for lamp sub-arrays A & C are set at a voltage of 152V with a current of 7.4A. And the power supply for sub-array B is set at a voltage of 21.4V with a current of 33.7A. The PV panel consists of 4×9 cells. The photodiode detector was placed onto 9 spots of each cell to take the measurements. The x and y axes correspond to the location of these spots (12×27 measuring spots). The z axis is the reading of the detector,

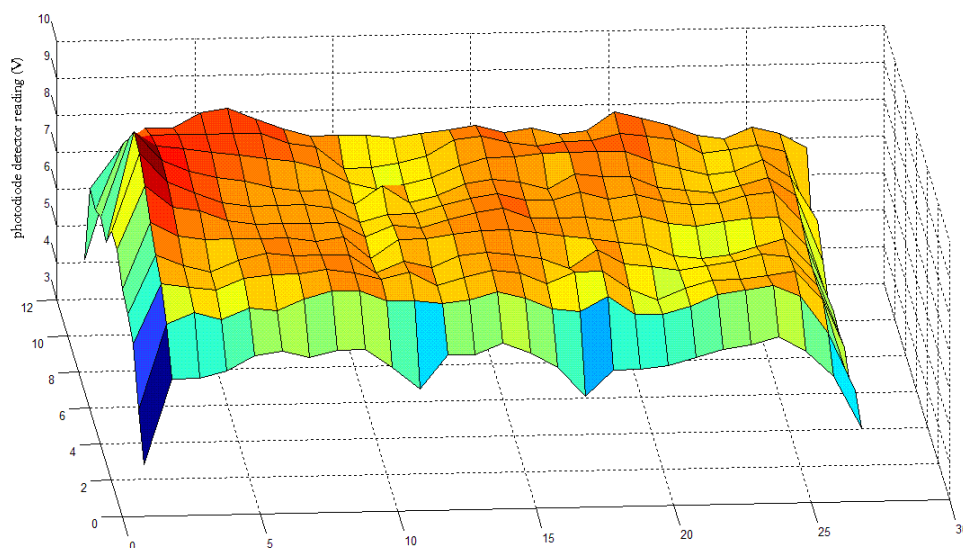


Fig 5-24. Measured irradiance distribution of the solar emulator

which has the corresponding relationship of $10V=1000W/m^2$.

It can be seen from Fig 5-24 that the largest deviation of irradiance level occurs at the edges. This is because a) the frame of the constructed solar emulator was slightly smaller than needed so that the mirrors at the edges was shadowing a small part of the PV cell edges; b) the mirrors are not all way down to the panel due to the essential gap for the cooling air flow; c) the mirrors were glued onto the fireboards and they are not perfectly flat.

Except at the edges, the other parts of the PV panel have very similar irradiance levels. Moreover, for each PV cell, it is the integrated irradiance level across the whole cell that determines its photocurrent. So the deviation of the irradiance level within a relatively small area (e.g. on the edges) will not greatly affect the photocurrent of the cell. Therefore, the uniformity of the irradiance distribution of the constructed solar emulator is likely to be within 10%.

5.5.2.2 Test of partial shading simulation

Fig 5-25 shows an characteristic of MSX60 PV panel under a partial shading condition created by the solar emulator, with three local maxima. More testing results will be shown in Chapter 6. Therefore, the solar emulator provides controllable testing conditions for the study of MPPT algorithms especially when dealing with partial shadings.

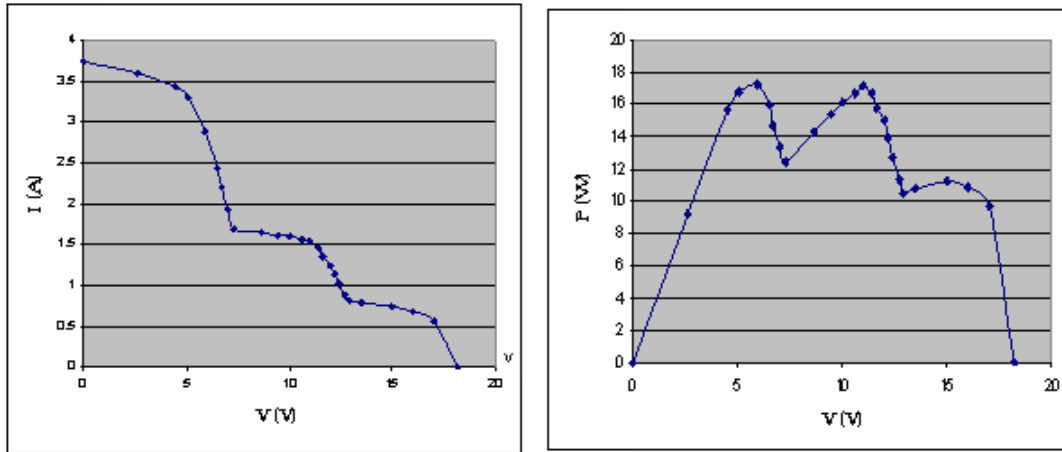


Fig 5-25. Characteristics of the PV panel under partial shading conditions

Left: I-V characteristic, right: P-V characteristic

5.6 Conclusions

After intensive investigation, a controllable steady-state solar emulator has been constructed using an array of Halogen lamps together with mirrors. Surrounding mirrors are used to create infinite light source so that uniform distribution of illumination to the PV panel(s) can be achieved. Partitioning mirrors are used to divide strings of PV cells so that different illumination levels can be controlled to create partial shading conditions. This prototype emulator is able to illuminate a large area (currently accommodating a PV panel of the size of 0.5m^2) and is affordable (approximately 1000 pounds) by a university. It is a very useful facility for the experiments in Chapter 6.

Chapter 6. Implementation of Intelligent MPP Tracking

Using a DSP controller

6.1 Introduction

Fig. 6-1 shows the block diagram of the new experimental set-up used in this work.

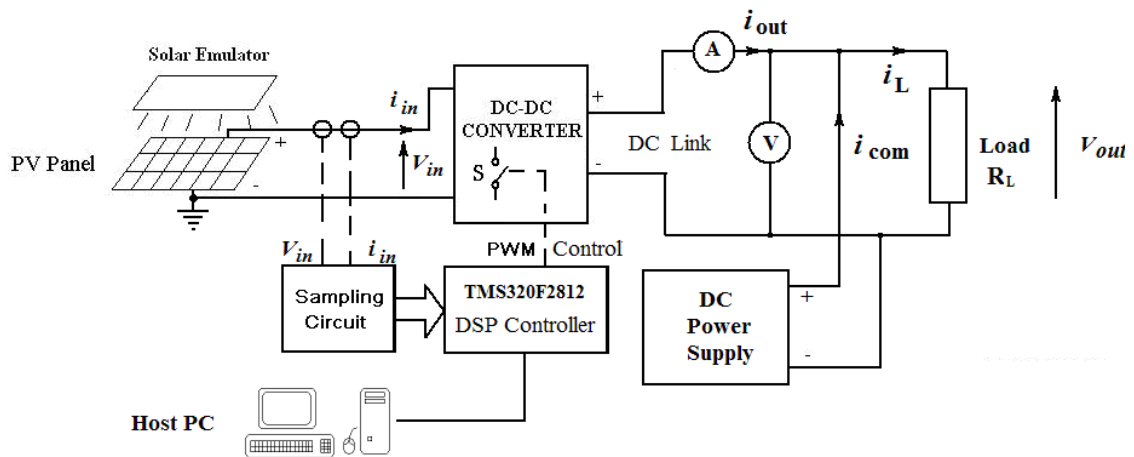


Fig 6-1. Hardware block diagram

(More details can be found in Appendix 8 and 9.)

The PV panel (BP Solar MSX60**), illuminated by the solar emulator described in Chapter 5, feeds power into the DC-DC converter. The open-circuit voltage of the PV panel under STC is 21.1 V, and the short circuit current is 3.8 A. This arrangement substitutes the original PV emulator using a Thevenin Source as described in Section 1.4.

** The MSX60 panel consists of two independent strings of 18 cells each. For the investigation under partial shading conditions, access was made to the middle of each string, so that the panel can be connected as 4 strings of 9 cells in series.

The original controller board of the DC-DC converter consisted of a TMS320C50 DSP starter kit, a Xilinx XC4003 FPGA and ADC converters. This has now been replaced with a new controller board based on a TMS320F2812 DSP starter kit, which provides on-chip PWM generation and integrated ADC. This DSP is faster and more powerful, and will be described in detail in Section 6.2. The host PC runs the software development package for the DSP.

The output of the DC-DC converter was originally connected to a grid-connected GD4000 inverter, which maintained the DC link voltage at 650V nominal (see Section 1.4). However, this arrangement is not suitable for experimentation with a single PV panel. The reasons are: Firstly, the output voltage of the PV panel is very low ($V_{OC}=21V$) and the DC-DC converter cannot step this voltage up to the required DC link voltage. Secondly, the inverter produced a lot of electrical noise causing problem in the sampling at the low power level of the PV panel (60Wp).

The inverter was therefore replaced by a DC power supply (300V/10A TCR Power Supply from Electronic Measurements Inc.) in parallel with a load resistor R_L (see Fig 6-1). Because the DC power supply cannot absorb power, to maintain the output voltage (DC link voltage) V_{out} constant, the load resistor R_L must be capable of consuming all the power generated by the PV panel. That is:

$$(V_{out})^2/R_L > \text{maximum output power } P_{max} \text{ of the PV panel.}$$

Considering the available step-up ratio of the DC-DC converter and the output voltage of the PV panel, V_{out} is set to 200V. Using the rated power of the panel (60W), the load

resistance must have a value: $R_L < 667 \Omega$. A variable power resistor of 800Ω (set to approx. 630Ω) is used in the experiment.

When the PV panel and converter start to deliver power, the DC power supply simply backs off but maintains the DC link voltage at 200V. The total power dissipated in R_L remains constant.

The experimental waveforms are recorded using a four channel Tektronix TDS7054 digital phosphor oscilloscope (DPO). The bandwidth is 500 MHz, and the sample rate is 5GS/s. It is able to record and store experimental waveforms/data in different file formats. The record length is 5,000 points, and the vertical resolution is 8-bits. The recorded data files can be further analysed using Matlab or Excel.

6.2 TMS320F2812 Digital Signal Processor

The F2812 DSP is a high performance 32-bit fixed-point DSP. It is a member of the TMS320C28xx DSP generation, which is designed to meet a wide range of applications, such as digital motor control (DMC), digital power supply and other embedded control systems. The F2812 DSP is able to generate 16 PWM signals and is equipped with many on-chip peripherals including ADCs, which makes it suitable for control of the PV system. The main features are [83]:

- 32-bit CPU and 6.67 ns instruction cycle (150 MHz). It is suitable for implementing complicated control algorithms for PV systems.
- 2 event managers (EV) provide 16 PWM signals to the power converter. Up to 8 PWM signals can be generated simultaneously by each EV: three independent pairs

(six outputs) by the three full-compare units with programmable deadbands, and two independent PWMs by the general-purpose timer compare units.

- Three 32-bit CPU timers.
- An on-chip 12-bit Analog-to-Digital Converter (ADC) module with 16 multiplexed input channels. The conversion time (including sample time) for each channel is 80 ns (at 25 MHz ADC clock), hence much faster than the MAX422 ADC module (333 kHz) used on the original controller board.
- 128 kb on-chip Flash EEPROM memory module allows the F2812 DSP to operate in the microcomputer mode. In the microcomputer mode, the F2812 DSP can run without the JTEG connection to the host PC.
- Code Composer Studio (CCS). CCS is the development package for the DSP, run on a PC. CCS extends the basic code generation tools with a set of debugging and real-time analysis capabilities. It provides a compiler, assembler, and linker to allow development of C or Assembly language code for the DSP. Additionally, it can record data in real-time mode for subsequent analysis.

6.3 Intelligent MPPT Controller with Partial Shading Identifier

The P&O MPPT algorithm with partial shading detection, proposed in Chapter 4, has been implemented using the TMS320F2812 DSP (see Appendix 10 for the complete DSP code). Fig 6-2 to Fig 6-6 show the program flowcharts.

Fig. 6-2 illustrates the main loop. After initializing all the parameters, the program runs the background routine (endless super loop) with timer interrupt service routine (ISR).

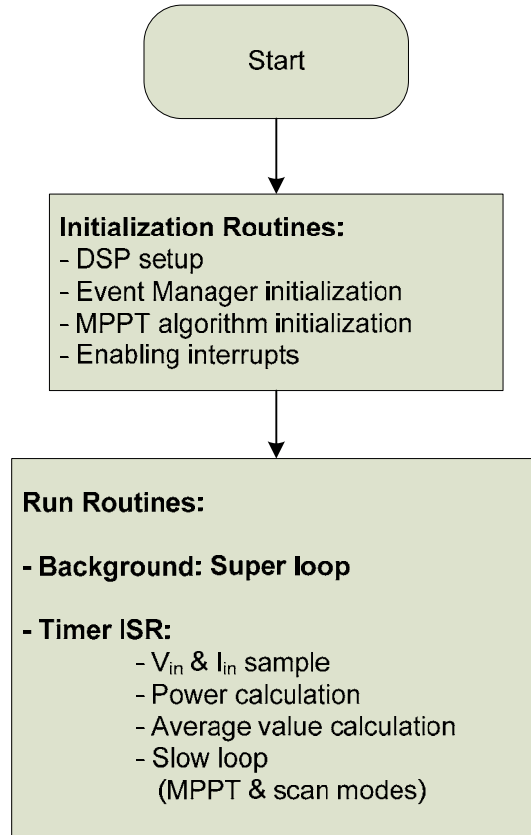
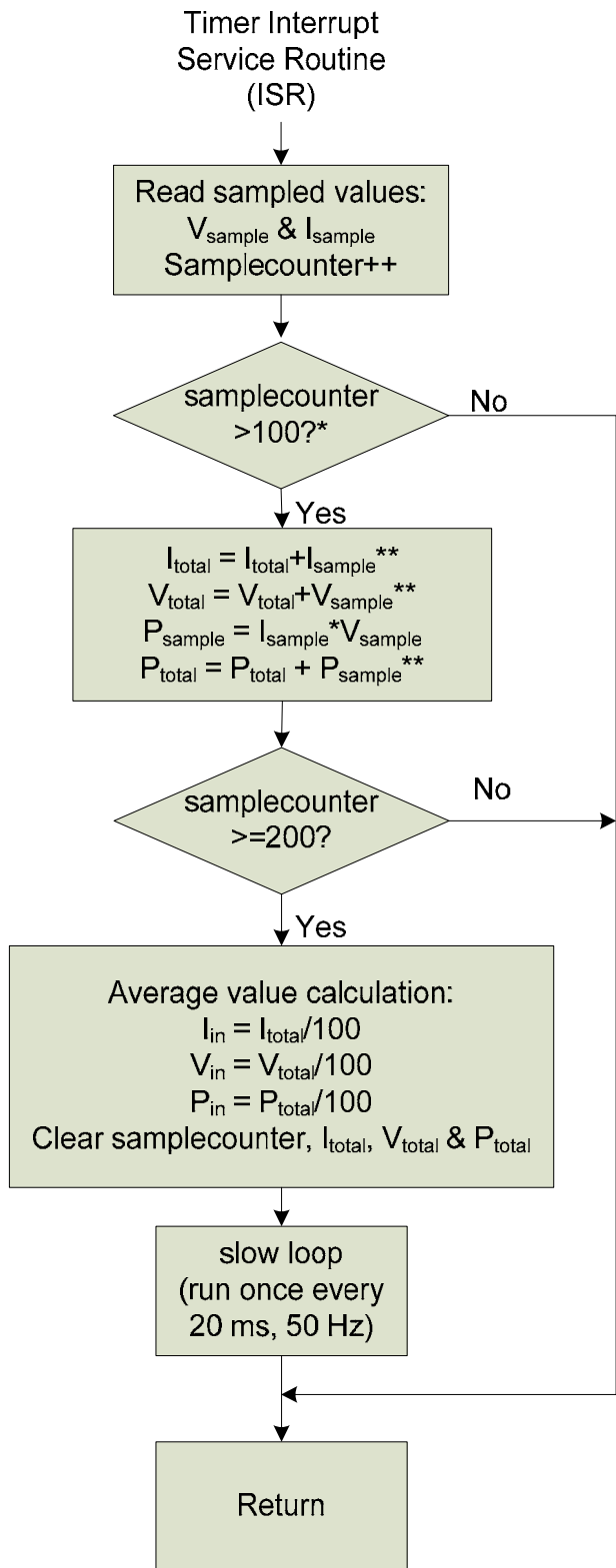


Fig 6-2 Main loop

Every 100 μs (10 kHz), the program enters the timer interrupt service routine. Fig. 6-3 shows the ISR program flowchart. The input voltage and current of the DC-DC converter are sampled every 100 μs . However, it was found that the output voltage of the DC power supply at the load side of the DC-DC converter contained a 100 Hz ripple (peak-to-peak is approx. 1% of the DC voltage) caused by the grid (shown in Fig 6-4). To eliminate the effect of this ripple, the perturbation period for the P&O method is chosen to be 20 ms (50 Hz). The program waits 10 ms for the voltage and current to settle. Then the sampled



Note:
*samplecounter=100,
means 10ms has elapsed.

**

$$I_{total} = \sum_{samplecounter=101}^{200} I_{sample}$$

$$V_{total} = \sum_{samplecounter=101}^{200} V_{sample}$$

$$P_{total} = \sum_{samplecounter=101}^{200} P_{sample}$$

Fig 6-3. Timer ISR Loop

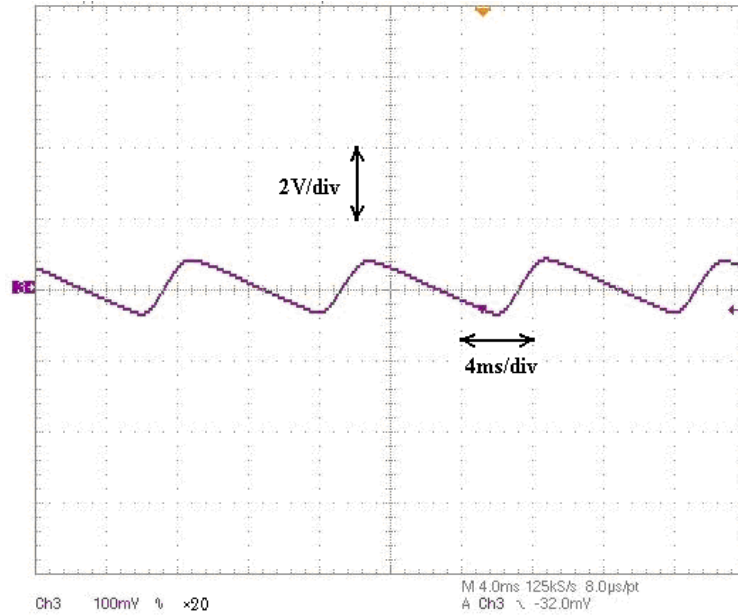


Fig 6-4. 100 Hz ripple of the output voltage

data within the latter 10 ms are averaged and stored. After that, the program runs a “slow loop” (as shown in Fig 6-5), which includes two operational modes: MPPT mode and Scan mode.

In MPPT mode, the P&O MPP tracking algorithm is implemented; the flowchart for this is shown in Fig 6-6. After an output power analysis process, the algorithm identifies if the PV system is operating at the MPP. If the operating point (OP) is changed from non-MPP status to MPP status, a judgment is made on potential partial shading, based on the deviation of the voltage from the standard trajectory (see Section 4.2). If partial shading is suspected, the algorithm enters the scan mode. If the OP remains at MPP status, the algorithm carries out the judgment every 1 minute.

Once the result of the above judgment indicates the existence of partial shading, the program enters the wide-range scan process (see Fig 6-7 for the flowchart). The power of

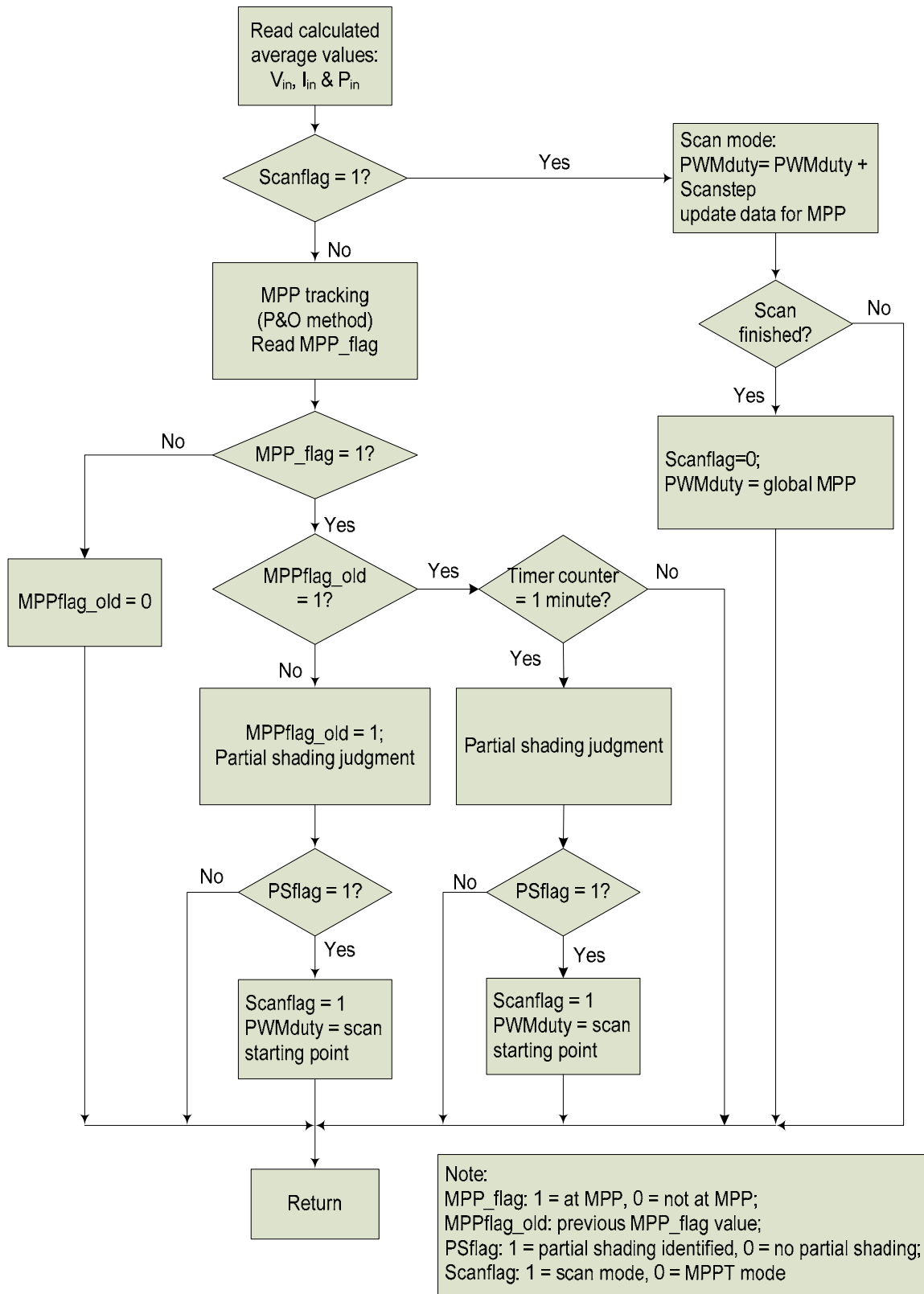


Fig 6-5. Slow Loop

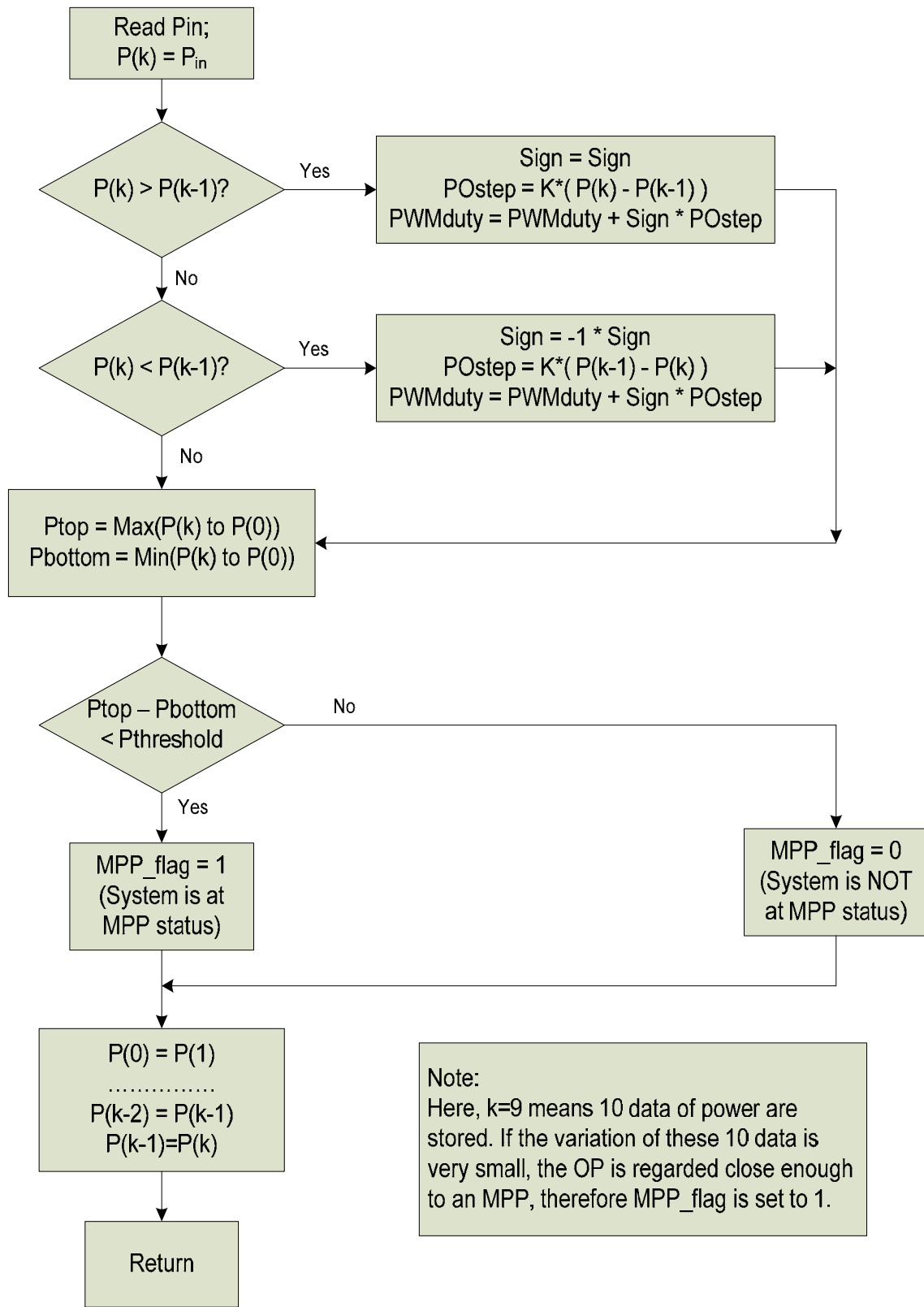


Fig 6-6. MPPT loop

every scanned point is compared, and the PWM duty is then set at the global maximum power point at the end of the scan mode.

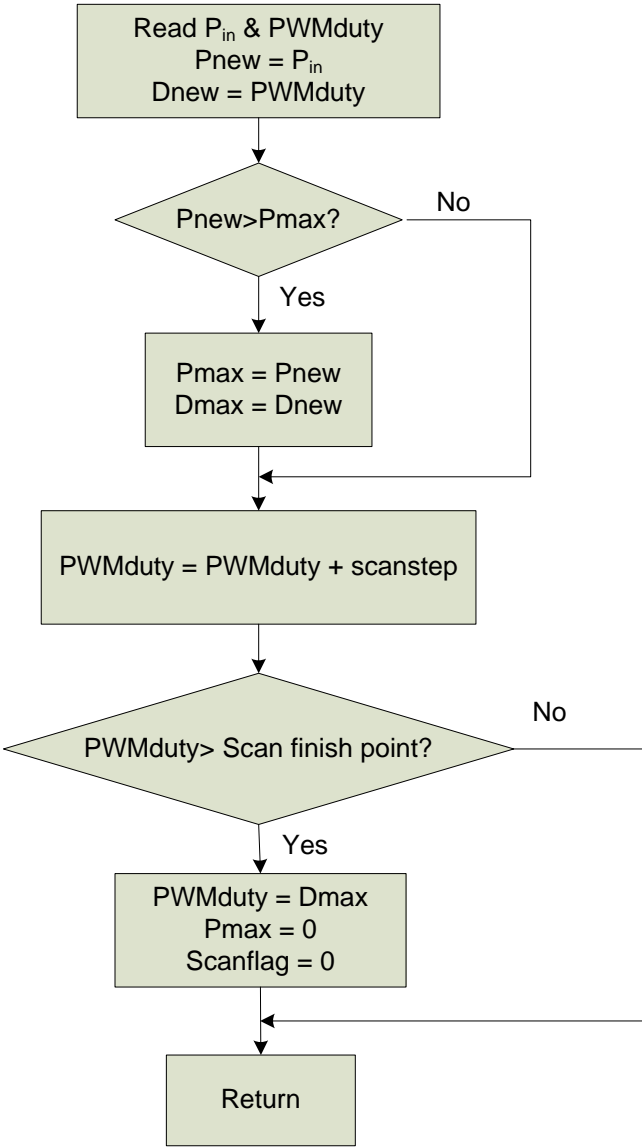


Fig 6-7. Scan loop

6.4 Testing and Performance

6.4.1 Measurement of Power-Voltage Curves under Partial Shading Conditions

The four strings of the PV panel under test are all connected in series with a bypass diode across each string. Thin wooden strips were cut to the length of a PV string and a width of approximately $\frac{1}{4}$ of that of a PV cell (square). They are used to manually cover the PV strings so that different patterns of partial shading can be created. If a PV string is not covered, it receives full irradiance, which is coded as level “4”. When a PV string is covered by 1, 2, or 3 wooden strips, the irradiance level it receives drops to “3”, “2”, or “1” respectively, compared to the full intensity “4”. These codes will be used to describe shading patterns. For example, if one PV string is covered by 2 wooden strips, another string is covered by 1, and the other two strings are not covered, the shading pattern will be coded as [2344].

Using only the scan loop of the implemented algorithm, data of the current, voltage and power of the PV panel under different shading patterns can be recorded and stored in the oscilloscope. The data can then be manipulated in Matlab afterwards. Fig 6-8 shows a group of measured P (V) curves under various shading conditions with reference to the measured standard MPP trajectory (see Section 4.2).

The trajectory does not have quite the same shape as the theoretical one because of the effect of a changing panel temperature with irradiance level. However, it is still obvious that the existence of a significant local MPP on the left-hand-side of the trajectory leads to a large deviation of $MPP_{(OC)}$ (the first local MPP from open-circuit, see Section 4.3)

from the trajectory. The higher the left-hand-side peak is, the more the deviation of $MPP_{(OC)}$. This confirms the theoretical behaviour, described in Chapter 4.

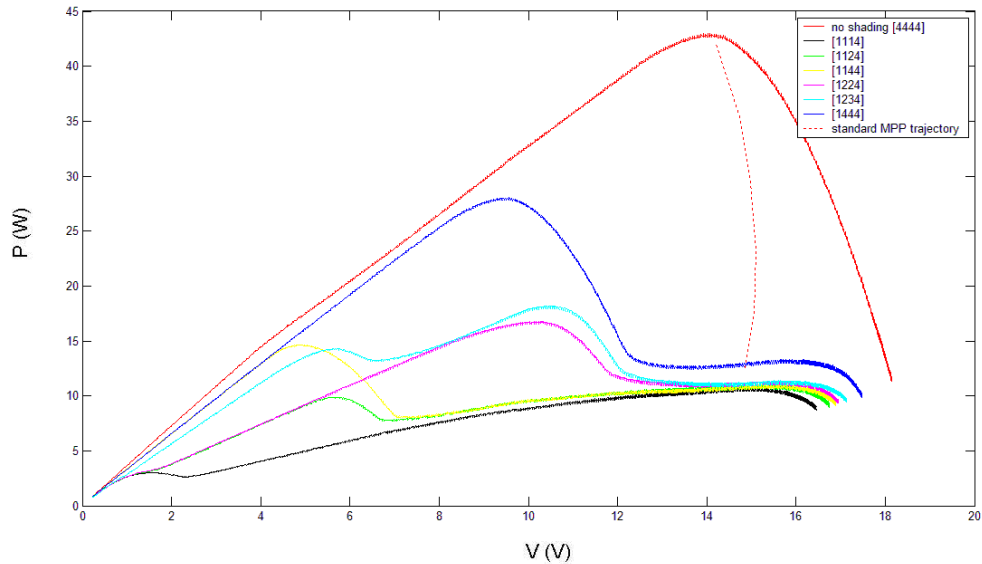


Fig 6-8. P (V) curves under various shading conditions

6.4.2 Test of the Proposed MPPT Algorithm with Partial Shading Identifier

The proposed MPPT algorithm was implemented and tested under different shading conditions using the constructed solar emulator.

Firstly, the algorithm was tested under partial shading conditions with 2 local MPPs.

Test A:

A transition from no shading to a shading pattern of [1444] was made by manually sliding 3 wooden strips, which are bound together, onto one of the PV strings. Fig 6-9

shows the transient waveforms captured by the oscilloscope, and Fig 6-10 plots the transient process using the data exported from the oscilloscope to Matlab.

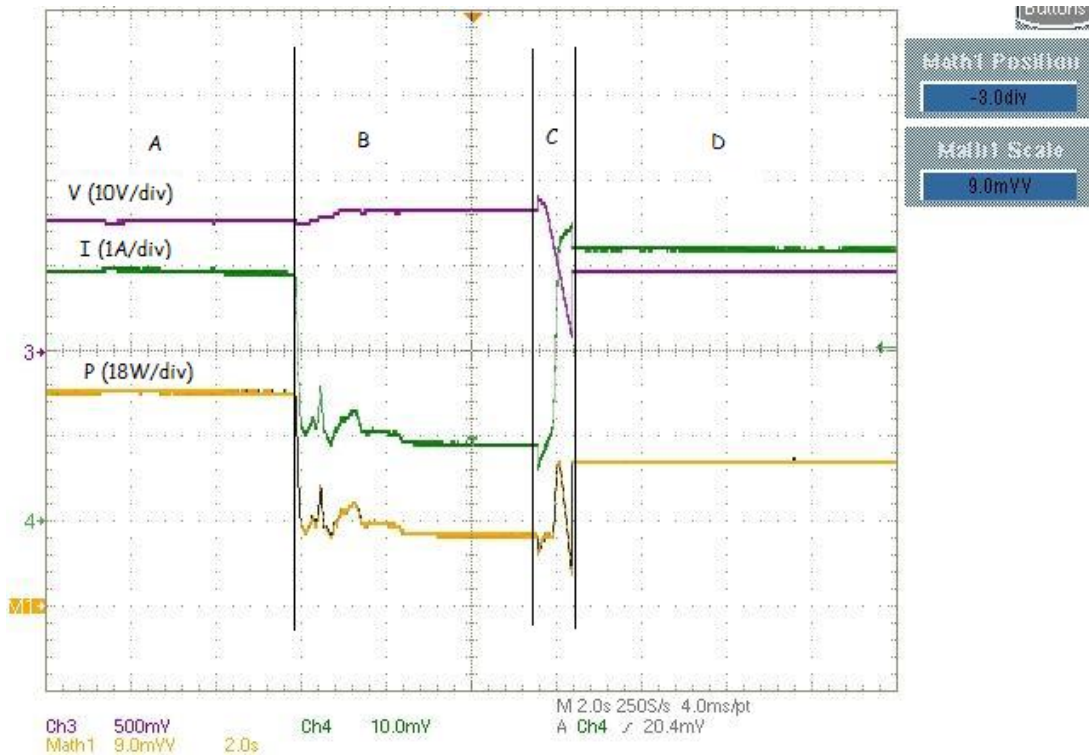


Fig 6-9. Waveforms during a transition from no shading to [1444] shading pattern

Interval A in Fig 6-9 shows operation under no shading. Interval B shows the transient waveforms during the transition to partial shading where the P&O method finds a local MPP which is not the global MPP (point P1 in Fig 6-10). Since this MPP is not adjacent to the standard MPP trajectory, the algorithm decides to carry out a global scan, as shown in interval C. Finally the global MPP is established and the operation point settles at the true MPP as shown in interval D (point P2 in Fig 6-10).

In this test, the proposed MPPT algorithm identified the occurrence of partial shading, therefore carried out a wide-range scan, and finally set the operation point at the true

MPP. Compared to OP P1 (15.2 W) originally found by P&O method, the power at OP P2 (30.8 W) has more than doubled.

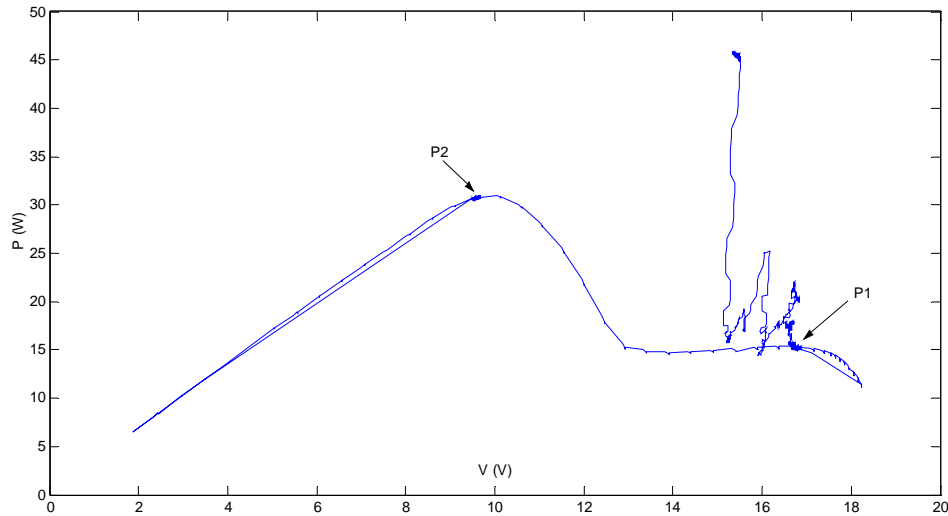


Fig 6-10. P (W) plot of MPP tracking process during a transition from no shading to [1444] shading pattern

Test B:

By binding two wooden strips together and sliding them onto a PV string, a transition from no shading to a shading pattern of [2444] was created. The experiment results are shown in Fig 6-11 and Fig 6-12. The transient process is similar to the above one and the algorithm manages to track the true MPP after successfully identifying partial shading.

Test C:

A very different shading pattern [1234] was also tested, which resulted in more local maxima. Due to the difficulty of creating pattern [1234] instantly, this experiment was carried out under static shading conditions, i.e. pattern [1234] was first created and the system was manually controlled to operate at a point away from the global MPP. As



Fig 6-11. Waveforms during a transition from no shading to [2444] shading pattern

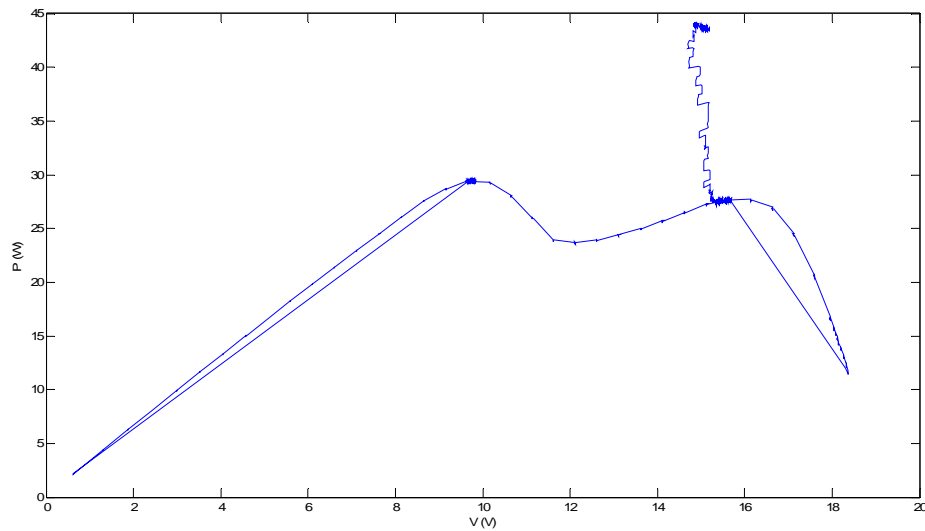


Fig 6-12. P (W) plot of MPP tracking process during a transition from no shading to [2444] shading pattern

shown in Fig 6-13, under shading pattern [1234], three local maxima exist within the operation range. The system initially operates at a lower local maximum as shown in Fig 6-14 (interval A). Then the algorithm identifies the existence of partial shading, therefore a global scan is initiated as shown in interval B. The global MPP is determined and the system settles at the true MPP as shown in interval C.

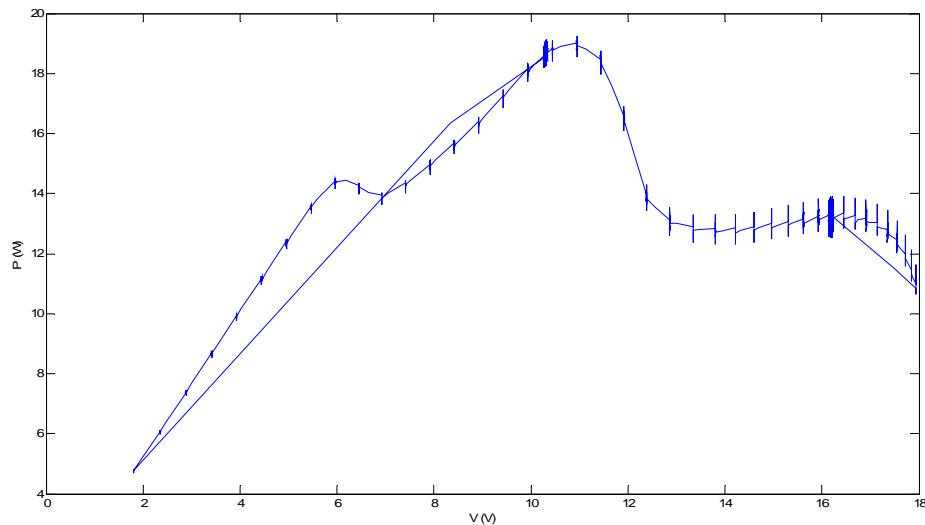


Fig 6-13. P (V) plot of the transition from a local MPP to the global MPP under [1234] shading pattern

It can be noticed that there are many “spikes” on the curve in Fig 6-13, which can also be seen in Fig 6-10 and Fig 6-12. One of the “spikes” in Fig 6-13 is zoomed as shown in Fig 6-15 (a). It can be seen that the “spike” actually consists of a lot of sampled points. The voltage waveform of these points is drawn in Fig 6-15 (b), where it can be seen that the voltage contains a 100 Hz ripple. This data is not sampled by the MPPT algorithm, but by the oscilloscope (sample interval 0.8 ms, i.e. sample rate 1.25 kHz). This plot confirms that it is necessary to average the calculation every 20 ms and that the algorithm needs to wait 10 ms for the waveforms to settle after each perturbation.

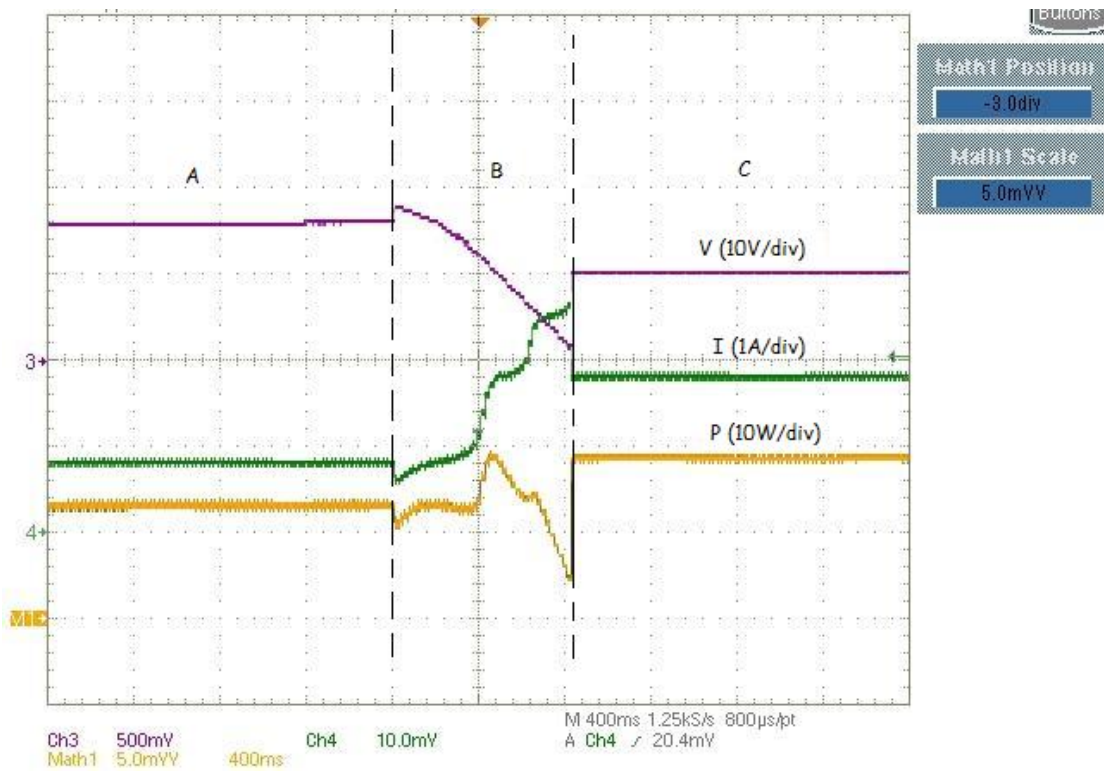
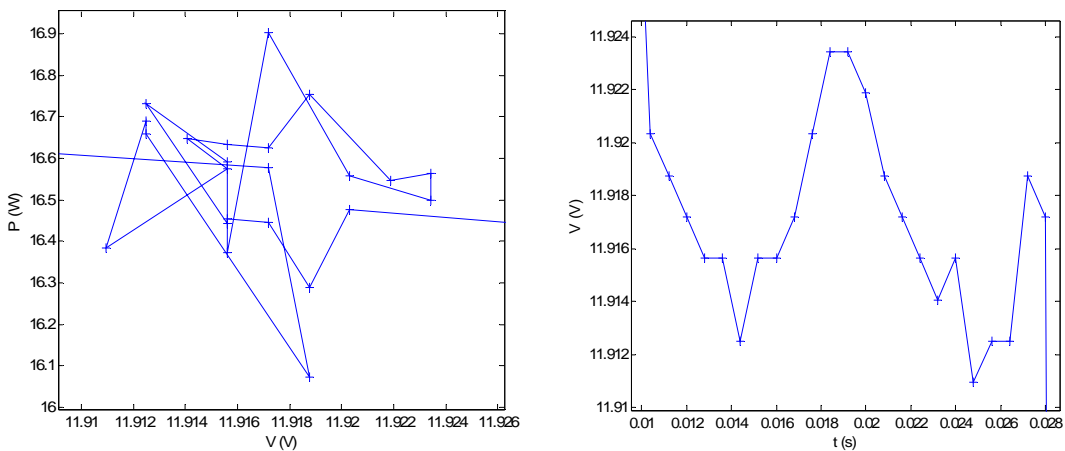


Fig 6-14. Waveform of the transition from a local MPP to the global MPP under [1234] shading pattern



(a) Zoomed “spike” in the P (V) curve (b) Zoomed “spike” in the Voltage waveform

Fig 6-15. A zoomed “spike”

6.5 Conclusions

An experimental indoor set-up of a PV system has been constructed based on a solar emulator and a (modified) PV panel. With the constructed solar emulator, various partial shading conditions are created for experimentation. A new controller board has been developed based on a TMS320F2812 DSP, which makes the implementation of the proposed intelligent MPPT algorithm and future update convenient. The original inverter at the output of the DC-DC converter is replaced by a DC Power Supply in parallel with a suitable load resistor, which is a simple alternative for low power testing.

The proposed MPPT algorithm with partial shading identification is implemented and verified by tests. Most conventional MPPT algorithms do not have a wide-range scan mechanism; therefore, under partial shading conditions, they tend to operate at a non-global MPP, potentially causing a large energy loss. Compared to this, the proposed algorithm can always track the global MPP hence is much more efficient under partial shading conditions. For example, there is accumulatively one hour of partial shading each day for a 1kW PV system. As in Test A (refer to 6.4.2), approximately a 60W PV panel has a Global MPP of 30W and a local MPP of 15W. To scale up to a 1KW system, it can produce only 250W of power using these conventional MPPT algorithms. However, the proposed algorithm can produce 500W. Therefore, there is an energy yield improvement of $(500-250) \text{ W} \cdot 1\text{h} = 0.25\text{kWh/day}$, which means 91.25kWh/year and 1825kWh if the PV system operates for 20 years.

Some other MPPT algorithms do carry out a global scan every certain period, e.g. every minute, to prevent operating at a non-global MPP. Such scans waste energy when the PV

system is already operating at the true MPP. Compared to this, the proposed algorithm actually knows when partial shading occurs, and then carries out a global scan. However, when there is no significant partial shading, it only carries out a judgment instead of a global scan at a set interval thus avoiding potential energy loss. For example, a 1kW PV system scans every minute and each scan takes 1 second. When there is no partial shading occurrence, the system spent $24\text{h} \times 1/60 = 0.4\text{h}$ each day doing useless scans. During one full-range scan of the PV characteristic, there is approx. 40% energy loss, which can be established by simulation or calculation. Therefore, for the 1kW system, there is an energy loss of $0.4\text{h} \times (40\% \times 1\text{kW}) = 0.16\text{kWh/day}$, which means 58.4kWh/year and 1168kWh over 20 years. On the contrary, the proposed algorithm can save 1168kWh over 20 years compared to these MPPT algorithms.

Chapter 7. Original Contributions, Conclusions and Future Work

This chapter firstly summarizes the major conclusions drawn from this work. Then the original contributions are described and claimed. Finally future work is suggested.

7.1 Original Contributions

- **Effect of PV dynamic on MPPT:** The presence of the capacitance in PV cells has so far only been investigated for studying loss mechanisms or flash characterization of PV cells. However, in this work, it has been shown that the presence of this capacitance may cause MPP tracking algorithms to deviate from the true MPP. This effect has been studied through simulations and experiments, and it has been shown that the PV dynamics may confuse MPPT algorithms if fast sampling and tracking are used. On one hand, fast switching (high frequency) is often implemented to reduce the size and weight of transformers in converters and to realize fast tracking. On the other hand, as investigated in this study, fast tracking may cause operation deviation from the true MPP due to the dynamic effect of the PV capacitance. Therefore, it is recommended that tracking speed is compromised and sampling is averaged to reduce the dynamic effect. Also it has been established that a good quality component analyzer can be used to directly measure the PV capacitance under illuminated conditions.
- **Standard Trajectory of Maximum Power Point:** It has not been reported that there is a trajectory linking the maximum power and the operating voltage at the maximum power point under idealized conditions (no series or parallel resistance). An equation has been derived in this work to describe this standard trajectory.

This standard trajectory can be used to fast track maximum power points under normal conditions as well as to identify partial shading occurrence.

- **Partial Shading Identification:** Partial shading conditions have been a big problem for existing converters with MPPT. So far there is no method to identify the occurrence of partial shading. Therefore, MPPT algorithms either do a global scan at a certain rate (during which some energy is lost), or have no global scan mechanism. When partial shading occurs, the tracking efficiency is low and energy is lost. In this work, it has been established that by monitoring the deviation of operating point from the standard trajectory of maximum power point, the occurrence of partial shading can be identified and a consequent global scan can be initiated. A novel control algorithm based on this finding has been proposed and verified by experiment.
- **Solar Emulator:** Commercial steady-state solar simulators are usually very large apparatus, but only illuminate a small area (a few square inches). They are very expensive (thousands of pounds) and are normally used in laboratories to test prototype PV cells/materials. They do not provide a facility to emulate partial shading conditions. A controllable solar emulator has been constructed using an array of Halogen lamps together with mirrors. Surrounding mirrors are used to create infinite light source so that uniform distribution of illumination to the PV panel(s) can be achieved. Partitioning mirrors are used to divide strings of PV cells so that different illumination levels can be controlled to create partial shading conditions. This prototype emulator is able to illuminate a large area

(currently accommodating a PV panel of the size of 0.5m²) and is affordable (approximately 1000 pounds) by the university.

- **Irradiance Detector:** A photodiode operating in the photovoltaic mode can be used as an irradiance measuring device. An irradiance detector using a photodiode has been constructed which is good to use for a solar emulator due to its small size.

7.2 Overview of Conclusions

- **Dynamic Effects on MPPT algorithms:** Dynamic effects due to the capacitance of PV cells and inverters should be taken into account when designing fast tracking MPPT algorithms. The timing of sampling is also important. It is therefore suggested that sampling speed shall not be too fast and that averaging or filtering is adopted in sampling.
- **Standard trajectory of Maximum Power Point:** There is a trajectory linking the maximum power and the operating voltage at the maximum power point under idealized conditions (no series or parallel resistance). Under normal conditions the operating point of an MPP tracker should locate on this trajectory.
- **Identification of partial shading:** The operating local maxima will deviate from the standard trajectory under partial shading conditions. The more severe the shading is, the more deviation there is. Therefore, by monitoring the deviation of operating point from the standard trajectory the occurrence of partial shadings can be identified.

7.3 Future Work

- Further investigation and study need to be carried out on the identification and compensation of the PV Capacitance to avoid deviation from the true MPPs due to the dynamic effect when fast tracking is used.
- The prototype solar emulator can be resized and made more flexible so that it can accommodate PV panel(s) of different sizes or multiple panels. The heat removing facility also needs improving so that constant panel temperature can be achieved to reduce its impact on PV characteristics.
- Further investigation and experimentation can be carried out on the power-voltage characteristics so that the proposed method to identify partial shading occurrence is more accurate and practical. For example, the impact of temperature variation or the characteristics for different materials.
- A self-learning mechanism of the standard trajectory can be included in the proposed MPP tracking algorithm, so that the effect of panel temperature variation and degrading can be compensated.
- Soft-switching other EMC design can be implemented to reduce the noise from the converter and inverter in the existing system, so that the sampling and control can be faster and more accurate and effective.

Appendices

Appendix 1. Matlab model of a PV source with only 1st quadrant characteristics

```
function o = PVmodel(i)
```

```
global A;  
global k;  
global T;  
global ns;  
global np;  
global Is;  
global q;
```

```
v=ns*A*k*T*log((i(2)-i(1)/np)/Is+1)/q;  
end
```

```
o=v;
```

Appendix 2 Matlab model of a PV source with 2nd quadrant characteristics

```
function o = PVmodel(in)
```

```
v=in(1);  
Iph=in(2);
```

```
global i;  
global M;  
global T;  
global np;  
global ns;  
global A;  
global k;  
global q;  
global Is;  
global Vbr;  
global aaa;  
global inf;
```

```
if v>0  
    M=1;  
elseif v<=Vbr  
    M=inf;  
else  
    M=1/(1-(v/Vbr)^aaa);  
end
```

```
i=np*(Iph-Is*exp(q*v/(ns*A*k*T)-1))*M;  
if i<0  
    i=0;  
end
```

```
o=i;
```

Appendix 3 Matlab model of a PV source with bypass diodes

```
function o = PVmodel(i)
```

```
global A;  
global k;  
global T;  
global ns;  
global np;  
global Is;  
global q;
```

```
if (i(2)-i(1)/np)>=0  
    v=ns*A*k*T*log((i(2)-i(1)/np)/Is+1)/q;  
else  
    v=0;  
end
```

```
o=v;
```

Appendix 4 Matlab function program of the Perturbation & Observation MPPT algorithm

```
function o = PnOmppt(u)
%u(2) is voltage, and u(3) is current
```

```
global io;
global po;
global vo;
global vro;
global flag;
global vrn;
global dsign;
```

```
delta=0.2;
```

```
if u(1)>=0.5
    if flag==0
        vn=u(2);
        in=u(3);
        pn=vn*in;
        if pn>=po
            dsign=dsign;
        else
            dsign=0-dsign;
        end
        vrn=vro+dsign*delta;
        vo=vn;
        io=in;
        po=pn;
        vro=vrn;
    end
    flag=1;
end
```

```
if u(1)<0.5
    flag=0;
end
```

```
o=vrn;
```

Appendix 5 Matlab function program of the Incremental Conductance MPPT algorithm

```
function o = incmpp(u)
%u(2) is voltage, and u(3)is current
```

```
global d;
global io;
global po;
global vo;
global vro;
global flag;
global vrn;
```

```
delta=0.5;
```

```
if u(1)>=0.5
    if flag==0
        vn=u(2);
        in=u(3);
        di=in-io;
        dv=vn-vo;
        if abs(dv)<=0.00005
            if abs(di)<=0.00005
                vrn=vro;
            elseif di>0.00005
                vrn=vro+delta;
            else
                vrn=vro-delta;
            end
        end
    else
        didv=di/dv;
        iv=-in/vn;
        if didv==iv
            vrn=vro;
        elseif didv>iv
            vrn=vro+delta;
        else
            vrn=vro-delta;
        end
    end
    vo=vn;
    io=in;
    vro=vrn;
end
```

```
    flag=1;
end
if u(1)<0.5
    flag=0;
end
```

```
o=vrn;
```

```
*****
```

Appendix 6 Matlab function program of the MPPT algorithm based on Intrinsic Ripple

```
function o = mpp(u)
%u(2) is voltage, and u(3)is current

global d;           %dp/di
global io;          %current_old (previous sample)
global po;          %power_old
global vo;          %voltage_old
global flag;

if u(1)<0
    if flag==0
        pn=u(2)*u(3);           %power_new
        vn=u(2);                 %voltage_new
        in=u(3);                 %current_new
        if in>io
            d=(pn-po)/(in-io);
            vo=vn;
            io=in;
            po=pn;
        end
        if in<io
            vo=vn;
            io=in;
            po=pn;
        end
    end
    flag=1;
end
if u(1)>0
    flag=0;
end

o=d;
*****
```

Appendix 7 Matlab program for irradiance distribution calculation

```
load Measured50W24d.dat % measured irradiance distribution data of Osram IRC 50W,  
24 degree lamp
```

```
length=13; % numbers of measured data
```

```
h0=184.5; % measured h
```

```
Eo=13.80; %measured E@h0 =1380W/m2
```

```
XMAX = 3;
```

```
YMAX = 3;
```

```
resolution=10; % points between two lamps/ division within one dis
```

```
dis = input(' Input the distance between two lamps (mm) = ');
```

```
%distance = 1;
```

```
hei = input (' Input the height (mm) = ');
```

```
%normalisation
```

```
distance = 1;
```

```
height = hei*1.0/dis;
```

```
% No. of lit lamps (same No. for row & column)
```

```
more=4; %how many lamps more at each direction outside the displayed area
```

```
imax = floor(XMAX*1.0/distance)+1+more*2; % eg: imax=12, then 12*12=144 lamps
```

```
maxtheta = Measured50W24d(length, 1);
```

```
theta_minor_influence=maxtheta;
```

```
factor=h0*h0*100/(hei*hei); % factor to convert E at h from normalized height
```

```
minor_intensity=0.05*Measured50W24d(1, 2)*factor; %define the value that is less than  
1% of the centre intensity
```

```
%initialization of intensity of each illuminated points
```

```
for j = 1:(XMAX*resolution+1)
```

```
    for k = 1:(XMAX*resolution+1)
```

```
        result(j,k) = 0; %initialization
```

```
        lx(j,k) = (j-1)*0.1*dis;
```

```
        ly(j,k) = (k-1)*0.1*dis; %real coordinates of illuminated points
```

```
    end
```

```
end
```

```
for ix = 1:imax
```

```
    for iy = 1:imax
```

```
        xl = (ix-(more+1))*distance;
```

```
        yl = (iy-(more+1))*distance; %normalized coordinates of the centres of lamps
```

```
        for j = 1:(XMAX*resolution+1)
```

```
            for k = 1:(XMAX*resolution+1)
```

```
                x = (j-1)*0.1*distance;
```

```

y = (k-1)*0.1*distance; %normalized coordinates of illuminated points
r = sqrt((x-xl)*(x-xl)+(y-yl)*(y-yl));
theta = atan(r/height)/pi*180;
index=1;
theta1 = Measured50W24d(index, 1);
theta2 = Measured50W24d(index+1, 1);

if theta <= maxtheta
    while theta > theta2
        index = index + 1;
        theta1 = Measured50W24d(index, 1);
        theta2 = Measured50W24d(index+1, 1);
    end
    deltat = theta-theta1;
    result1 = Measured50W24d(index, 2);
    result2 = Measured50W24d(index+1, 2);
    result = (result1 + deltat*(result2-result1)/(theta2-theta1))*factor;
    if result < minor_intensity %if the intensity is less than 5% of the centre
intensity,
        if theta < theta_minor_influence
            theta_minor_influence=theta; %then the current theta is where minor
influence the lamp has on the calculated point
        end
    end
    result(j,k) = result(j,k)+ result;
end
end
end
end
end
end

surf(lx, ly, result); %plot the 3D figure

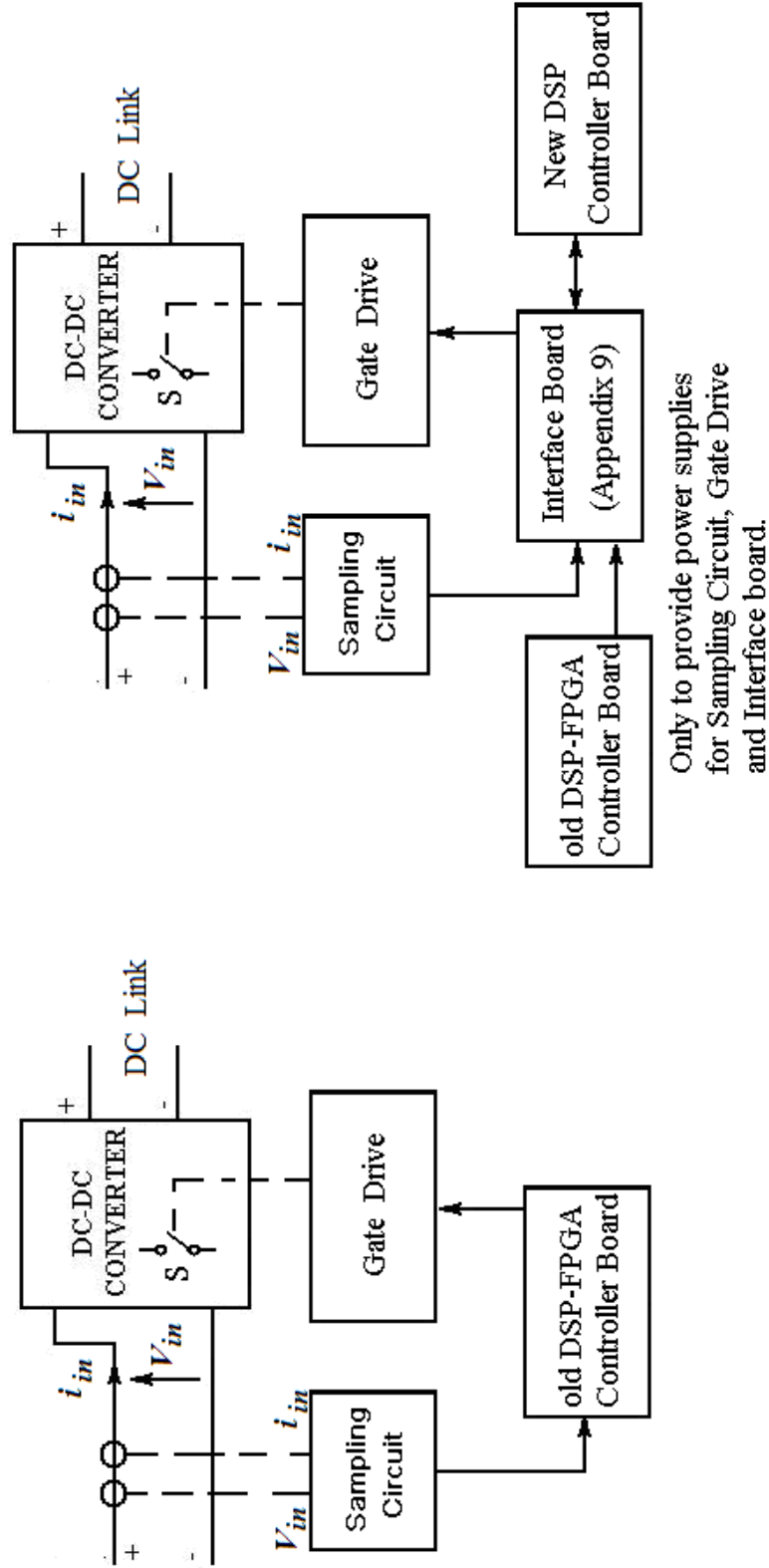
%display some calculated info
max_intensity = max(max(result));
min_intensity = min(min(result));
mean_intensity = mean(mean(result));
variation = max((max_intensity -mean_intensity), (mean_intensity-
min_intensity))/mean_intensity*100;
%theta_zero_cd=maxtheta;
r_no_influence=tan(theta_minor_influence/180*pi)*hei;

disp('The average intensity is (W/m2)');
disp (mean_intensity);
disp('The maximum intensity is (W/m2)');
disp (max_intensity);

```

```
disp('The minimum intensity is (W/m2)');
disp( min_intensity);
disp ('The variation is (%)');
disp (variation)
disp('The no influence distance is (mm)');
disp(r_no_influence);
disp('The no influence angle is (degree)');
disp(theta_minor_influence);
*****
```

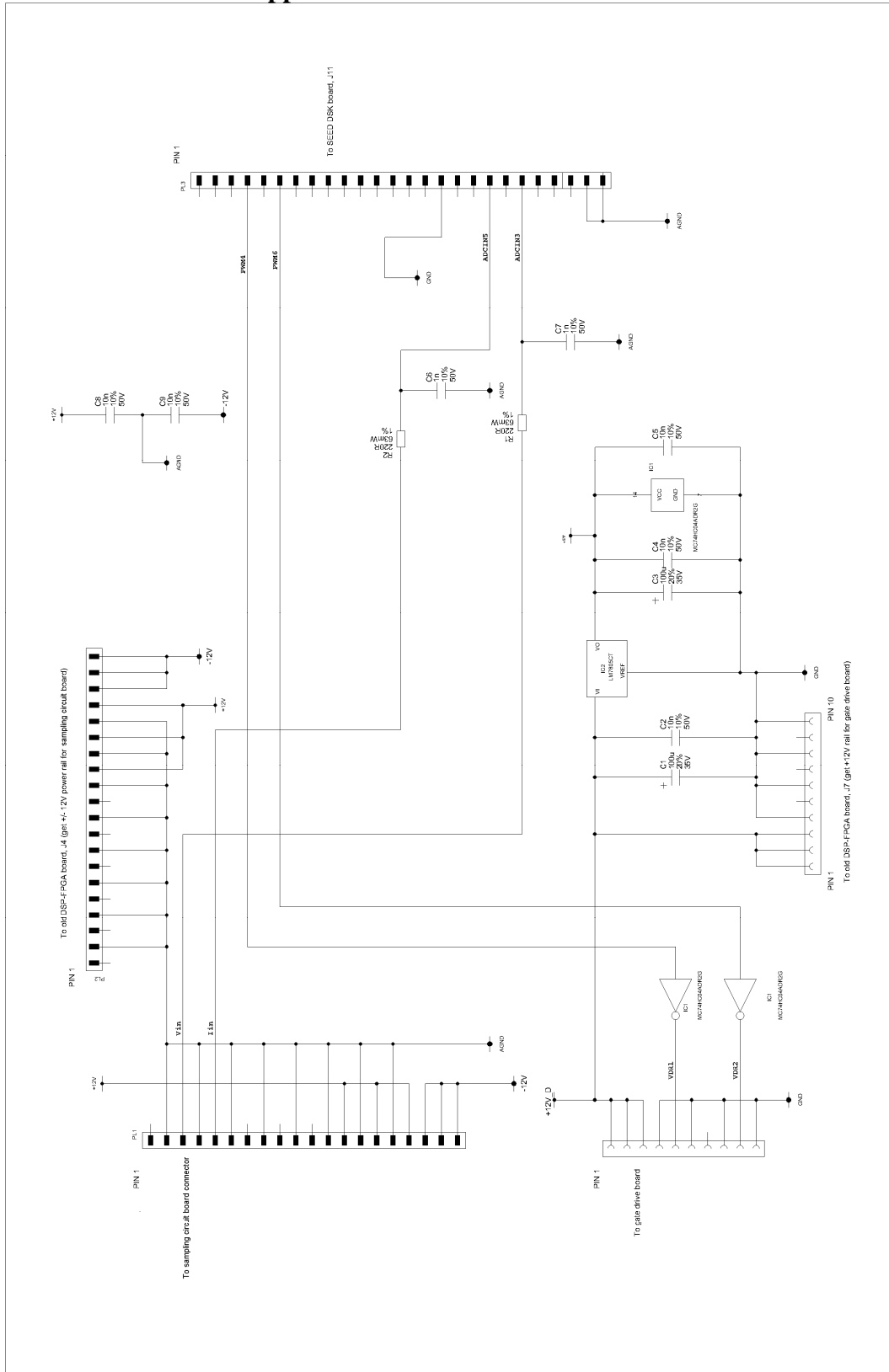
Appendix 8 Diagrams of existing and modified circuits



(a) Existing Circuit [18] [38]

(b) Modified Experimental Circuit used in this work

Appendix 9 Interface board circuit



Appendix 10 DSP code

```
//#####  
//  
// FILE:                PVcontrol.c  
//  
// TITLE:               PV MPPT control program  
//  
//#####  
  
#include "DSP28_Device.h"  
#include "math.h"  
#include "DSK2812_DA.H"  
#include "stdlib.h"  
  
interrupt void t1_timeruf_isr(void);  
  
int Id=0,Ie=0;  
int count=0,cn=0;  
int Iinbuff[400];  
int Vinbuff[400];  
int viewbuff4[400];  
int viewbuff5[400];  
int scanrecordI[400];  
int scanrecordV[400];  
int scanrecordP[400];  
int scanreccount=0;  
int sri=0;  
int maxpp=0;  
int maxpv=0;  
int maxpd=1000;  
int scancount=0;  
int scanflag=0;  
int Prec[16];  
int Pindex;  
int Pmppmax;  
int Pmppmin;  
int MPP_flag=0;  
int MPP_old=0;  
int MPP_c=0;  
int PS_flag = 0;  
int avi=0;  
long int Iaver=0;  
long int Vaver=0;  
int Iave;  
int Vave;
```

```

int Iold=0;
int Vold=0;
int deltaI=0;
int deltaV=0;
long int Pave;
long int Paver=0;
long int Paver2;
int Ppaonew=0;
int Ppaold=0;
int Ppaold2=0;
int paosign=1;
int paocn=0;
int postep=1;
int pwmduty=1125;
int currentperiod=3750;           //3750-10KHz;           1875-20KHz
int halfpe = 1875;               // = currentperiod/2
int sectimer = 0;
int msectimer = 0;
int i,j;
int an;
long int iref;
int tcount=0;
int tcount2=0;

void main(void)
{
    InitSysCtrl();
    EALLOW;                       // Enable PWM pins
    GpioMuxRegs.GPAMUX.all = 0x00BF;           // EVA PWM 1-6 pins
    GpioMuxRegs.GPBMUX.all = 0x00FF;           // EVB PWM 7-12 pins
    GpioMuxRegs.GPADIR.bit.GPIOA6=0;
    GpioMuxRegs.GPADIR.bit.GPIOA8=1;
    GpioMuxRegs.GPADIR.bit.GPIOA9=1;
    GpioMuxRegs.GPADIR.bit.GPIOA10=1;
    GpioMuxRegs.GPADIR.bit.GPIOA11=0;           //GPIOA11 input
    GpioDataRegs.GPACLEAR.bit.GPIOA6=1;
    GpioDataRegs.GPASET.bit.GPIOA8=1;           // LED D101 on
    GpioDataRegs.GPACLEAR.bit.GPIOA9=1;           // LED D102 off
    GpioDataRegs.GPACLEAR.bit.GPIOA10=1;           // LED D103 off
    GpioMuxRegs.GPBDIR.bit.GPIOB10=1;
    SysCtrlRegs.HISPCP.all=0x0001;           //High speed clock set to 75MHz
    EDIS;

    // Disable and clear all CPU interrupts:
    DINT;
    IER = 0x0000;

```

```

IFR = 0x0000;

// Initialize Pie Control Registers To Default State:
InitPieCtrl();

// Initialize the PIE Vector Table To a Known State:
InitPieVectTable();

InitCpuTimers();

// Initialize all the Device Peripherals to a known state:
InitAdc();

// EVA Configure T1PWM, T2PWM, PWM1-PWM6
EvaRegs.T1PR = currentperiod;    // Timer1 period 20 KHz
EvaRegs.T1CMPR = 0x03C0;    // Timer1 compare
EvaRegs.T1CNT = 0x0000;    // Timer1 counter
// TMODE = continuous up/down
// Timer enable
// Timer compare enable
EvaRegs.T1CON.all = 0x0842;    //4842

// Initalize EVA Timer2
EvaRegs.T2PR = currentperiod*2-1;    // Timer2 period
EvaRegs.T2CMPR = 0x03C0;    // Timer2 compare
EvaRegs.T2CNT = 0x0000;    // Timer2 counter
// TMODE = continuous up/down
// Timer enable
// Timer compare enable
EvaRegs.T2CON.all = 0x1042;

// Setup T1PWM and T2PWM
// Drive T1/T2 PWM by compare logic
EvaRegs.GPTCONA.bit.TCOMPOE = 1;
// Polarity of GP Timer 1 Compare = Active low
EvaRegs.GPTCONA.bit.T1PIN = 1;
// Polarity of GP Timer 2 Compare = Active high
EvaRegs.GPTCONA.bit.T2PIN = 1;

// Step 3 Enable compare for PWM1-PWM6
EvaRegs.CMPR1 = 938;
EvaRegs.CMPR2 = 469;
EvaRegs.CMPR3 = 235;

// Compare action control. Action that takes place
// on a compare event

```

```

// output pin 1 CMPR1 - active high
// output pin 2 CMPR1 - active low
// output pin 3 CMPR2 - active high
// output pin 4 CMPR2 - active low
// output pin 5 CMPR3 - active high
// output pin 6 CMPR3 - active low
EvaRegs.ACTRA.all = 0x0A5A;
// EvaRegs.DBTCONA.all = 0x09F0; // 2.0 us under-lap
// 0000 1001 1111 1000
EvaRegs.COMCONA.all = 0xA600;

EvaRegs.EVAIMRA.bit.T1PINT =1;

// EVB Configure T3PWM, T4PWM and PWM7-PWM12
// Initalize the Timers

// Initalize EVB Timer3
// Timer3 controls T3PWM and PWM7-12
EvbRegs.T3PR = currentperiod; // Timer3 period
EvbRegs.T3CMPR = 0x03C0; // Timer3 compare
EvbRegs.T3CNT = 0x0000; // Timer3 counter
// TMODE = continuous up/down
// Timer enable
// Timer compare enable
EvbRegs.T3CON.all = 0x4842;

// Initalize EVB Timer4
// Timer4 controls T4PWM
EvbRegs.T4PR = currentperiod; // Timer4 period
EvbRegs.T4CMPR = 0x0030; // Timer4 compare
EvbRegs.T4CNT = 0x0000; // Timer4 counter
// TMODE = continuous up/down
// Timer enable
// Timer compare enable
EvbRegs.T4CON.all = 0x1042;

// Setup T3PWM and T4PWM
// Drive T3/T4 PWM by compare logic
EvbRegs.GPTCONB.bit.TCOMPOE = 1;
// Polarity of GP Timer 3 Compare = Active low
EvbRegs.GPTCONB.bit.T3PIN = 1;
// Polarity of GP Timer 4 Compare = Active high
EvbRegs.GPTCONB.bit.T4PIN = 2;

// Enable compare for PWM7-PWM12
EvbRegs.CMPR4 = 0x0753;

```

```

EvbRegs.CMPR5 = 0x3C00;
EvbRegs.CMPR6 = 0xFC00;

// Compare action control. Action that takes place
// on a compare event
// output pin 1 CMPR4 - active high
// output pin 2 CMPR4 - active low
// output pin 3 CMPR5 - active high
// output pin 4 CMPR5 - active low
// output pin 5 CMPR6 - active high
// output pin 6 CMPR6 - active low
EvbRegs.ACTRB.all = 0x0666;
    EvbRegs.DBTCNB.all = 0x09F8;
    // Enable deadband and set to 1/75MHz*32*6(p=32,m=6)

EvbRegs.COMCONB.all = 0xA600;

//setting up of the A to D converter
AdcRegs.ADCTRL3.bit.ADCCLKPS=0x6; //ADC clock pulse is 75/6MHz=13.3ns
AdcRegs.ADCTRL1.bit.SEQ_CASC=1; // two sequencers are cascaded
AdcRegs.ADCTRL1.bit.ACQ_PS=0x1;
    //sample window is set to 4*ADCCLKPS=40ns
AdcRegs.ADCCHSELSEQ1.bit.CONV00=0x0; //A0 in ADCRESULT0
AdcRegs.ADCCHSELSEQ1.bit.CONV01=0x1; //A1 in ADCRESULT1
AdcRegs.ADCCHSELSEQ1.bit.CONV02=0x2; //A2 IN ADCRESULT2
AdcRegs.ADCCHSELSEQ1.bit.CONV03=0x3; //A4 IN ADCRESULT3
AdcRegs.ADCCHSELSEQ2.bit.CONV04=0x5; //B0 in ADCRESULT4
AdcRegs.ADCTRL1.bit.CONT_RUN=0; //sequencers in continuous running
AdcRegs.ADCMAXCONV.bit.MAX_CONV=0x4; //5 maximum conversions
AdcRegs.ADCTRL2.all=0x2000; //start of the sequencer

//Pie Vector table is modified to point to the new interrupt service routine
EALLOW;
PieVectTable.T1PINT =&t1_timeruf_isr;
EDIS;

//Interrupt group 1 is enabled at CPU level
IER |=M_INT1;
IER |=M_INT2;

//Group 1 interrupt line 7 is enabled at PIE level
PieCtrlRegs.PIEIER1.bit.INTx7 = 0;
PieCtrlRegs.PIEIER2.bit.INTx4 = 1;

//Interrupt enabled at CPU level
EINT;

```

```

ERTM;

// IDLE loop
while (1)
{

}

interrupt void t1_timeruf_isr(void)
{
    tcount++;
    tcount2++;

    GpioDataRegs.GPBDAT.bit.GPIOB10=1;
    AdcRegs.ADCTRL2.bit.RST_SEQ1=1; //sequencers stoped and reset for reading
    Id=AdcRegs.ADCRESULT3>>4; //Vin
    Ie=AdcRegs.ADCRESULT4>>4; //Iin

    Id = Id - 36; // offset
    Ie = Ie - 22; // offset
    AdcRegs.ADCTRL2.bit.SOC_SEQ1=1; //sequencers restarted from start
    if (AdcRegs.ADCST.bit.INT_SEQ1==1)
    {
        an=an+1;
        AdcRegs.ADCST.bit.INT_SEQ1_CLR=1;
    }
    if (an==10)
    {
        an=5;
    }

    /*----- average V I P calculation -----*/
    if (avi<100){
        avi++;
    }
    else{
        Iaver=Iaver+Ie;
        Vaver=Vaver+Id;
        Paver2 = (long) Ie*Id;
        Paver = Paver+(Paver2>>8);
        avi++;
    }

    if (avi>=200){
        Iave = Iaver>>6;

```

```

Vave = Vaver>>6;
Pave = Paver>>9;
avi=0;
Iaver=0;
Vaver=0;
Paver=0;
msectimer ++;
if (msectimer>50){
    sectimer ++;
    msectimer = 0;
}

linbuff[cn]=Vave;
Vinbuff[cn]=MPP_flag;
viewbuff4[cn]=pwmduty;
viewbuff5[cn++]=Pave;
if (cn>400)
    cn=0;

/*----- Scan -----*/
if (scanflag ==1){
    pwmduty = pwmduty + 40;           //40 is the scan step
    scanreccount++;
    scanrecordI[sri]=Iave;
    scanrecordV[sri]=Vave;
    scanrecordP[sri++]=Pave;
    if (Pave>maxpp){
        maxpp=Pave;
        maxpv=Vave;
        maxpd=pwmduty;
    }
    if (pwmduty>1800){
        scancount =0;
        scanflag = 0;
        if (maxpd>100)
            pwmduty = maxpd;
    }
}
/*----- end of Scan -----*/

/*----- MPPT (P&O)-----*/
if (scanflag == 0){
    Ppaonew = Pave;
    if (Ppaonew>(Ppaold+1)){
        if (Ppaold>(Ppaold2+1)){
            postep = Ppaonew-Ppaold;

```

```

    postep = (postep)>>2;
    if (postep>10)
        postep = 10;
    pwmduty = pwmduty + paosign*postep;
}
}
if (Ppaonew<(Ppaold-1)){
    if (Ppaold<(Ppaold2-1)){
        postep = Ppaold - Ppaonew;
        postep = (postep)>>2;
        if (postep>10)
            postep = 10;
        paosign = -1*paosign;
        pwmduty = pwmduty +paosign*postep;
    }
}
if (pwmduty < 100)
    pwmduty = 100;
if (pwmduty >1400)
    pwmduty = 1400;
Ppaold2 = Ppaold;
Ppaold = Ppaonew;
for (Pindex = 9; Pindex>0; Pindex--){
    Prec[Pindex]=Prec[Pindex-1];
}
Prec[0]=Ppaonew;
Pmppmin = Prec[0];
Pmppmax = Prec[0];
for (Pindex =1; Pindex < 10; Pindex++){
    if (Prec[Pindex]>Pmppmax)
        Pmppmax=Prec[Pindex];
    if (Prec[Pindex]<Pmppmin)
        Pmppmin = Prec[Pindex];
}
if ((Pmppmax-Pmppmin)<100){
    MPP_c++;
    if (MPP_c>10){
        MPP_c=10;
        MPP_flag = 1;
    }
}
if ((Pmppmax - Pmppmin)>99){
    MPP_flag = 0;
    MPP_c = 0;
}
deltaI = Iave - Iold;

```

```

if (abs(deltaV)< 2){
  if (abs(deltaI)>1){
    if (deltaI>0){
      pwmduty = pwmduty + 10;
    }
    if (deltaI<0){
      pwmduty = pwmduty -10;
    }
  }
}
if (abs(deltaV)>1){
  if ((Vave*deltaI) > (Iave*deltaV)){
    if (deltaV>0){
      pwmduty = pwmduty + 10;
    }
    if (deltaV<0){
      pwmduty = pwmduty - 10;
    }
  }
  if ((Vave*deltaI)< (Iave*deltaV)){
    if (deltaV<0){
      pwmduty = pwmduty -10;
    }
    if (deltaV>0){
      pwmduty = pwmduty +10;
    }
  }
}
Vold = Vave;
Iold = Iave;
if (pwmduty < 100)
  pwmduty = 100;
if (pwmduty >1400)
  pwmduty = 1400; */

```

```

/*----- if want to scan -----*/
if (MPP_flag == 1){
  if ((MPP_old == 0)&&(PS_flag == 0)){
    if ((Vave>3400)&&(Vave<3800)){
      PS_flag = 0;
    }
  }
  if ((Vave < 3400) || (Vave> 3800)){
    PS_flag = 1;
    scanflag=1;
    maxpp=0;
    maxpv=0;
  }
}

```

```

        maxpd=1000;
        sri=0;
        pwmduty = 100;
        MPP_flag = 0;
    }
}
MPP_old = MPP_flag;
if (sectimer > 10) {
    if (sectimer < 12){
    }
    if (sectimer > 40) {
        sectimer = 0;
        if ((Vave > 3400) && (Vave < 3800)) {
            PS_flag = 0;
        }
        if ((Vave < 3400) || (Vave > 3800)) {
            PS_flag = 1;
            scanflag=1;
            maxpp=0;
            maxpv=0;
            maxpd=1000;
            sri=0;
            pwmduty = 100;
            MPP_flag = 0;
        }
    }
}
}
/*----- end of MPPT -----*/
}

EvaRegs.CMPR2 = halfpe - pwmduty;
EvaRegs.CMPR3 = halfpe + pwmduty;
EvaRegs.T2CMPR = 4000;
EDIS;

if (count > 400)
{
    count=0;
}

PieCtrlRegs.PIEACK.bit.ACK2=1;
EvaRegs.EVAIFRA.bit.T1PINT=1;
GpioDataRegs.GPBDAT.bit.GPIOB10=0;
}

```

References

- [1] Great Britain. Department of Trade and Industry, **Meeting the energy challenge - A white paper on energy**, TSO, 2007, ISBN: 9780101712422
- [2] World Energy Council, **New renewable energy resources: a guide to the future**, Kogan Page, 1994, ISBN: 0749412631
- [3] Renewable Energy Policy Network for the 21st Century, “Renewables 2007 global status report”, available at http://www.ren21.net/pdf/RE2007_Global_Status_Report.pdf, accessed on 29/11/2008
- [4] Great Britain. Parliament. House of Lords. European Union Committee, **The EU's target for renewable energy : 20% by 2020 : report and evidence**, TSO, 2008, ISBN: 9780104013656
- [5] Great Britain Parliament, House of Commons, Innovation, Universities, Science and Skills Committee, **Renewable electricity generation technologies: report**, TSO, 2008, ISBN: 9780215523860
- [6] <http://www.restats.org.uk/electricity.htm>, accessed on 29/11/2008
- [7] Tomas Markvart, **Solar electricity**, 2nd edition, Wiley, 1999, ISBN: 0471988537
- [8] <http://www.renewableenergyworld.com>, accessed on 29/11/2008
- [9] E. Becquerel, “On electron effects under the influence of solar radiation”, *Comptes Rendues*, 1839
- [10] International Solar Energy Society. United Kingdom Section, **Solar energy : a UK assessment**, 1976, ISBN: 090496308
- [11] Eduardo Lorenzo, **Solar electricity: Engineering of Photovoltaic systems**, Published by PROGNSA, 1994, ISBN 8486505550
- [12] Matt Boreland and Darren Bagnall, “Current and future photovoltaics”, available at http://www.foresight.gov.uk/Energy/current_and_future_photovoltaics_.pdf, accessed on 30/11/2008
- [13] Robert Foster, “Japan photovoltaics market overview”, October 2005, available at <http://solar.nmsu.edu/publications/Japan%20Report.pdf>, accessed on 30/11/2008
- [14] Federal Ministry for the Environment, Nature Conservation and Nuclear Safety

Public Relations Division (Germany), **Renewable energy sources in figures - National and international development**, June 2008

- [15] UK energy research centre (UKERC), **Solar PV Landscape**, July 2007, available at: <http://ukerc.rl.ac.uk/ERL0301.html>, accessed on 01/12/2008
- [16] J. A. M. Bleijs, and A. D. Simmons, "Flexible PV demonstration and research system at the University of Leicester: Performance and modelling", Proceedings of the 20th European Union Photovoltaic Solar Energy Conference, 6-10 June 2005, Barcelona, pp. 2705-2708
- [17] J. A. M. Bleijs, and A. L. U. Mayere, "PV system at the University of Leicester: Performance and Developments", Proceedings of the 22nd European PV Solar Energy Conference, 3 - 7 September 2007, Milan, pp. 3089-3093
- [18] J. A. Gow, and J. A. M. Bleijs, "A modular DC-DC converter and maximum power tracking controller for medium to large scale photovoltaic generating plant", Proceedings of the 8th European Conference on Power Electronics and Applications. EPE'99, 1999, 8p
- [19] A. L. Fahrenbruch, and R. H. Bube, **Fundamentals of solar cells: photovoltaic solar energy conversion**, Academic Press, 1983, ISBN: 0122476808
- [20] D. F. Dunster, **Semiconductors for engineers**, Business Books, 1969, ISBN: 0220798621
- [21] Charles E. Backus, **Solar Cells**, IEEE Press, 1976, ISBN: 0879420693
- [22] Jenny Nelson, **The Physics of Solar Cells**, Imperial College Press, 2003, ISBN: 978-1-86094-340-9
- [23] S. J. Ransome, J. H. Wohlgemuth, and K. C. Heasman, "Quantifying PV Losses from Equivalent Circuit Models, Cells, Modules and Arrays", Proceedings of the 19th European Photovoltaic Solar Energy Conference, 7-11 June 2004, Paris, pp. 2346-2349
- [24] Tim Bruton, et al, "Towards 20% Efficient Silicon Solar Cells Manufactured at 60 MWp Per Annum", Proceedings of the 3rd World Conference on Photovoltaic Energy Conversion, 2003, Vol.1, pt. 1, pp. 899-902
- [25] M. Oukachmih, "New organic discotic materials for photovoltaic conversion, Solar Energy Materials and Solar Cells", v 85, n 4, 1 Feb. 2005, pp. 535-543
- [26] <http://www.n-e-renewables.org.uk>, North east renewable energy directory, accessed on 01/12/2008

- [27] J.A. Gow, and C.D. Manning, "Development of a photovoltaic array model for use in power-electronics simulation studies", IEE Proceedings-Electric Power Applications, v 146, n 2, March 1999, pp. 193-200
- [28] C. Protopoulos, B.J. Brinkworth, R.H. Marshall, and B.M. Cross, "Evaluation of two theoretical models in simulating the performance of amorphous-silicon solar cells", 10th E.C. Photovoltaic Solar Energy Conference, Proceedings of the International Conference, 1991, pp. 412-415
- [29] J.P. Charles, I. Mekkaoui-Alaoui, G. Bordure, and P. Mialhe, "A critical study of the effectiveness of the single and double exponential models for I-V characterization of solar cells", Solid-State Electronics, Vol. 28, No. 8, Aug. 1985, pp. 807-820
- [30] N. Veissid, D. Bonnet, and H. Richter, "Experimental investigation of the double exponential model of a solar cell under illuminated conditions: considering the instrumental uncertainties in the current, voltage and temperature values", Solid-State Electronics, Vol. 38, No. 11, Nov. 1995, pp. 1937-1943
- [31] Luis Castaner, and Santiago Silvestre, **Modelling Photovoltaic Systems Using Pspice**, J. Wiley, 2002, ISBN: 0470845287
- [32] A. Woyte, J. Nijs, and R. Belmans, "Partial shadowing of photovoltaic arrays with different system configurations: literature review and field test results", Solar Energy, Vol. 74, Issue 3, March 2003, pp. 217-233
- [33] W. Xiao, N. Ozog, and W. G. Dunford, "Topology Study of Photovoltaic Interface for Maximum Power Point Tracking", IEEE Transactions on Industrial Electronics, Vol. 54, No. 3, June 2007, pp. 1696-1704
- [34] Solar Cells and PV Systems, http://paris.fe.uni-lj.si/pvnet/strona_PV/index.html, accessed on 12/12/2008
- [35] G. Scheible, H. Solmecke, and D. Hackstein, "System Engineering Aspects and Power Electronics in an Autonomous Photovoltaic-Hydrogen System", International Journal of Renewable Energy Engineering, Vol. 1, No. 3, Dec 1999, pp. 98-103
- [36] M. A. Abella and F. chenlo, "Choosing the Right Inverter for Grid-connected PV systems", Renewable Energy Word, Mar-Apr 2004, pp. 131-146
- [37] G. R. Walker and P. C. Sernia, "Cascaded DC-DC Converter Connection of Photovoltaic Modules", IEEE Transactions on Power Electronics, Vol. 19, No. 4, July 2004, pp. 1130-1139

- [38] J. A. Gow, J. A. M. Bleijs, and R. Jones, "Optimization of a utility interface for large-scale photovoltaic power systems", Proceedings of the 9th European Conference on Power Electronics and Applications, EPE 2001, 10p
- [39] D. P. Hohm and M. E. Ropp, "Comparative study of maximum power point tracking algorithms", Progress in Photovoltaics: Research and Application, 2003, 11, pp. 47-62
- [40] T. Esum, and P.L. Chapman, "Comparison of Photovoltaic Array Maximum Power Point Tracking Techniques", IEEE Transaction on Energy Conversion, Vol. 22, No. 2, June 2007, pp. 439-449
- [41] K. H. Hussein, I. Muta, T. Hoshino, and M. Osakada, "Maximum photovoltaic power tracking: an algorithm for rapidly changing atmospheric conditions", IEE Proceedings, Generation, Transmission and Distribution, Vol. 142, No. 1, Jan. 1995, pp. 59-64
- [42] N. Khaehintung, T. Wiangtong, and P. Sirisuk, "FPGA implementation of MPPT using variable step-size P and O algorithm for PV applications", 2006 International Symposium on Communications and Information Technologies, ISCIT 2006, pp. 212-215
- [43] S. Jain, and V. Agarwal, "A New Algorithm for Rapid Tracking of Approximate Maximum Power Point in Photovoltaic Systems", IEEE Power Electronics Letters, Vol. 2, No. 1, March 2004, pp. 16-19
- [44] D. Sera, R. Teodorescu, J. Hantschel, and M. Knoll, "Optimized maximum power point tracker for fast-changing environmental conditions", IEEE Transactions on Industrial Electronics, Vol. 55, No. 7, July 2008, pp. 2629-2637
- [45] D. Shmilovitz, "On the control of photovoltaic maximum power point tracker via output parameters", IEE Proceedings, Electric Power Application, Vol. 152, No. 2, March 2005, pp. 239-248
- [46] G. Petrone, G. Spagnuolo, R. Teodorescu, M. Veerachary, and M. Vitelli, "Reliability Issues in Photovoltaic Power Processing Systems", IEEE Transactions on Industrial Electronics, Vol.55, No. 7, July 2008, pp. 2569-2580
- [47] R. Bruendlinger, B. Bletterie, M. Milde, and H. Oldenkamp, "Maximum power point tracking performance under partially shaded PV array conditions," Proceedings of the 21st European Union Photovoltaic Solar Energy Conference, Dresden, 4-8 September 2006, pp. 2157- 2160

- [48] K. Kobayashi, I. Takano, and Y. Sawada, "A study of a two stage maximum power point tracking control of a photovoltaic system under partially shaded insolation conditions," *Sol. Energy Mater. Sol. Cells*, Vol. 90, No. 18/19, Nov. 2006, pp. 2975–2988
- [49] H. Patel and V. Agarwal, "Maximum Power Point Tracking Algorithm for PV Systems Operating Under Partially Shaded Conditions", *IEEE Transactions on Industrial Electronics*, Vol. 55, No. 4, April 2008, pp. 1689-1698
- [50] R. Alonso, E. Román, S. Elorduizapatarietxe, P. Ibáñez, and I. Canales, "A new MPPT method solving problems with local maximum power points", *Proceedings of the 21st European Union Photovoltaic Solar Energy Conference*, Dresden, 4-8 September 2006, pp. 2293-2296
- [51] T. Noguchi, S. Togashi, and R. Nakamoto, "Short current Pulse-based Maximum-power-point Tracking Method for Multiple Photovoltaic-and-Converter Module System", *IEEE Transactions on Industrial Electronics*, Vol. 49, No. 1, February 2002, pp. 217-223
- [52] W. Liang, X. Han, and Q. Xie, "The Design of Maximum Power Point Tracker for a Racing Solar Car", *Application of Electronic Technique*, Vol. 30, No. 8, 2004, pp. 34-36 (in Chinese)
- [53] N.A. Ahmed, and M. Miyatake, "A novel maximum power point tracking for photovoltaic applications under partially shaded insolation conditions", *Electric Power Systems Research*, Vol. 78, No. 5, 2008, pp. 777-784
- [54] H. Patel and V. Agarwal, "MATLAB-based modeling to study the effects of partial shading on PV array characteristics", *IEEE Transactions on Energy Conversion*, Vol. 23, No. 1, March 2008, pp. 302-310
- [55] M.C. Alonso and F. Chenlo, "Experimental Study of Reverse Biased Silicon Solar Cells", *2nd World Conference and Exhibition on Photovoltaic Solar Energy Conversion*, July 1998, pp. 2376-2379
- [56] G. Friesen and H. A. Ossenbrink, "Capacitance Effects in High-efficiency Cells", *Solar Energy Materials and Solar Cells*, Vol. 48, No. 1-4, Nov. 1997, pp. 77-83
- [57] J. H. Scofield, M. Contreras, A. M. Gabor, and R. Noufi: "Admittance Measurements on Cu(In,Ga)Se₂ Polycrystalline Thin-film Solar Cells", *Proceedings of 24th IEEE Photovoltaic Specialists Conference*, New York, 1995, pp. 291-294

- [58] S. Mau and T. Krametz: "Influence of solar cell capacitance on the measurement of I-V-curves of PV-modules", 20th Symposium on Photovoltaic Solar Energy, Germany, 2005, 3p
- [59] G. Friesen, M. Mertens, E. Dunlop, W. Zaaiman, and H. A. Ossenbrink, "Investigation of Solar Cell Capacitance and its Dependence on Temperature Using the Photocurrent-Response Method", 14th European Photovoltaic Solar Energy Conference, Barcelona, Spain, 1997, pp. 2385-2388
- [60] T. Chayavanich, C. Limsakul, N. Chayavanich, D. Chenvidhya, C. Jivacate, and K. Kirtikara, "Describing Dynamic Behavior of Static IV Characteristics of PV Modules Using Dynamic Impedance", Proc. of 21st European Photovoltaic Solar Energy Conference, Dresden, Sept. 2006, pp. 2464-2465
- [61] C. Honsberg and S. Bowden, **Photovoltaics**, Beta of the 2nd Edition of CDROM, <http://www.pvcdrom.pveducation.org/index.html>, accessed 30/09/2008
- [62] U.S. Department of Energy - Energy Efficiency and Renewable Energy, http://www1.eere.energy.gov/solar/printable_versions/pv_cell_light.html, accessed 30/09/2008
- [63] Solar Resource Data from National Renewable Energy Laboratory of the U.S, <http://rredc.nrel.gov/solar/spectra/>, accessed 30/09/2008
- [64] J. A. Merrigan, **Sunlight to electricity : prospects for solar energy conversion by photovoltaics**, MIT Press, 1975, ISBN: 0262131161
- [65] H. Field, "UV-VIS-IR spectral responsivity measurement system for solar cells", AIP Conference Proceedings, Vol. 462, 1999, pp. 629-35
- [66] A. Goetzberger and V. U. Hoffmann, **Photovoltaic solar energy generation**, Springer, 2005, ISBN: 3540236767
- [67] W. Palz, **Solar Electricity: an Economic Approach to Solar Energy**, Unesco., 1978, ISBN: 9231014277
- [68] Establishment and Operation of a Photovoltaic Cell Test Facility, www.berr.gov.uk/files/file16539.pdf, accessed 30/09/2008
- [69] H. Cotal, R. Sherif, G. Glenn, D. Krut, A. Paredes, T. Meza, and H. Hayden, "High Concentration Testing and Performance of Multijunction Solar Cells", Conference Record of the IEEE Photovoltaic Specialists Conference, 2002, pp. 1612-1615

- [70] Reactive sputtering produces durable coatings for a demanding environmental test application, <http://www.ptbmagazine.com/Jan00/ptb.0100coat.html>, accessed 30/09/2008
- [71] John G. Webster, **Wiley Encyclopedia of Electrical and Electronics Engineering**, John Wiley, 1999, ISBN: 0471139467
- [72] Glenn James, **Mathematics dictionary**, Van Nostrand Reinhold, 1976, ISBN: 0442240910
- [73] J. E. Kaufman and J. F. Christensen, **IES Lighting Handbook**, Illuminating Engineering Society of North America, 5th edition 1972, ISBN: 0879950005
- [74] Juno and Aculux Residential Recessed Lighting, <http://www.junolightinggroup.com/>, accessed 02/07/2009
- [75] Binning and Labelling, <http://www.philipslumileds.com/pdfs/AB21.pdf>, accessed 30/09/2008
- [76] Luxeon K2 Emitter, <http://www.philipslumileds.com/pdfs/DS51.pdf>, accessed 30/09/2008
- [77] All in One Plug and Play Guide, <http://www.philipslumileds.com/pdfs/PG01.pdf>, accessed 30/09/2008
- [78] Wide Area Lighting Design Guide, <http://www.philipslumileds.com/pdfs/BR07.pdf>, accessed 30/09/2008
- [79] Mega-Ray SB 100-Watt flood lamp, www.reptielenlampen.nl/MegaRay.htm, accessed 30/09/2008
- [80] C. Prapanavarat, M. Barnes and N. Jenkins, "Investigation of the performance of a photovoltaic AC module", IEE Proceedings: Generation, Transmission and Distribution, Vol. 149, Issue 4, pp. 472-478
- [81] www.osram.com, accessed 30/09/2008
- [82] DIALux - a planning software for your project presentation, <http://www.dial.de/CMS/English/Articles/DIALux/Features/Features.html>, accessed 30/09/2008
- [83] <http://www.mirosolar.com/reflection.html>, accessed 30/09/2008
- [84] TMS320F281x Data Sheet, <http://focus.ti.com/lit/ds/symlink/tms320f2812.pdf>, accessed 30/09/2008

Publications

- [1] Y. Liu, and J.A.M. Bleijs, “Dynamic Effect of PV Cell Capacitance on MPPT Algorithms”, Proceedings of the 21st European Union Photovoltaic Solar Energy Conference, Dresden, 4-8 September 2006, pp. 2604- 2607
- [2] Y. Liu, and J.A.M. Bleijs, “Design of a Flexible Solar Emulator to Facilitate the Study on MPPT Control of PV Panels Using a DSP Based DC/DC Converter”, Proceedings of the 22nd European PV Solar Energy Conference, 3 - 7 September 2007, Milan, pp. 3059-3063